March 3, 1976

To the Graduate Council:

I am submitting herewith a dissertation written by Sen-I Chang entitled "A Method for Systematic Interpretation of Dynamic Measurements in a High Temperature Gas-Cooled Reactor." I recommend that it be accepted in partial fulfillment of the requirements for the degree of Doctor of Philosophy, with a major in Nuclear Engineering.

T. W. Kerlin, Major Professor

We have read this dissertation
and recommend its acceptance:

Accepted for the Council:

Vice Chancellor
Graduate Studies and Research

A METHOD FOR SYSTEMATIC INTERPRETATION OF DYNAMIC MEASUREMENTS IN A HIGH TEMPERATURE GAS-COOLED REACTOR

A Dissertation

Presented for the

Doctor of Philosophy

Degree

The University of Tennessee

Sen-I Chang

March 1976

1270489

ACKNOWLEDGEMENTS

The author wishes to express his indebtedness to his advisor Professor T. W. Kerlin for suggesting the problem considered in this dissertation and for the many helpful discussions and continuing advice throughout the course of this study.

The author would like to thank Messrs. D. G. Renfro, J. G. Thakkar, and M. H. Lee for their help in the check-out and use of the steam generator model for Fort St. Vrain to perform the dynamic analysis.

A special note of appreciation is for Mrs. Juanita Rye for her effort in preparing the final documentation.

The work reported herein was performed under a contract between the Nuclear Engineering Department, The University of Tennessee and Oak Ridge National Laboratory (Subcontract Number 4122).

ABSTRACT

Large linear dynamic models for nuclear reactor systems are widely used for simulation and control system design. It is important to be able to verify these models and the parameters in them. Existing parameter identification techniques are very time-consuming for use with large systems. This study presents the development and application of a new technique for practical parameter identification of systems whose dynamics are described by up to 110 first order, linear differential and algebraic equations. A partitioned matrix technique was developed for this purpose. This technique which takes advantage of the matrix form of the system equations, constitutes a very efficient analysis algorithm when implemented on the digital computer.

The identification procedure is to be used to analyze test results from the Fort St. Vrain high temperature, gas cooled reactor.

In order to validate the important physical parameters in the overall system model of Fort St. Vrain, reliable models for each component in the system are necessary. A linear, three node moving boundary model of a once-through steam generator for the Fort St. Vrain nuclear plant was developed for use with other subsystem models developed at the General Atomic Company.

To demonstrate the efficiency of the proposed technique which was used in the parameter identification algorithm in this study, three system models were analyzed: (a) Oconee I nuclear system described by twenty-nine differential equations; (b) Fort St. Vrain

steam generator, described by thirteen differential and seven algebraic equations, (c) Fort St. Vrain nuclear steam supply system, described by fifty-eight differential and twenty-three algebraic equations. Computer programs were written in FORTRAN IV to make the necessary calculations; the programs were executed on the IBM 360 Model 65 computer.

The accuracy and computing time of the new technique were studied. Also, the use of the Fisher information matrix for answering the question of parameter identifiability was studied. The information matrix which was generated could be used to evaluate the goodness of the parameters estimated. Using the new technique, the simulated analysis of the 81st order model of the Fort St. Vrain nuclear system required only 12 minutes and 50 seconds on the IBM 360 Model 65 computer.

TABLE OF CONTENTS

CHAPTER		PAGE
1.	INTRODUCTION	1
	Statement of the Problem	1
	Approach Used in This Study	1
	Scope and Organization of the Text	3
2.	FORT ST. VRAIN STEAM GENERATOR MODELING	5
	Introduction	5
	A Description of the System	6
	Helium Circuitry	9
	Main Steam Circuitry	9
	Integral Reheater Circuitry	11
	Lumped Parameter Analysis	11
	Model Formulation	12
	Basic Equations	12
	Summary of Equations	20
	Linearization of Equations	22
	Equation (2.20) Linearization	22
	Equation (2.21) Linearization	25
	Equation (2.22) Linearization	28
	Equation (2.23) Linearization	31
	Results and Discussion	36
	Discussion of Results for Run No. 1 (Figures 4 to 7)	37

CHAPTER PAGE

Discussion of Results for Run No. 2 (Figures 8 to 11) 48

Discussion of Results for Run No. 3 (Figures 12 to 15) 48

Discussion of Results for Run No. 4 (Figures 16 to 19) 57

Discussion of Results for Run No. 5 (Figures 20 to 23) 57

3. A METHOD FOR AUTOMATIC IDENTIFICATION OF PARAMETERS IN LARGE DYNAMIC SYSTEM 66

Introduction 66

Descent Methods-the Method of Steepest Descent and the Method of Conjugate Gradients 68

The Method for Calculating the Frequency Response and Its Sensitivity to Parameter Changes 76

The Application of the Partitioned Matrix Technique in the Optimization Scheme 79

The Partitioned Matrix Algorithm 81

Identifiability of the Parameters 84

4. DEMONSTRATION OF THE METHOD-CASE STUDY I: OCONEE I NUCLEAR SYSTEM 96

Introduction 96

The Theoretical Model of the Oconee I System 97

Reactor and Core Heat Transfer Model 97

CHAPTER PAGE

Piping and Plenums 106
Steam Generator 108
Pressurizer 110
Overall System 112
Experimental Results 113
Results and Discussion 118

5. DEMONSTRATION OF THE METHOD-CASE STUDY II: FORT ST. VRAIN STEAM GENERATOR 134
Introduction 134
A Description of the System 135
Results and Discussion 137

6. DEMONSTRATION OF THE METHOD-CASE STUDY III: FORT ST. VRAIN NUCLEAR STEAM SUPPLY SYSTEM 146
Introduction 146
The Fort St. Vrain Nuclear Power Plant Description 148
Theoretical Model of the System 150
Neutronics 150
Core Thermal 155
Helium Transport Delays 159
Secondary Coolant Pressure-Flow Equations . . . 159
Secondary Coolant Thermal Balance Equations . . 163
Helium Flow Rate 169
Overall System 170
Results and Discussion 182

CHAPTER PAGE

7. CONCLUSIONS AND RECOMMENDATIONS 189

Conclusions 189

Recommendations 191

LIST OF REFERENCES 192

APPENDIXES 196

A. THE ERROR FUNCTION BASED ON THE DIFFERENCE OF GAIN AND PHASE IN THE FREQUENCY DOMAIN 197

B. HFFT-A METHOD FOR DIGITAL FOURIER ANALYSIS 200

C. THE ELEMENTARY ROW/COLUMN OPERATION ON A GENERAL COMPLEX SQUARE MATRIX 207

D. DESCRIPTION OF COMPUTER CODE, PARAPE 211

VITA 219

LIST OF TABLES

TABLE		PAGE
2.1.	Fort St. Vrain Nuclear Power Plant Steam Generator Design Conditions	8
2.2.	The Variables Associated with CPSG for A and B Matrix	38
2.3.	The State Variables Associated with CPSG for Reduced A_d Matrix	39
2.4.	Elements of A Matrix for CPSG	40
2.5.	Elements of B Matrix for CPSG	41
2.6.	Elements of A_d Matrix for CPSG	42
2.7.	Description of Each Analysis Run	43
4.1.	Core Design, Thermal, and Hydraulic Data Oconee I FSAR	99
4.2.	Nuclear Design Data Oconee I FSAR	102
4.3.	Reactor Vessel Design Data Oconee I FSAR	103
4.4.	Steam Generator Design Data Oconee I FSAR	104
4.5.	State Variable Index for Oconee I System	114
4.6.	Oconee I System Coefficient Matrix	115
4.7.	Input Data for Algebra Table: Case Study I	122
4.8.	Results of PARARI Computer Code Run: Case Study I	126
4.9.	Results of PARAGP Code Run: Case Study I	130
5.1.	The Algebra Table for Case Study II	138
5.2.	The Results of PARAGP Code Run for the Fort St. Vrain Steam Generator	142

TABLE PAGE

5.3. The Results of PARARI Calculation for the Fort St. Vrain Steam Generator 145

6.1. Fort St. Vrain Neutronics Parameters 151

6.2. Data on Major Design Characteristics Fort St. Vrain FSAR 152

6.3. State Variable Index for Fort St. Vrain System 172

6.4. Elements of A Matrix for Case Study III 175

6.5. Elements of B Matrix for Case Study III 176

6.6. The Algebra Table for Case Study III 183

6.7. The Results of PARARI Code Run for the Fort St. Vrain Nuclear System 184

6.8. The Results of PARAGP Code Run for the Fort St. Vrain Nuclear System 185

LIST OF FIGURES

FIGURE		PAGE
1.	Fort St. Vrain 330-MW(e) HTGR	7
2.	Fort St. Vrain Nuclear Power Plant Steam Generator Module	10
3.	The Schematiced Lump Division of Once Through Steam Generator Model	13
4.	CFSG Time Response to a 1 lb/sec Step Increase of Helium Flow	44
5.	Frequency Response of Main Steam Temperature to Helium Flow (CFSG)	45
6.	Frequency Response of Helium Outlet Temperature to Helium Flow (CFSG)	46
7.	Frequency Response of Main Steam Pressure to Helium Flow (CFSG)	47
8.	CPSG Time Response to a 1 lb/sec Step Increase of Helium Flow	49
9.	Frequency Response of Main Steam Temperature to Helium Flow (CPSG)	50
10.	Frequency Response of Helium Outlet Temperature to Helium Flow (CPSG)	51
11.	Frequency Response of Main Steam Pressure to Helium Flow (CPSG)	52
12.	CFSG Time Response to a 1°F Step Increase of Helium Inlet Temperature	53

FIGURE PAGE

13. Frequency Response of Main Steam Temperature to Helium Inlet Temperature (CFSG) 54

14. Frequency Response of Helium Outlet Temperature to Helium Inlet Temperature (CFSG) 55

15. Frequency Response of Main Steam Pressure to Helium Inlet Temperature 56

16. CPSG Time Response to a 1°F Steam Increase of Helium Inlet Temperature 58

17. Frequency Response of Main Steam Temperature to Helium Inlet Temperature (CPSG) 59

18. Frequency Response of Helium Outlet Temperature to Helium Inlet Temperature 60

19. Frequency Response of Main Steam Pressure to Helium Inlet Temperature (CPSG) 61

20. CFSG Time Response to a 1 lb/sec Step Increase of Feedwater Flow 62

21. Frequency Response of Main Steam Temperature to Feedwater Flow (CFSG) 63

22. Frequency Response of Helium Outlet Temperature to Feedwater Flow (CFSG) 64

23. Frequency Response of Main Steam Pressure to Feedwater Flow (CFSG) 65

24. The Descent Vector $\bar{V}_i$ Lies in the Tangent Plane to the Level Surface through $\bar{P}_{i+1}$ 71

25. Descent Methods when Ellipses are Elongated 73

FIGURE PAGE

26. Level Surfaces for Different Values of ΔE 88

27. The Ellipses for Different Matrices, J 91

28. Schematic of Oconee I System 98

29. Schematic of Fuel-Coolant Heat Transfer Model 107

30. Model of Oconee I Once Through Steam Generator 111

31. Frequency Response Based on Reference Coefficients Values: 95 Percent Power 117

32. The Experiment Response Data in Time-Domain 119

33. Frequency Response Calculated from Experiment Data . . 120

34. Signs of System Matrix B for Case Study I 123

35. Signs of System Matrix B After Row/Column Shifting . . 124

36. Comparison Between Theoretical and Experimental Frequency Response (PARARI Calculation) 127

37. The Curves of $J_{kk\ell}$ Versus Frequencies for Case Study I 128

38. Comparison Between Theoretical and Experimental Frequency Response (PARAGP Calculation) 131

39. The Contour Map for Case Study I 132

40. Comparison Between the Results of PARAGP Calculation and Reference Model's Frequency Response (Case Study II) 136

41. The Signs of System Matrix B for Case Study II 139

42. The Signs of System Matrix B After Elemental Row/Column Shifting 141

43. The Curves of $J_{ii\ell}$ Versus Frequencies for Case Study II Steam Generator 143

FIGURE PAGE

44. Schematic Diagram of Fort St. Vrain Nuclear Steam Supply System 149

45. Core Thermal Model for Fort St. Vrain Nuclear System . 156

46. Pressure/Flow Model for Secondary Coolant Flow 161

47. Thermal Model of Reheater and Turbines 164

48. Comparison Between the Results of PARARI Calculation and Reference Model's Frequency Response 180

49. The Curves of $J_{ii\ell}$ Versus Frequencies for Fort St. Vrain Nuclear System 187

CHAPTER 1

INTRODUCTION

1.1 Statement of the Problem

The main objectives of the research reported in this dissertation are:

a. To develop a new method for practical parameter identification in large dynamic systems (involving up to 110 coupled, linear differential equations) with special emphasis on the Fort St. Vrain nuclear plant.

b. To prepare a suitable plant model for Fort St. Vrain to use for simulated applications of the identification procedure and for subsequent use in parameter identification using actual plant data to be obtained in future tests.

c. To evaluate the new identification procedure using both actual plant test data (from a pressurized water reactor) and simulated experiments.

1.2 Approach Used in This Study

The choice of a theoretical model in this study is restricted to one in which the only independent variable is time. As in several other applications of the parameter space approach,[1,2,3] a model consisting of n first-order, differential equations with the following form was used:

$$\dot{\bar{x}} = B\bar{x} + \bar{f}g \qquad (1.1)$$

where

$\cdot$ = derivative with respect to time

n = the order of the system

$\bar{x}$ = the state variable vector of the system (nxl)

B = the system's constant coefficient matrix (nxn)

g = a scalar which represents the input disturbance, and

$\bar{f}$ = the contribution vector of g to each state variable (nxl).

This type of model is used to simulate the system dynamics because the coefficients that appear in the equation have physical significance.

In this dissertation, a more general form of n first-order, differential equations will be used:

$$A\dot{\bar{x}} = B\bar{x} + \bar{f}g \qquad (1.2)$$

where

A = the differential system matrix (nxn)

B = the algebraic system matrix (nxn).

The form of Equation (1.2) is equivalent to Equation (1.1) if A is the identity matrix.

In a plant dynamic test, measurement of the frequency response is a convenient way to obtain the information for experimental determination of parameters in the theoretical model.

The adjustment of the parameters is accomplished by changing the parameters in such a way that the differences between the theoretical model frequency response and the experimental frequency response from the plant are minimized. Three important advantages of the minimization in the frequency domain[4] are (a) the ease in obtaining the theoretical model's frequency response, (b) the

algebraic nature of calculations in the frequency domain, and (c) the small additional calculation required to obtain the sensitivities needed in the optimization. Changes in the parameters are made according to an optimization scheme such as the conjugate gradient method.[5]

1.3 Scope and Organization of the Text

In Chapter 2, the development of a linear, 3 node moving boundary model for Fort St. Vrain steam generator is presented. The model equations are derived from first principles to provide a complete, physical model for the identification work. The results of model responses in the time domain and frequency domain are discussed.

In Chapter 3, a new method for identifying parameters in very large models (up to 110th order) of dynamic systems is developed. It is based on optimizing the parameter estimates by minimizing differences between model-predicted frequency responses and experimentally measured frequency responses. The method employs a new matrix partitioning technique to achieve the required efficiency. The method is implemented in a new computer program called PARAPE.

Chapter 4 contains the results obtained using PARAPE to adjust the important design parameter in a theoretical model for the Oconee 1 pressurized water reactor in order to obtain better agreement with previously measured experimental results. This will provide the experience needed for efficient handling of the data to be obtained in future applications such as the one anticipated at Fort St. Vrain.

In Chapter 5, the model for the Fort St. Vrain steam generator is used to provide data for a simulated parameter identification. A reference calculation was performed with a selected data set. Then a calculation was performed using a modified data set. The reference calculation was used to provide simulated experimental frequency response data and the starting estimate in the parameter estimation was taken as the modified data set. The PARAPE code was used to adjust the parameters so as to improve agreement with the reference case. In this simulated case, the correct parameter values were known, permitting an evaluation of the success of the identification.

Chapter 6 is also devoted to a simulated test. In this case, the model represents the overall Fort St. Vrain plant and is 81st order. This task was performed to demonstrate the capability of the PARAPE program to deal with very large models.

Some concluding remarks and suggestions for future work in this study are given in Chapter 7.

CHAPTER 2

FORT ST. VRAIN STEAM GENERATOR MODELING

2.1 Introduction

A linear model, called LAP, which was developed by General Atomic Company (GA) to simulate Fort St. Vrain includes the primary coolant system, secondary coolant system, and reactor system. Each of these sub-system models was derived from first principles at GA (conservation of mass, momentum, energy, and neutrons) except for an approximation used for the main steam section in the once-through steam generator (OTSG) in early studies.

An empirical or transfer function approach was adopted by GA for the main steam section. This emperical model was obtained by tuning arbitrary constants in LAP's[6] transfer function type model to produce agreement between LAP and the Transient Analysis Program,[7] a detailed, nonlinear model.

The development and implementation of a linear steam generator model derived from first principles was undertaken at GA (work performed by W. D. Leech)[8] because it was believed that an OTSG linear model based on first principles would be superior to the original model for two reasons. First, a model based on first principles yields a better physical understanding. Second, the tuning of the arbitrary constants which appear in the transfer function involved a large degree of qualitative judgement as to when satisfactory agreement was reached between TAP and LAP.

A dynamic analysis was performed by the author using this new steam generator model and the preliminary results were not satisfactory. The decision was made to revise the steam generator model in order to provide a reliable steam generator representation in the overall system model of Fort St. Vrain for use in the system identification project. The revised model is described in the following sections.

2.2 A Description of the System

The Fort St. Vrain plant has two identical once-through type steam generator loops arranged in parallel, each of which consists of six individual steam generator modules, located within the cavity of the prestressed concrete reactor vessel (PCRV) and beneath the reactor core (see Figure 1). Each steam-generator module contains a heat-transfer section with a main steam production region and an integral reheater, as well as a PCRV penetration section with suitable inlet and outlet connections and helium-pressure barriers.

The steam generator is used to transfer the heat from the helium coolant to the water/steam. The helium flow that cools the reactor core enters the steam generator at high temperature and gives up its heat, first to the reheat steam section, then to the once-through main steam/water section. The sections produce main steam and reheat steam as demanded by the plant load and main turbine requirements.

The main design parameters of the system are shown in Table 2.1.

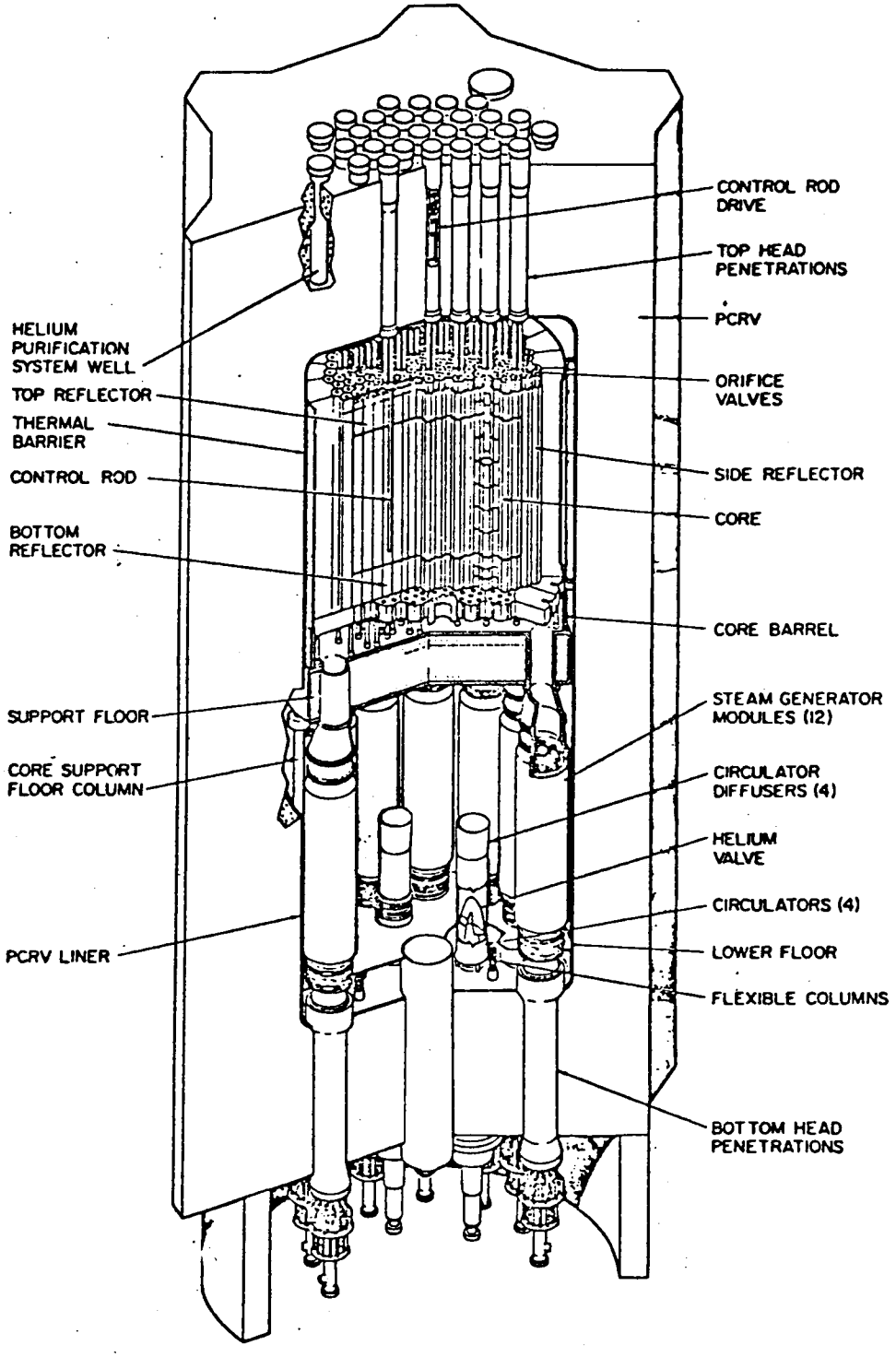


Figure 1. Fort St. Vrain 330-MW(e) HTGR.

TABLE 2.1

FORT ST. VRAIN NUCLEAR POWER PLANT
STEAM GENERATOR DESIGN CONDITIONS

	100% Steam Flow	25% Steam Flow
Load		
Generator Output (MW)	342.0	81.2
Station Output (MW)	330.2	67.4
Helium		
Flow (lb/hr)	2,452,400	1,026,000
Outlet Pressure (psia)	686	589
Inlet Temperature (F)	1,268	1,085
Outlet Temperature (F)	632	501
Pressure Drop (psi)	3.47	0.36
Feedwater/Main Steam		
Flow (lb/hr)	2,305,326	574,776
Outlet Pressure (psia)	2,512	2,419
Inlet Temperature (F)	403	299
Outlet Temperature (F)	1005	1,000
Pressure Drop (psi)	590	45
Reheat Steam		
Flow (lb/hr)	2,245,366	556,928
Outlet Pressure (psia)	600	151
Inlet Temperature (F)	673	570
Outlet Temperature (F)	1,002	1,000
Pressure Drop (psi)	42	11

The modules (Figure 2) are divided into three bundles (heating surface sections) arranged one above the other, made up of helically wound tubes supported by perforated plates attached to the central support structure.

Helium Circuitry

Helium leaves the core and travels downward to the steam generator. The gas then passes over the reheater, finishing superheater, pre-superheater, evaporator, and economizer surfaces consecutively. Cold helium exits at the bottom of the steam generator modules and flows into the four suction chambers of the helium circulators.

Main Steam Circuitry

Feedwater is distributed to the 12 modules through flow-control valves and enters each module through a ringheader. The heat-transfer surfaces of the economizer-evaporator-pre-superheater (EES) and finishing superheater (SHII) bundles are composed of helically wound tubes originating at the feedwater subheaders. In the bottom EES bundle, the water is preheated, evaporated, and pre-superheated. The steam flow is counter current to the helium flow passing over these tubes. Then the crossover tubes lead the pre-superheated steam to the finishing superheater (SHII) which is arranged for co-current flow above the EES bundle. This arrangement is required to minimize tube metal temperatures and enhances stability in this section. Superheated steam leaves the SHII bundle via tubes and

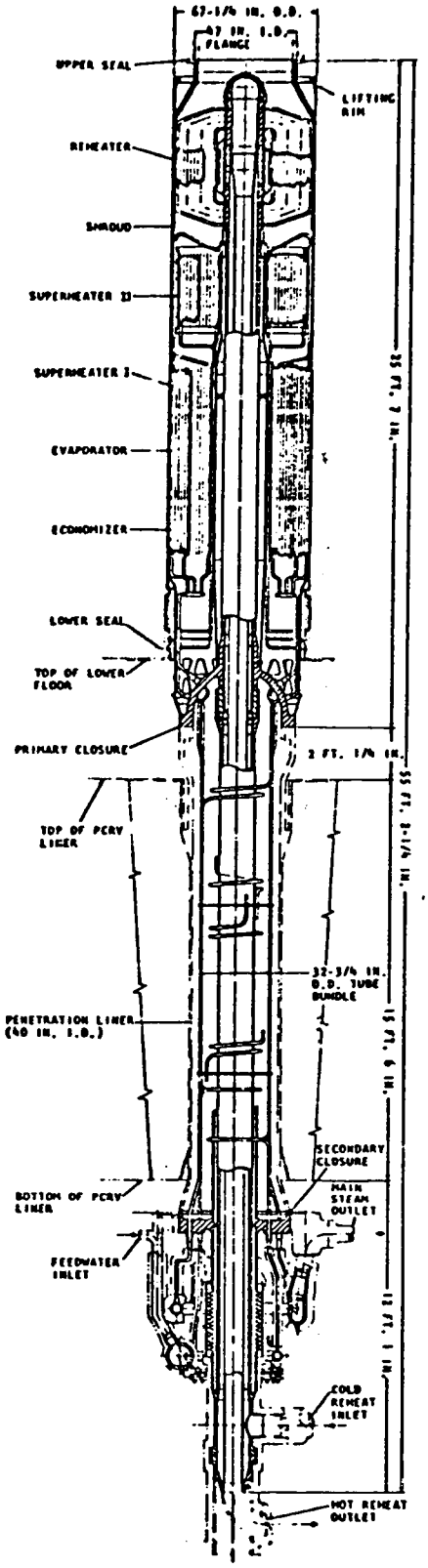


Figure 2. Fort St. Vrain Nuclear Power Plant Steam Generator Module.

is collected in the main steam ringheader, which is connected to the main steam piping.

Integral Reheater Circuitry

Cold reheat steam enters each steam-generator module through an annulus. The steam is discharged from the annulus to the reheater (RH) bundle. The RH bundle, also composed of helically wound tubes, is the uppermost heating surface in the steam generator, and is arranged for counter current flow. Hot reheat steam is carried via the central reheat pipe through the primary and secondary closures and returns to the intermediate pressure (IP) turbine.

2.3 Lumped Parameter Analysis

The dynamic analysis of a sub-system such as a once through steam generator (OTSG) is a distributed parameter problem. However, a lumped parameter approach is commonly used for its simplicity and ease of solution by either analog or digital techniques. For dynamic analysis, it is often desirable to have a linear set of coupled differential equations. Equations can be linearized by expanding each term in a Taylor series about an operating point. If the terms above first order are neglected, the result is valid as long as the variables stay close to the operating point. The linearized set of equations has the form of Equation (1.2):

$$A \frac{d\bar{x}}{dt} = B\bar{x} + \bar{f}g. \qquad (2.1)$$

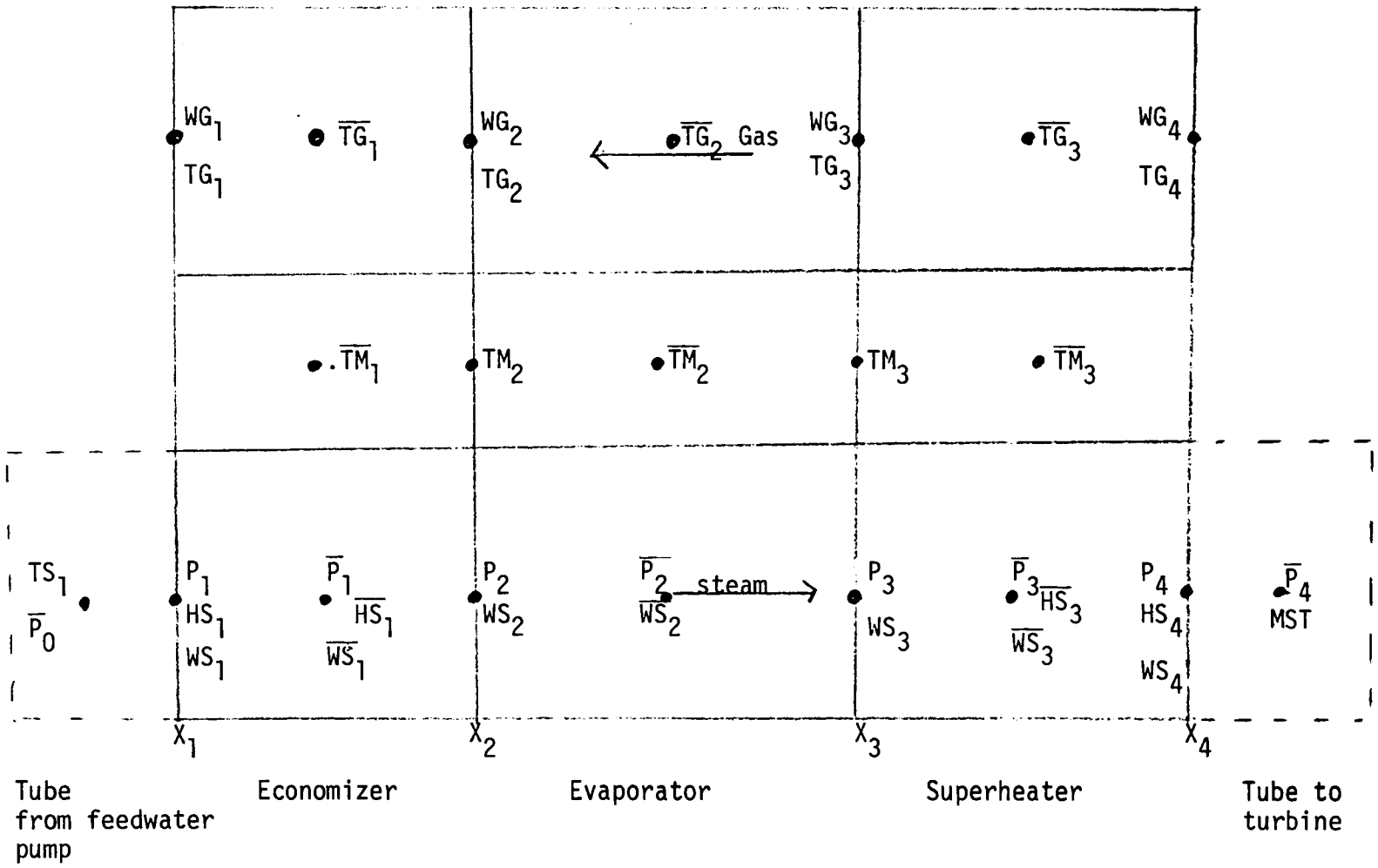
A set of equations of this form was obtained by the System Analysis Branch of the Reactor Engineering Department of General Atomic in the mathematical model LAP (Linear Analysis Program).

Model Formulation

In order to account for movement of the beginning and end of the boiling zone, the main steam section was divided into three regions with moving boundaries corresponding to the economizer, evaporator, and superheater as shown in Figure 3. The first node upper boundary was defined as the length (from the inlet) required for the water to be heated to saturation. The second node upper boundary, was defined by the additional length required to heat the water from saturated liquid to saturated vapor. The third node was defined as the remaining length by the steam generator. This formulation allows movement of the points where boiling begins (0 percent quality) and ends (100 percent quality) and yields a low order representation of the physical system that retains all of the physical processes usually considered important.

Basic Equations

Figure 3 shows a counter flow heat exchanger. The locations X_2 and X_3 are free to move but always remain at fixed quality. For the steam generator model, X_2 is the location of saturated liquid (0 percent quality) and X_3 is the location of saturated vapor (100 percent quality).



TS_1: feedwater temperature

MST: main steam temperature.

Figure 3. The Schematiced Lump Division of Once Through Steam Generator Model.

Conservation of Mass. The basic relationship is:

Flow in - Flow out = rate of change of mass stored.

a. Gas side

$$WG_i = WG_{in} \quad (i = 1, 2, 3)$$

where WG = gas flow rate (lb/sec)

WG_{in} = inlet gas flow rate.

Here we assume the gas flow rate is a function of time only and the same in every section.

b. Water/steam side

$$(WS_i - \frac{1}{V_i} A \dot{X}_i) - (WS_{i+1} - \frac{1}{V_{i+1}} A \dot{X}_{i+1}) =$$

$$A \frac{d}{dt} [\frac{1}{\bar{V}_i} (X_{i+1} - X_i)] \qquad (2.2)$$

where

$\cdot$ = indicated derivative with respect to time

$-$ = indicates average quantity in the node

WS = water/steam flow rate (lb/sec)

V = specific volume (ft^3/lb)

$\bar{V}$ = average specific volume in the node (ft^3/lb)

A = water/steam flow cross section (ft^2)

X = location along the flow path (ft)

i = 1, 2, 3. Note that the X_1 and X_4 are fixed, so that $\dot{X}_1 = \dot{X}_4 = 0$.

Rewriting Equation (2.2)

$$WS_i - WS_{i+1} = A \frac{d}{dt}[\frac{1}{\bar{V}_i} (X_{i+1} - X_i)] + \frac{1}{V_i} A \dot{X}_i - \frac{1}{V_{i+1}} A \dot{X}_{i+1} \qquad (2.3)$$

Conservation of Energy. The basic relationship is:

Energy flow in - Energy flow out - Rate of energy transferred out = rate of energy stored.

a. Gas side

$$(WG_{i+1}\ HG_{i+1} + A_g\ \rho_{i+1}\ HG_{i+1}\ \dot{X}_{i+1}) - (WG_i\ HG_i + A_g\ \rho_i\ HG_i\ \dot{X}_i) - Q_{gm} = A_g\ C_v\ \frac{d}{dt}[\bar{\rho}_i\ \overline{TG}_i(X_{i+1} - X_i)] \qquad (2.4)$$

where

HG = enthalpy of gas (Btu/lb)

ρ_i = gas density (lb/ft^3)

Q_{gm} = heat transfer rate from gas to metal (Btu/sec)

C_v = constant volume specific heat for the gas (Btu/lb°F)

TG = gas temperature (°F).

We assume that the helium is an ideal gas under the conditions that exist in the steam generator. Then

$$HG = C_p(TG + 459.6) \qquad (2.5)$$

where

C_p = constant pressure specific heat for the gas (Btu/lb°F).

The gas density can also be related to the gas pressure and gas temperature by the perfect gas law as follows:

$$\rho_i = PG_i\ 0.373343/(TG_i + 459.6)\ (i = 1, 2, 3, 4). \qquad (2.6)$$

Equation (2.4) can be rearranged to yield

$$WG_{i+1}\ HG_{i+1} - WG_i\ HG_i - Q_{gm} = A_g\ C_v\ \frac{d}{dt}[\bar{\rho}_i\ \overline{TG}_i\ (x_{i+1} - x_i)]$$

$$- A_g\ \rho_{i+1}\ HG_{i+1}\ \dot{x}_{i+1} + A_g\ \rho_i\ HG_i\ \dot{X}_i. \qquad (2.7)$$

b. Metal tube

The basic relationship is:

Heat flow in - Heat flow out = rate of heat stored in the metal.

$$Q_{gm} - TM_i\ M\ C_{Pm}\ \dot{X}_i - Q_{ms} + TM_{i+1}\ M\ C_{Pm}\ \dot{X}_{i+1} =$$

$$M\ C_{Pm}\ \frac{d}{dt}[\overline{TM}_i\ (X_{i+1} - X_i)] \qquad (2.8)$$

where

$\overline{TM}$ = average metal temperature for the node (°F)

C_{Pm} = metal heat capacity (Btu/lb-°F)

Q_{ms} = heat transfer rate from metal to steam (Btu/lb)

M = metal mass per unit length (lb/ft).

We assume the metal boundary temperature to be given by the arithmetic average of adjacent node temperatures

$$TM_i = \frac{1}{2}\ (\overline{TM}_{i-1} + \overline{TM}_i) \text{ for } i = 2, 3. \qquad (2.9)$$

Substitute Equation (2.9) into (2.8) and rearrange to yield

$$Q_{gm} - Q_{ms} = M\ C_{Pm}\ [(X_{i+1} - X_i)\ \dot{\overline{TM}}_i + \frac{1}{2}\ (\overline{TM}_i - \overline{TM_{i+1}})\cdot$$

$$\dot{X}_{i+1} - \frac{1}{2}\ (\overline{TM}_i - \overline{TM}_{i-1})\ \dot{X}_i]. \qquad (2.10)$$

The heat transfer rates are evaluated as follows:

$$Q_{gm} = [\text{Heat transfer area} \cdot (\overline{TG}_i - \overline{TM}_i)]/[K_{gi} (\overline{WG}_i)^{-C_{gi}} + R_i \cdot 0.5] \quad (2.11)$$

$$Q_{ms} = [\text{Heat transfer area} \cdot (\overline{TM}_i - \overline{TS}_i)]/[K_{si} (\overline{WS}_i)^{-C_{si}} + R_i \cdot 0.5] \quad (2.12)$$

where

K_g = constant for gas to metal heat transfer

C_g = flow exponent for gas to metal heat transfer

K_s = constant for metal to water heat transfer

C_s = flow exponent for metal to water heat transfer

R = thermal resistivity of the metal times the tube thickness

TS = water/steam temperature.

c. Water/steam

$$(WS_i\ HS_i - \frac{1}{V_i} HS_i\ A\ \dot{X}_i) - (WS_{i+1}\ HS_{i+1} - \frac{1}{V_{i+1}}\ HS_{i+1}$$

$$A\ \dot{X}_{i+1}) + Q_{ms} = A \frac{d}{dt}[\frac{1}{V_i} \bar{u}_i\ (X_{i+1} - X_i)] \quad (2.13)$$

where

HS = enthalpy of water/steam (Btu/lb)

u = internal energy of water/steam (Btu/lb).

Rearranging Equation (13) yields:

$$WS_i\ HS_i - WS_{i+1}\ HS_{i+1} + Q_{ms} = A \frac{d}{dt}[\frac{1}{V_i} \bar{u}_i\ (X_{i+1} - X_i)]$$

$$+ A\ [\frac{1}{V_i} HS_i\ \dot{X}_i - \frac{1}{V_{i+1}} HS_{i+1}\ \dot{X}_{i+1}]. \quad (2.14)$$

Conservation of Momentum. Since it is assumed the flow on the gas side of the steam generator is time dependent only, there is no need for a momentum equation in that region.

In the water/steam, the basic principle is:

$$\sum \text{forces} = \text{Rate of change of momentum}$$

$$P_i - P_{i+1} - K_f \overline{WS}_i^2 - \left(\frac{1}{144 \cdot \bar{V}_i}\right) \text{PITCH} \, (X_{i+1} - X_i)$$

$$= \left(\frac{1}{144 \cdot g \cdot A}\right) \frac{d}{dt} \left[\overline{WS}_i \, (X_{i+1} - X_i)\right] \qquad (2.15)$$

where

K_f = friction drop coefficient (PSIA/(lbm/sec)^2)

g = gravitational constant (ft/sec^2)

PITCH = height increase per unit length of tube.

In Equation (2.15) the first two terms are the pressure force. The third term is the friction loss. The fourth term is pressure change due to changes in elevation. Due to the coiled nature of the steam generator, the PITCH $\approx$ 0.05, so we can cancel the fourth term. The coefficient $\left(\frac{1}{144 \cdot g \cdot A}\right)$ of the differential term in the momentum equation is quite small. Furthermore, the sign of $\dot{X}_i$ and $\dot{X}_{i+1}$ are the same all the time. So, it can be cancelled without introducing significant error in the model. After cancelling these terms in Equation (2.15), we have the general form of the flow pressure drop relation:

$$\overline{WS}_i = \sqrt{(P_i - P_{i+1})/K_i}$$

where K_i is a head loss coefficient. The algebraic relationships are

$$WS_1 = \sqrt{(\bar{P}_0 - \bar{P}_1)/K_1} \tag{2.16}$$

$$WS_2 = \sqrt{(\bar{P}_1 - \bar{P}_2)/K_2} \tag{2.17}$$

$$WS_3 = \sqrt{(\bar{P}_2 - \bar{P}_3)/K_3} \tag{2.18}$$

$$WS_4 = \sqrt{(\bar{P}_3 - \bar{P}_4)/K_4} \tag{2.19}$$

The Weighting Factor. The equations which were derived in the above include both the average quantities and end point quantities for the nodes. Additional relationships will be necessary in order to have as many equations as unknowns.

For each node, a weighting factor is defined and the average value for any quantity, $\bar{Y}$, is calculated as follows:

$$\bar{Y}_i = Y_i F_i + Y_{i+1} (1 - F_i) F_i \leq 1.$$

Note that if F equals 0.5, $\bar{Y}$ is the linear average. This averaging method is used to calculate $\overline{TG}$, $\overline{TM}$, $\overline{WS}$, $\overline{P}$, and $\overline{HS}$. The average quantities $\overline{U}$, $\overline{V}$, and $\overline{TS}$ are then calculated from steam tables using $\overline{P}$ and $\overline{HS}$ as the independent variables.

This concludes the derivation of the lumped nodes equations for a once-through steam generator. Before further development, the assumptions behind the derivation are summarized as follows:

1. Gas flow rate is a function only of time.
2. The enthalpy at X_2 and X_3 are functions of pressure with fixed quality.

3. No heat conduction in the flow direction.
4. Balanced flow and uniform heat flux exists at any node.
5. In the economizer, the flow in equals flow out.
6. The average water/steam flow rate used in the equation is assumed to be a linear average of the flow in and out of each node.
7. The water/steam flow rate is proportional to the square root of pressure difference.

2.4 Summary of Equations

Now for the purpose of review, the following equations are a summary of those that must be solved for each node of a moving boundary heat exchanger.

The twelve differential equations are:

$$WS_i - WS_{i+1} = A \left\{\frac{d}{dt}\left[\frac{1}{\bar{V}_i}(X_{i+1} - X_i) - \frac{1}{V_{i+1}}\dot{X}_{i+1} + \frac{1}{V_i}\dot{X}_i\right\}\right. \quad (i = 1, 2, 3). \tag{2.20}$$

Note that $\dot{X}_1 = \dot{X}_4 = 0$

$$WG_{i+1}\, HG_{i+1} - WG_i\, HG_i - Q_{gm} = A_g\, C_v \frac{d}{dt}\cdot$$

$$[\bar{\rho}_i\, \overline{TG}_i\, (X_{i+1} - X_i)] - A_g\, \rho_{i+1}\, HG_{i+1}\, \dot{X}_{i+1} + A_g\, \rho_i\, HG_i\, \dot{X}_i \quad (i = 1, 2, 3) \tag{2.21}$$

$$Q_{gm} - Q_{ms} = M \cdot C_{Pm} [(X_{i+1} - X_i) \dot{\overline{TM}}_i$$

$$+ \frac{1}{2} (\overline{TM}_i - \overline{TM}_{i+1}) \dot{X}_{i+1} - \frac{1}{2} (\overline{TM}_i - \overline{TM}_{i-1}) \dot{X}_i]$$

$$(i = 1, 2, 3) \qquad (2.22)$$

$$WS_i \cdot HS_i - WS_{i+1} HS_{i+1} + Q_{ms} = A \cdot \frac{d}{dt} [\frac{1}{\bar{V}_i} \bar{u}_i \cdot$$

$$(X_{i+1} - X_i)] + A \cdot [\frac{1}{V_i} HS_i \dot{X}_i - \frac{1}{V_{i+1}} HS_{i+1} \dot{X}_{i+1}]$$

$$(i = 1, 2, 3) \qquad (2.23)$$

where HS_2 and HS_3 are functions of pressure with fixed quality only.

The six algebraic equations are

$$WG_i = WG_{in} \qquad (i = 1, 2, 3) \qquad (2.24)$$

$$WS_i = \sqrt{(\bar{P}_{i-1} - \bar{P}_i)/K_i} \qquad (i = 2, 3, 4). \qquad (2.25)$$

The eighteen unknowns for the model are:

1. Three average gas temperature ($\overline{TG}_1$, $\overline{TG}_2$, $\overline{TG}_3$) described by differential Equation (2.21).
2. Three metal temperature ($\overline{TM}_1$, $\overline{TM}_2$, $\overline{TM}_3$) described by differential Equation (2.22).
3. Three water/steam flow ($\overline{P}_1$, $\overline{P}_2$, $\overline{P}_3$) described by differential Equation (2.20).

4. Two locations (X_2, X_3) and one enthalpy (HS_4) described by differential Equation (2.23).
5. Three gas flows (WG_1, WG_2, WG_3) described by algebraic Equation (2.24).
6. Three water/steam flow (WS_2, WS_3, WS_4) described by algebraic Equation (2.25).

The assumed knowns, or inputs to the problem are:

1. Inlet water pressure (P_1).
2. Inlet water flow and enthalpy (WS_1, HS_1).
3. Fixed locations (X_1, X_4).
4. Inlet gas temperature and flow (TG_4, WG_{in}).

2.5 Linearization of Equations

The previously derived equations are linearized in the following sections.

Equation (2.20) Linearization

Equation (2.20) is repeated as follows:

$$WS_i - WS_{i+1} = A \left\{\frac{d}{dt}\left[\frac{1}{\bar{V}_i}(X_{i+1} - X_i) - \frac{1}{V_{i+1}}\dot{X}_{i+1} + \frac{1}{V_i}\dot{X}_i\right\}\right. . \qquad (2.20)$$

We assume $\bar{V}_i$ is a function of $\overline{HS}_i$ and $\bar{P}_i$. The average quantities $\overline{HS}_i$ and $\bar{P}_i$ are obtained by weighting the end point values for each node as follows:

$$\overline{HS}_i = W_i\, HS_i + (1 - W_i)\, HS_{i+1} \qquad (2.26)$$

$$\bar{P}_i = W_i P_i + (1 - W_i) \cdot P_{i+1} \qquad (i = 1, 2, 3) \tag{2.27}$$

where

$W_1 = 0.75$, $W_2 = 0.67$, and $W_3 = 0.30$ (weighting factors for water/steam side).

The linearized form of Equation (2.20) is

$$\delta WS_i - \delta WS_{i+1} = A_{1,i}\, \delta \dot{X}_{i+1} + A_{2,i}\, \delta \dot{HS}_i + A_{3,i}\, \delta \dot{HS}_{i+1}$$

$$+ (A_{4,i} + A_{5,i})\, \delta \dot{\bar{P}}_i + A_{6,i}\, \delta \dot{X}_i$$

where

$$A_{1,i} = A \left(\frac{1}{\bar{V}_i} - \frac{1}{V_{i+1}}\right).$$

(Note: All the values for each variable in the coefficients represent the steady state in the systems.)

$$L_i = X_{i+1} - X_i$$

$$A_{2,i} = - A \cdot L_i \left(\frac{\partial \bar{V}_i}{\partial HS_i}\right)_{P_i} / \bar{V}_i^{\,2} \qquad i = 1$$

$$= 0 \qquad i = 2, 3$$

($\bar{V}$ is only a function of pressure when i = 2, 3).

$$A_{3,i} = - A\, L_i \left(\frac{\partial \bar{V}_i}{\partial HS_{i+1}}\right)_{P_{i+1}} / \bar{V}_i^{\,2} \qquad i = 3$$

$$= 0 \qquad i = 1, 2$$

$$A_{4,i} = - A\, L_i \left(\frac{\partial \bar{V}_i}{\partial P_i}\right)_{HS_i} / \bar{V}_i^{\,2}$$

$$A_{5,i} = - A L_i \left(\frac{\partial \bar{V}_i}{\partial P_{i+1}}\right)_{HS_{i+1}} / \bar{V}_i^2$$

$$A_{6,i} = - A \left(\frac{1}{\bar{V}_i} - \frac{1}{V_i}\right)$$

δHS_i can be related to the temperature TS_i as follows:

$$\delta HS_i = \left(\frac{\partial HS_i}{\partial P_i}\right)_{TS_i} \delta P_i + \left(\frac{\partial HS_i}{\partial TS_i}\right)_{P_i} \delta TS_i.$$

Since enthalpy is almost independent of pressure for subcooled water, i.e.,

$$\left(\frac{\partial HS_1}{\delta P_1}\right)_{TS_1} \simeq 0.$$

For $i = 1$, we have

$$\delta HS_1 = \left(\frac{\partial HS_1}{\partial TS_1}\right)_{P_1} \delta TS_1.$$

The final form of the linearized Equation (2.20) is:

for $i = 1$,

$$\delta WS_1 - \delta WS_2 = A_{1,1}\delta \dot{X}_2 + A_{2,1} \left(\frac{\partial HS_1}{\partial TS_1}\right)_{P_1} \delta \dot{T}S_1 + (A_{4,1} + A_{5,1}) \delta \dot{\bar{P}}_1 \qquad (2.28)$$

$i = 2$,

$$\delta WS_2 - \delta WS_3 = A_{6,2}\delta \dot{X}_2 + (A_{4,2} + A_{5,2}) \delta \dot{\bar{P}}_2 + A_{1,2}\delta \dot{X}_3. \qquad (2.29)$$

For i = 3, the term HS_4 can be related to the main steam temperature (TS_4) and pressure ($\bar{P}_3$) as follows:

$$\delta HS_4 = \left(\frac{\partial HS_4}{\delta \bar{P}_3}\right)_{TS_4} \delta \bar{P}_3 + \left(\frac{\partial HS_4}{\partial \overline{TS_4}}\right)_{\bar{P}_3} \delta TS_4$$

$$\tilde{=} (1 - W_3) \left(\frac{\partial HS_4}{\partial P_4}\right)_{TS_4} \delta \bar{P}_3 + \left(\frac{\partial HS_4}{\partial \overline{TS_4}}\right)_{P_4} \delta TS_4.$$

After δHS_4 is replaced by $\delta \bar{P}_3$ and δTS_4, we have

$$\delta WS_3 - \delta WS_4 = A_{3,3} \left(\frac{\partial HS_4}{\partial \overline{TS_4}}\right)_{P_4} \dot{\delta TS_4} + G_1 \dot{\delta \bar{P}_3}$$

$$+ A_{6,3} \dot{\delta X}_3 \qquad (2.30)$$

where

$$G_1 = (A_{4,3} + A_{5,3}) + A_{3,3} (1 - W_3) \left(\frac{\partial HS_4}{\partial P_4}\right)_{TS_4}.$$

Equation (2.21) Linearization

Equation (2.21) is repeated as follows:

$$WG_{i+1} HG_{i+1} - WG_i HG_i - Q_{gm} = A_g C_v \frac{d}{dt} [\bar{\rho}_i \overline{TG}_i (X_{i+1} - X_i)]$$

$$- A_g \rho_{i+1} HG_{i+1} \dot{X}_{i+1} + A_g \rho_i HG_i \dot{X}_i \quad (i = 1, 2, 3). \qquad (2.21)$$

We assume HG is a function of TG only and we have

$$HG_i = C_{pg} (TG_i + 459.6)$$

$$\overline{TG}_i = TG_i F_i + TG_{i+1} (1 - F_i)$$

$$\overline{WG}_i = WG_i F_i + WG_{i+1} (1 - F_i) \qquad (i = 1, 2, 3) \qquad (2.31)$$

where

$F_1 = 0.75$, $F_2 = 0.67$, and $F_3 = 0.30$ (weighting factors for the helium side).

The linearized form of Equation (2.21) is as follows

$$B_{1,i}\, \delta WG_{i+1} + B_{2,i}\, \delta WG_i + B_{3,i}\, \delta TG_{i+1} + C_{4,i}\, \delta \overline{TG}_i$$

$$+ B_{4,i}\, \delta TG_i + B_{5,i}\, \delta X_{i+1} + B_{6,i}\, \delta X_i + B_{7,i}\, \delta \overline{TM}_i =$$

$$A_{7,i}\, \delta \dot{X}_{i+1} + A_{8,i}\, \delta \dot{X}_i + A_{9,i}\, \delta \dot{\overline{TG}}_i$$

where

$$E_{1,i} = \pi \cdot OD \cdot L_i (\overline{TG}_i - \overline{TM}_i) \cdot K_{gi} \cdot C_{gi}\, WG^{-(C_{gi} + 1)} /$$

$$(K_{gi}\, WG^{-C_{gi}} + 0.5 R_i)^2$$

$$E_{2,i} = \pi \cdot OD\, (K_{gi} \cdot WG^{-C_{gi}} + 0.5\, R_i)^{-1}$$

$$B_{1,i} = HG_{i+1} - E_{1,i} (1 - F_i)$$

$$B_{2,i} = - HG_i - E_{1,i} F_i$$

$$B_{3,i} = WG_{i+1}\, C_{pg}$$

$$C_{4,i} = - E_{2,i}\, L_i$$

$$B_{4,i} = - WG_i\, C_{pg}$$

$$B_{5,i} = - E_{2,i} (\overline{TG}_i - \overline{TM}_i)$$

$$B_{6,i} = - B_{5,i}$$

$$B_{7,i} = E_{2,i} L_i$$

$$A_{7,i} = A_g (C_{vg} \cdot \bar{\rho}_i \cdot \overline{TG}_i - \rho_{i+1} \cdot HG_{i+1})$$

$$A_{8,i} = - A_g (C_{vg} \cdot \bar{\rho}_i \cdot \overline{TG}_i - \rho_i \cdot HG_i)$$

$$A_{9,i} = A_g C_{vg} L_i \bar{\rho}_i .$$

For i = 1

$$B_{1,1} \delta WG_2 + B_{2,1} \delta WG_1 + B_{3,1} \delta TG_2 + C_{4,1} \delta\overline{TG}_1 + B_{4,1} \delta TG_1 + B_{5,1} \delta X_2 + B_{7,1} \delta\overline{TM}_1 = A_{7,1} \delta\dot{X}_2 + A_{9,1} \dot{\delta\overline{TG}}_1 \quad (2.32)$$

i = 2

$$B_{1,2} \delta WG_3 + B_{2,2} \delta WG_2 + B_{3,2} \delta TG_3 + C_{4,2} \delta\overline{TG}_2 + B_{4,2} \delta TG_2 + B_{5,2} \delta X_3 + B_{6,2} \delta X_2 + B_{7,2} \delta\overline{TM}_2 = A_{7,2} \delta\dot{X}_3 + A_{8,2} \delta\dot{X}_2 + A_{9,2} \dot{\delta\overline{TG}}_2 \quad (2.33)$$

i = 3

$$B_{1,3} \delta WG_4 + B_{2,3} \delta WG_3 + B_{3,3} \delta TG_4 + C_{4,3} \delta\overline{TG}_3 + B_{4,3} \delta TG_3 + B_{6,3} \delta X_3 + B_{7,3} \delta\overline{TM}_3 = A_{8,3} \delta\dot{X}_3 + A_{9,3} \dot{\delta\overline{TG}}_3 \quad (2.34)$$

Note that either the variable $\delta\overline{TG}$ or the variable δTG can be eliminated by using Equation (2.31). In order to make changes of the weight factor (F_i) in the system dynamic response study convenient, we keep both variables in the equation.

Equation (2.22) Linearization

Equation (2.22) is repeated as follows:

$$Q_{gm} - Q_{ms} = M\, C_{pm} \left[(X_{i+1} - X_i)\, \dot{\overline{TM}}_i + \frac{1}{2}\,(\overline{TM}_i - \overline{TM}_{i+1})\cdot \dot{X}_{i+1} - \frac{1}{2}\,(\overline{TM}_i - \overline{TM}_{i-1})\cdot \dot{X}_i\right] \quad (i = 1, 2, 3). \tag{2.22}$$

We assume the term $\overline{TS}_i$ in Q_{ms} is a function of $\bar{P}_i$ and $\overline{HS}_i$. And, let

$$\bar{P}_i = W_i\, P_i + (1 - W_i)\, P_{i+1}$$

$$\overline{HS}_i = W_i\, HS_i + (1 - W_i)\, HS_{i+1}.$$

The values of weighting factors, W_i, are shown in Equation (2.27). The linearized form of Equation (2.22) is as follows:

$$B_{8,i}\,\delta X_{i+1} - B_{8,i}\,\delta X_i + B_{9,i}\,\delta\overline{TM}_i + B_{10,i}\,\delta\overline{TG}_i + B_{12,i}\,\delta WG_{i+1} + B_{13,i}\,\delta WG_i + (B_{14,i} + B_{15,i})\,\delta\bar{P}_i + B_{16,i}\,\delta HS_i + B_{17,i}\,\delta HS_{i+1} + B_{18,i}\,\delta WS_i + B_{19,i}\,\delta WS_{i+1} = A_{11,i}\,\delta\dot{\overline{TM}}_i + A_{12,i}\,\delta\dot{X}_{i+1} + A_{13,i}\,\delta\dot{X}_i$$

where

$$E_{4,i} = \pi \cdot OD \left(KS_i \, WS^{-CS_i} + 0.5 \, R_i\right)^{-1}$$

$$E_{5,i} = \pi \cdot OD \, L_i \, KS_i \, CS_i \, WS^{-(CS_i + 1)} \left(\overline{TM}_i - \overline{TS}_i\right) \cdot$$

$$\left(KS_i \, WS^{-CS_i} + 0.5 \, R_i\right)^{-2}$$

$$B_{8,i} = E_{2,i} \left(\overline{TG}_i - \overline{TM}_i\right) - E_{4,i} \left(\overline{TM}_i - \overline{TS}_i\right) = 0.$$

(For at the steady state, the heat transferred in equals the heat transferred out.)

$$B_{9,i} = - E_{2,i} \, L_i - E_{4,i} \, L_i$$

$$B_{10,i} = E_{2,i} \, L_i$$

$$B_{12,i} = E_{1,i} \left(1 - F_i\right)$$

$$B_{13,i} = E_{1,i} \, F_i$$

$$B_{14,i} = E_{4,i} \left(\frac{\partial \overline{TS}_i}{\partial P_i}\right)_{HS_i} L_i$$

$$B_{15,i} = E_{4,i} \left(\frac{\partial \overline{TS}_i}{\partial P_{i+1}}\right)_{HS_{i+1}} L_i$$

$$B_{16,i} = E_{4,i} \left(\frac{\partial \overline{TS}_i}{\partial HS_i}\right)_{P_i} L_i \qquad i = 1$$

$$= 0 \qquad\qquad i = 2, 3$$

(For $i = 2, 3$, TS_i is function of P_i only with fixed quality.)

$$B_{17,i} = E_{4,i} \left(\frac{\partial \overline{TS}_i}{\partial HS_{i+1}}\right)_{P_{i+1}} L_i \qquad i = 3$$

$$= 0 \qquad i = 1, 2$$

$$B_{18,i} = - E_{5,i} W_i$$

$$B_{19,i} = - E_{5,i} (1 - W_i)$$

$$A_{11,i} = M C_{pm} L_i$$

$$A_{12,i} = \frac{1}{2} M C_{pm} (\overline{TM}_i - \overline{TM}_{i+1})$$

$$A_{13,i} = - \frac{1}{2} M C_{pm} (\overline{TM}_i - \overline{TM}_{i-1}).$$

The final linearized equations for each node are:

For i = 1

$$B_{9,1}\ \delta\overline{TM}_1 + B_{10,1}\ \delta\overline{TG}_1 + B_{12,1}\ \delta WG_2 + B_{13,1}\ \delta WG_1$$

$$+ (B_{14,1} + B_{15,1})\ \delta\bar{P}_1 + B_{16,1} \left(\frac{\partial HS_1}{\partial TS_1}\right)_{P_1} \delta TS_1 + B_{18,1}\ \delta WS_1$$

$$+ B_{19,1}\ \delta WS_2 = A_{11,1}\ \dot{\delta\overline{TM}}_1 + A_{12,1}\ \delta\dot{X}_2 \qquad (2.35)$$

i = 2

$$B_{9,2}\ \delta\overline{TM}_2 + B_{10,2}\ \delta\overline{TG}_2 + B_{12,2}\ \delta WG_3 + B_{13,2}\ \delta WG_2$$

$$+ (B_{14,2} + B_{15,2})\ \delta\bar{P}_2 + B_{18,2}\ \delta WS_2 + B_{19,2}\ \delta WS_3$$

$$= A_{11,2}\ \dot{\delta\overline{TM}}_2 + A_{12,2}\ \delta\dot{X}_3 + A_{13,2}\ \delta\dot{X}_2 \qquad (2.36)$$

$i = 3$

$$B_{9,3}\,\delta TM_3 + B_{10,3}\,\delta\overline{TG}_3 + B_{12,3}\,\delta WG_4 + B_{13,3}\,\delta WG_3$$

$$+ G_2\,\delta\bar{P}_3 + B_{17,3}\cdot\left(\frac{\partial HS_4}{\partial TS_4}\right)_{P_4}\cdot\delta TS_4 + B_{18,3}\,\delta WS_3 + B_{19,3}\,\delta WS_4$$

$$= A_{11,3}\,\delta\dot{\overline{TM}}_3 + A_{13,3}\,\delta\dot{X}_3 \qquad (2.37)$$

where

$$G_2 = \left[B_{14,3} + B_{15,3} + B_{17,3}\,(1 - W_3)\left(\frac{\partial HS_4}{\partial P_4}\right)_{TS_4}\right].$$

Equation (2.23) Linearization

Equation (2.23) is repeated as follows:

$$WS_i\,HS_i - WS_{i+1}\,HS_{i+1} + Q_{ms} = A\,\frac{d}{dt}\left[\frac{1}{\bar{V}_i}\,\bar{U}_i\cdot\right.$$

$$\left.(X_{i+1} - X_i)\right] + A\left[\frac{1}{\bar{V}_i}\,HS_i\,\dot{X}_i - \frac{1}{V_{i+1}}\,HS_{i+1}\,\dot{X}_{i+1}\right]$$

$$(i = 1, 2, 3). \qquad (2.23)$$

Assume the $\bar{U}_i$ and $\bar{V}_i$ are functions of $\bar{P}_i$ and $\overline{HS}_i$.

Let

$$\delta HS_i = \left(\frac{\partial HS_i}{\partial P_i}\right)_{\text{quality}}\delta P_i \qquad (i = 2, 3).$$

Note: It is 0% quality at boundary 2 and 100% quality at boundary 3. The linearized form of Equation (2.23) is as follows:

$$B_{20,i}\,\delta HS_i + B_{21,i}\,\delta WS_i + B_{22,i}\,\delta HS_{i+1} + B_{23,i}\,\delta WS_{i+1}$$

$$- B_{24,i}\,\delta X_{i+1} + B_{24,i}\,\delta X_i - B_{25,i}\,\delta\overline{TM}_i + B_{26,i}\,\delta\bar{P}_i$$

$$+ B_{27,i}\ \delta\bar{P}_{i+1} + B_{28,i}\ \delta\bar{P}_{i-1} = A_{14,i}\ \delta\dot{HS}_i + A_{16,i}\ \delta\dot{HS}_{i+1}$$

$$+ (A_{15,i} + A_{17,i})\ \delta\dot{\bar{P}}_i + A_{18,i}\ \delta\dot{X}_{i+1} + A_{19,i}\ \delta\dot{X}_i$$

where

$$B_{20,i} = WS_i - E_{4,i}\left(\frac{\partial\overline{TS}_i}{\partial HS_i}\right) L_i \qquad i = 1$$

$$= 0 \qquad i = 2, 3$$

$$B_{21,i} = HS_i + W_i\ E_{5,i}$$

$$B_{22,i} = - WS_{i+1} - E_{4,i}\left(\frac{\partial TS_i}{\partial HS_{i+1}}\right) L_i \qquad i = 3$$

$$= 0 \qquad i = 1, 2$$

$$B_{23,i} = - HS_{i+1} + (1 - W_i)\ E_{5,i}$$

$$B_{24,i} = - E_{4,i}\ (\overline{TM}_i - \overline{TS}_i)$$

$$B_{25,i} = - E_{4,i}\ L_i$$

$$D_i = - E_{4,i}\ L_i\left[\left(\frac{\partial\overline{TS}_i}{\partial P_i}\right)_{HS_i} + \left(\frac{\partial\overline{TS}_i}{\partial P_{i+1}}\right)_{HS_{i+1}}\right]$$

In $B_{26,i}$, $B_{27,i}$, and $B_{28,i}$, we let

$$\delta P_i = \frac{1}{2}\left(\delta\bar{P}_{i-1} + \delta\bar{P}_i\right)$$

for i = 1

$$B_{26,1} = D_1 - \frac{1}{2} WS \left(\frac{\partial HS_2}{\partial P_2}\right)_{quality}$$

$$B_{27,1} = -\frac{1}{2} WS \left(\frac{\partial HS_2}{\partial P_2}\right)_{quality} \quad \text{and } B_{28,1} = 0$$

i = 2

$$B_{26,2} = D_2 - \frac{1}{2} WS \left[\left(\frac{\partial HS_3}{\partial P_3}\right)_{quality} - \left(\frac{\partial HS_2}{\partial P_2}\right)_{quality}\right]$$

$$B_{27,2} = -\frac{1}{2} WS \left(\frac{\partial HS_3}{\partial P_3}\right)_{quality}$$

$$B_{28,2} = \frac{1}{2} WS \left(\frac{\partial HS_2}{\partial P_2}\right)_{quality}$$

i = 3

$$B_{26,3} = D_3 + \frac{1}{2} WS \left(\frac{\partial HS_3}{\partial P_3}\right)_{quality}$$

$$B_{27,3} = 0$$

$$B_{28,3} = \frac{1}{2} WS \left(\frac{\partial HS_3}{\partial P_3}\right)_{quality}$$

$$A_{14,i} = A L_i \bar{V}_i^{-2} \left[\bar{V}_i \left(\frac{\partial \bar{U}_i}{\partial HS_i}\right)_{P_i} - \bar{U}_i \left(\frac{\partial \bar{V}_i}{\partial HS_i}\right)_{P_i}\right] \quad i = 1$$

$$= 0 \qquad i = 2, 3$$

$$A_{15,i} = A L_i \bar{V}_i^{-2} \left[\bar{V}_i \left(\frac{\partial \bar{U}_i}{\partial P_i}\right)_{HS_i} - \bar{U}_i \left(\frac{\partial \bar{V}_i}{\partial P_i}\right)_{HS_i}\right]$$

$$A_{17,i} = A L_i \bar{V}_i^{2} \left[\bar{V}_i \left(\frac{\partial \bar{U}_i}{\partial P_{i+1}}\right)_{HS_{i+1}} - \bar{U}_i \left(\frac{\partial \bar{V}_i}{\partial P_{i+1}}\right)_{HS_{i+1}}\right]$$

$$A_{16,i} = A\, L_i\, \bar{V}_i^2 \left[\bar{V}_i \left(\frac{\partial \bar{U}_i}{\partial HS_{i+1}}\right)_{P_{i+1}} - \bar{U}_i \left(\frac{\partial \bar{V}_i}{\partial HS_{i+1}}\right)_{P_{i+1}}\right] \quad i = 3$$

$$= 0 \qquad i = 1, 2$$

$$A_{18,i} = A \left[\frac{\bar{U}_i}{\bar{V}_i} - \frac{HS_{i+1}}{V_{i+1}}\right]$$

$$A_{19,i} = -A \left[\frac{\bar{U}_i}{\bar{V}_i} - \frac{HS_i}{V_i}\right]$$

The linearized equations for each node are:

for $i = 1$

$$B_{20,1} \left(\frac{\partial HS_1}{\partial \overline{TS}_1}\right)_{P_1} \delta TS_1 + B_{21,1}\, \delta WS_1 + B_{23,1}\, \delta WS_2$$

$$- B_{24,1}\, \delta X_2 - B_{25,1}\, \delta \overline{TM}_1 + B_{26,1}\, \delta \bar{P}_1 + B_{27,1}\, \delta \bar{P}_2$$

$$= A_{14,1} \left(\frac{\partial HS_1}{\partial \overline{TS}_1}\right)_{P_1} \delta \dot{TS}_1 + (A_{15,1} + A_{17,1})\, \delta \dot{\bar{P}}_1 + A_{18,1}\, \delta \dot{X}_2 \qquad (2.37)$$

$i = 2$

$$B_{21,2}\, \delta WS_2 + B_{23,2}\, \delta WS_3 - B_{24,2}\, \delta X_3 + B_{24,2}\, \delta X_2$$

$$- B_{25.2}\, \delta \overline{TM}_2 + B_{26,2}\, \delta \bar{P}_2 + B_{27,2}\, \delta \bar{P}_3 + B_{28,2}\, \delta \bar{P}_1$$

$$= (A_{15,2} + A_{17,2})\, \delta \dot{\bar{P}}_2 + A_{18,2}\, \delta \dot{X}_3 + A_{19,2}\, \delta \dot{X}_2 \qquad (2.38)$$

i = 3

$$B_{21,3}\ \delta WS_3 + B_{22,3}\ \left(\frac{\partial HS_4}{\partial TS_4}\right)_{P_4}\ \delta TS_4 + B_{23,3}\ \delta WS_4 + B_{24,3}\ \delta X_3$$

$$- B_{25,3}\ \delta\overline{TM}_3 + G_3\ \delta\bar{P}_3 + B_{28,3}\ \delta\bar{P}_2$$

$$= G_4\ \delta\dot{\bar{P}}_3 + A_{16,3}\ \left(\frac{\partial HS_4}{\partial TS_4}\right)_{P_4}\ \delta\dot{TS}_4 + A_{19,3}\ \delta\dot{X}_3 \qquad (2.39)$$

where

$$G_3 = B_{26,3} + (1 - W_3)\ B_{22,3}\ \left(\frac{\partial HS_4}{\partial P_4}\right)_{TS_4}$$

$$G_4 = A_{15,3} + A_{17,3} + (1 - W_3)\ A_{16,3}\ \left(\frac{\partial HS_4}{\partial P_4}\right)_{TS_4}. \qquad (2.40)$$

The nine linearized algebraic equations are

$$\delta WG_i = \delta WG_{in} \qquad (i = 1, 2, 3) \qquad (2.41)$$

$$\delta\overline{TG}_i = F_i\ \delta TG_i + (1 - F_i)\ \delta TG_{i+1} \qquad (i = 1, 2, 3) \qquad (2.42)$$

$$\delta WS_2 = KK_2\ (\delta\bar{P}_1 - \delta\bar{P}_2) \qquad (2.43)$$

where

$$KK_2 = \frac{WS}{2(\bar{P}_1 - \bar{P}_2)}$$

$$\delta WS_3 = KK_3\ (\delta\bar{P}_2 - \delta\bar{P}_3) \qquad (2.44)$$

where

$$KK_3 = \frac{WS}{2(\bar{P}_2 - \bar{P}_3)}$$

$$\delta WS_4 = KK_4\ (\delta\bar{P}_3 - \delta\bar{P}_4) \qquad (2.45)$$

where

$$KK_4 = \frac{WS}{2(\bar{P}_3 - \bar{P}_4)} .$$

The linearized equations from (2.28) to (2.45) can then be arranged in a matrix form as Equation (2.1).

2.6 Results and Discussion

The linearized equations presented in the above section were used to calculate the frequency response and time response of the main steam generator (no reheater) for selected inputs. In obtaining these results, two different sets of equations were used. In the first set, the feedwater pressure, $\bar{P}_0$, (see Figure 3, page 13) is held constant; hence, the description "constant pressure model" (CPSG). In the second set, the variable WS_1 (feedwater flow) is held constant; hence, the description "constant flow model" (CFSG). The frequency response and time responses for the constant pressure and constant flow models were calculated for each input selected.

The code SFRMOD[9] was used to calculate the frequency response. The input to SFRMOD is of the form as Equation (2.1).

Before calculating the time response, it was necessary to transfer the system of algebraic and differential Equation (2.1) describing the steam generator to the following form

$$\frac{d\bar{X}_d}{dt} = A_d + \bar{f}_d \qquad (2.46)$$

where

$\bar{X}_d$ = vector of state variables

A_d = matrix of constant coefficients

$\bar{f}_d$ = forcing terms for the system input.

This was performed using the computer code PUREDIFF.[9] The input to PUREDIFF consists of the A and B matrices and $\bar{f}$ vector as in Equation (2.1). The state variables of $\bar{X}$ and $\bar{X}_d$ are listed in Tables 2.2 and 2.3. The elements of A, B, and A_d matrices appear in Tables 2.4, 2.5, and 2.6.

The time response calculations were performed using the computer code MATEXP.[10] The input to MATEXP consists of the A_d matrix and $\bar{f}_d$ vectors, as defined in Equation (2.46).

Results of the frequency response and time response calculation at 100 percent load point were calculated for the following inputs: helium flow, helium inlet temperature, and feedwater flow. The five runs were labeled in Table 2.7.

The selected outputs to be plotted for each run were: (a) main steam outlet temperature (TS4), (b) Helium outlet average temperature at node 1 (TG1B), and (c) main steam outlet average pressure at node 3 (P3B).

Discussion of Results for Run No. 1 (Figures 4 to 7)

Run No. 1 shows the CFSG model time response and frequency response for a 1 lb/sec increase in helium flow rate. Increased helium flow rate increases the heat transfer rate from the helium to the secondary coolant through the tube wall. For constant outlet steam header pressure and feedwater flow rate, the steam pressure

TABLE 2.2

THE VARIABLES ASSOCIATED WITH CPSG FOR A AND B MATRIX

Number	Variables
1, 2, 3	$\delta\bar{P}_1$, $\delta\bar{P}_2$, $\delta\bar{P}_3$
4, 5, 6, 7	δTG_1, δTG_2, δTG_3, δTG_4
8, 9, 10	$\delta\overline{TM}_1$, $\delta\overline{TM}_2$, $\delta\overline{TM}_3$
11, 12	δX_2, δX_3
13	δMST
14, 15, 16	$\delta\overline{TG}_1$, $\delta\overline{TG}_2$, $\delta\overline{TG}_3$
17, 18, 19, 20	δWS_1, δWS_2, δWS_3, δWS_4

TABLE 2.3

THE STATE VARIABLES ASSOCIATED WITH CPSG
FOR REDUCED A_d MATRIX

Number	State Variables
1, 2, 3, 4	$\delta\bar{P}_1$, $\delta\bar{P}_2$, $\delta\bar{P}_3$, δTG_4
5, 6, 7	$\delta\overline{TM}_1$, $\delta\overline{TM}_2$, $\delta\overline{TM}_3$
8, 9	δX_2, δX_3
10	δMST
11, 12, 13	$\delta\overline{TG}_1$, $\delta\overline{TG}_2$, $\delta\overline{TG}_3$

TABLE 2.4

ELEMENTS OF A MATRIX FOR CPSG

I	J	Value	I	J	Value
1	1	2.61100E-01	1	11	3.38100E 01
2	2	1.01500E 00	2	11	2.28600E 01
2	12	1.47400E 01	3	3	3.13900E-01
3	12	1.05200E 01	3	13	-5.05800E-01
7	7	1.00000E 00	8	8	7.41000E 03
8	11	-7.91700E 03	9	9	4.71100E 03
9	11	-7.91700E 03	9	12	-1.09600E 04
10	10	7.51100E 03	10	12	-1.09600E 04
11	1	4.14200E 02	11	11	-6.98900E 02
12	2	9.45500E 02	12	11	1.57900E 04
12	12	8.68800E 03	13	3	3.67400E 02
13	12	9.52200E 03	13	13	-4.25700E 02
14	11	-3.11100E 02	14	14	3.67500E 01
15	11	3.11100E 02	15	12	-3.11100E 02
15	15	1.97900E 01	16	12	3.11100E 02
16	16	2.59200E 01			

TABLE 2.5

ELEMENTS OF B MATRIX FOR CPSG

I	J	Value	I	J	Value
1	17	1.00000E 00	1	18	-1.00000E 00
2	18	1.00000E 00	2	19	-1.00000E 00
3	19	1.00000E 00	3	20	-1.00000E 00
4	4	7.50000E-01	4	5	2.50000E-01
4	14	-1.00000E 00	5	5	6.70000E-01
5	6	3.30000E-01	5	15	-1.00000E 00
6	6	3.00000E-01	6	7	7.00000E-01
6	16	-1.00000E 00	7	7	-2.00000E 00
8	1	8.77400E 01	8	8	-3.54900E 03
8	14	9.37200E 02	8	17	-8.58400E 01
8	18	-2.86100E 01	9	2	9.14300E 01
9	9	-2.35900E 03	9	15	5.95800E 02
9	18	-4.74800E 01	9	19	-2.33800E 01
10	3	-1.42600E 02	10	10	-3.89900E 03
10	13	1.83200E 03	10	16	9.50000E 02
10	19	-3.52900E 01	10	20	-8.23500E 01
11	1	-1.13700E 02	11	2	-2.59300E 01
11	8	2.61200E 03	11	11	1.39500E 03
11	17	4.71600E 02	11	18	-7.48700E 02
12	1	2.59300E 01	12	2	-3.78800E 01
12	3	2.76200E 01	12	9	1.76300E 03
12	11	-1.54100E 03	12	12	1.54100E 03
12	18	8.24800E 02	12	19	-1.02900E 03
13	2	-2.76200E 01	13	3	1.25800E 02
13	10	2.94900E 03	13	12	-1.81300E 03
13	13	-2.04700E 03	13	19	1.08800E 03
13	20	-1.48600E 03	14	4	-5.95500E 02
14	5	5.95500E 02	14	8	9.37200E 02
14	11	-1.45900E 03	14	14	-9.37200E 02
15	5	-5.95500E 02	15	6	5.95500E 02
15	9	5.95800E 02	15	11	1.61200E 03
15	12	-1.61200E 03	15	15	-5.95800E 02
16	6	-5.95500E 02	16	7	5.95500E 02
16	10	9.50000E 02	16	12	1.89600E 03
16	16	-9.50000E 02	17	1	-6.18100E 00
17	17	-1.00000E 00	18	1	7.24500E 00
18	2	-7.24500E 00	18	18	-1.00000E 00
19	2	1.86000E 00	19	3	-1.86000E 00
19	19	-1.00000E 00	20	3	1.37700E 00
20	20	-1.00000E 00			

TABLE 2.6

ELEMENTS OF A_d MATRIX FOR CPSG

I	J	Value	I	J	Value
1	1	-2.08069E 01	1	2	1.32226E 01
1	5	6.22502E 00	1	8	3.32462E 00
2	1	6.56259E 00	2	2	-8.12296E 00
2	3	2.43416E 00	2	5	3.20625E-01
2	6	5.07714E 00	2	8	-4.26658E 00
2	9	4.43782E 00	3	1	-2.62943E 00
3	2	5.67584E 00	3	3	-1.15497E 01
3	5	-3.39635E-01	3	6	2.26271E 00
3	7	2.85728E 01	3	8	-2.15917E 00
3	9	-1.55883E 01	3	10	-1.98333E 01
4	4	-2.00000E 00	5	1	-1.97124E-01
5	2	1.47821E-01	5	5	-5.30310E-01
5	8	-2.74313E-02	5	11	1.26478E-01
6	1	4.74859E-01	6	2	-2.68791E-01
6	3	-8.71540E-02	6	5	4.12984E-02
6	6	-1.31411E 00	6	8	7.33000E-01
6	9	-7.10944E-01	6	12	1.26470E-01
7	1	5.92834E-01	7	2	-3.47747E-01
7	3	-8.57976E-02	7	5	7.65746E-02
7	6	-5.10153E-01	7	7	-5.19105E-01
7	8	4.86810E-01	7	9	-4.45914E-01
7	10	2.43909E-01	7	13	1.26481E-01
8	1	-2.36419E-01	8	2	1.12173E-01
8	5	-4.80731E-02	8	8	-2.56746E-02
9	1	4.06275E-01	9	2	-2.32326E-01
9	3	-4.14297E-02	9	5	5.24774E-02
9	6	-3.49613E-01	9	8	3.33616E-01
9	9	-3.05589E-01	10	1	6.81819E 00
10	2	-4.98699E 00	10	3	-1.62970E 00
10	5	8.80685E-01	10	6	-5.86727E 00
10	7	1.77323E 01	10	8	5.59880E 00
10	9	-1.60300E 01	10	10	-1.23086E 01
11	1	-2.00136E 00	11	2	9.49582E-01
11	4	2.48301E 01	11	5	2.50951E 01
11	8	-3.99180E 01	11	11	-4.71075E 01
11	12	3.22469E 01	11	13	-3.54716E 01
12	1	1.01032E 01	12	2	-5.41555E 00
12	3	-6.51277E-01	12	4	-1.04794E 02
12	5	1.58066E 00	12	6	2.46102E 01
12	8	8.71034E 01	12	9	-8.62592E 01
12	12	-7.50180E 01	12	13	1.49706E 02
13	1	-4.87624E 00	13	2	2.78844E 00
13	3	4.97252E-01	13	4	7.65818E 01
13	5	-6.29849E-01	13	6	4.19616E 00
13	7	3.66512E 01	13	8	-4.00416E 00
13	9	7.68159E 01	13	13	-1.13233E 02

TABLE 2.7

DESCRIPTION OF EACH ANALYSIS RUN

Run No.	Description of Perturbed Input Variable	Constant Flow Model or Constant Pressure Model
1	Helium flow rate (1 lb/sec)	CFSG
2	Helium flow rate (1 lb/sec)	CPSG
3	Helium inlet temperature (1°F)	CFSG
4	Helium inlet temperature (1°F)	CPSG
5	Feedwater flow rate (1 lb/sec)	CFSG

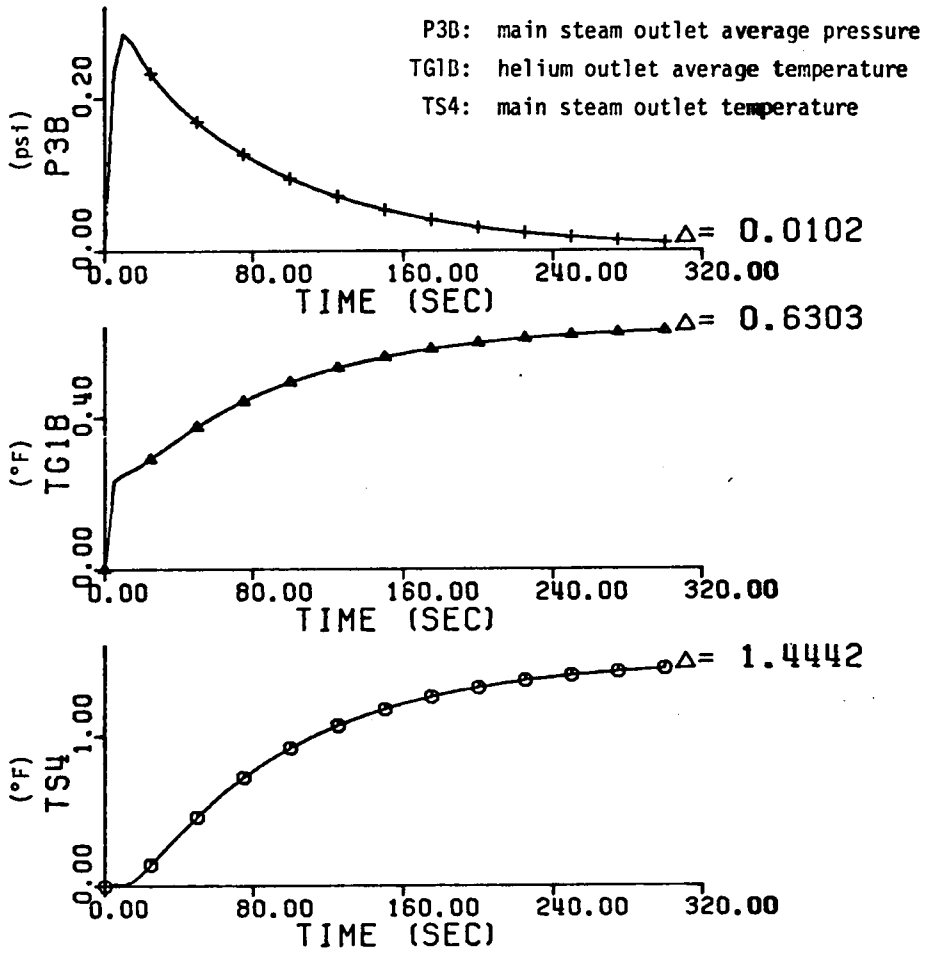


Figure 4. CFSG Time Response to a 1 lb/sec Step Increase of Helium Flow.

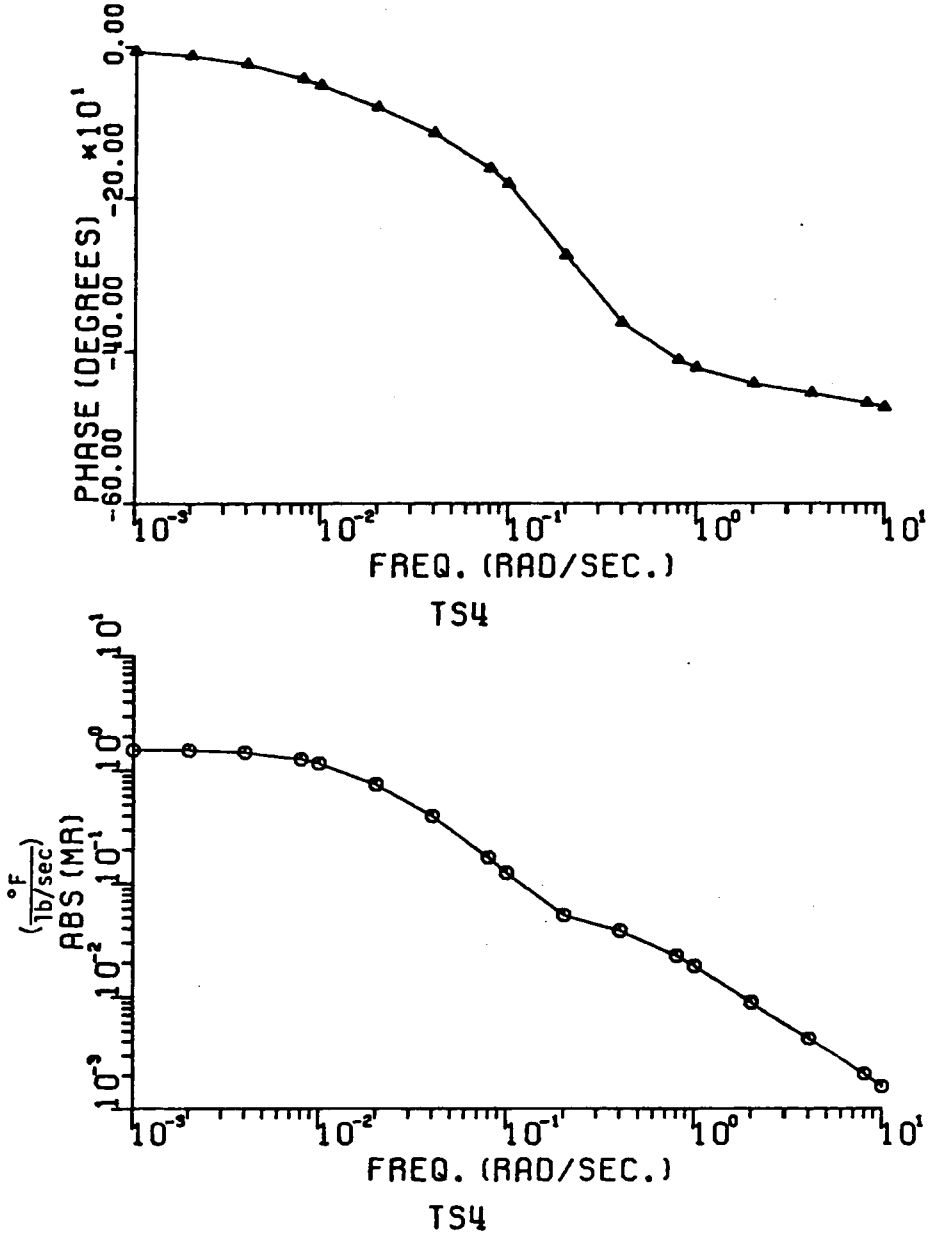


Figure 5. Frequency Response of Main Steam Temperature to Helium Flow (CFSG).

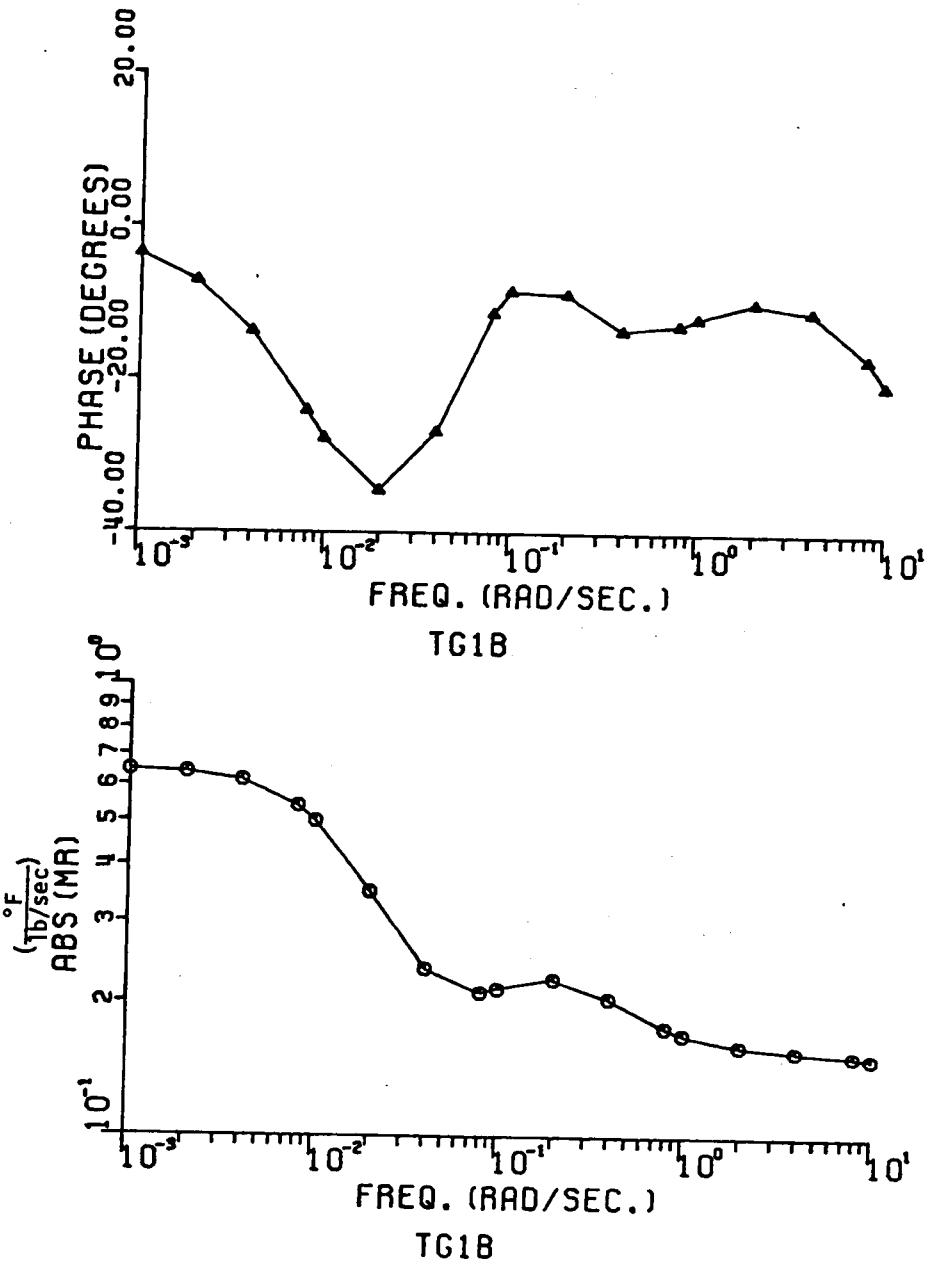


Figure 6. Frequency Response of Helium Outlet Temperature to Helium Flow (CFSG).

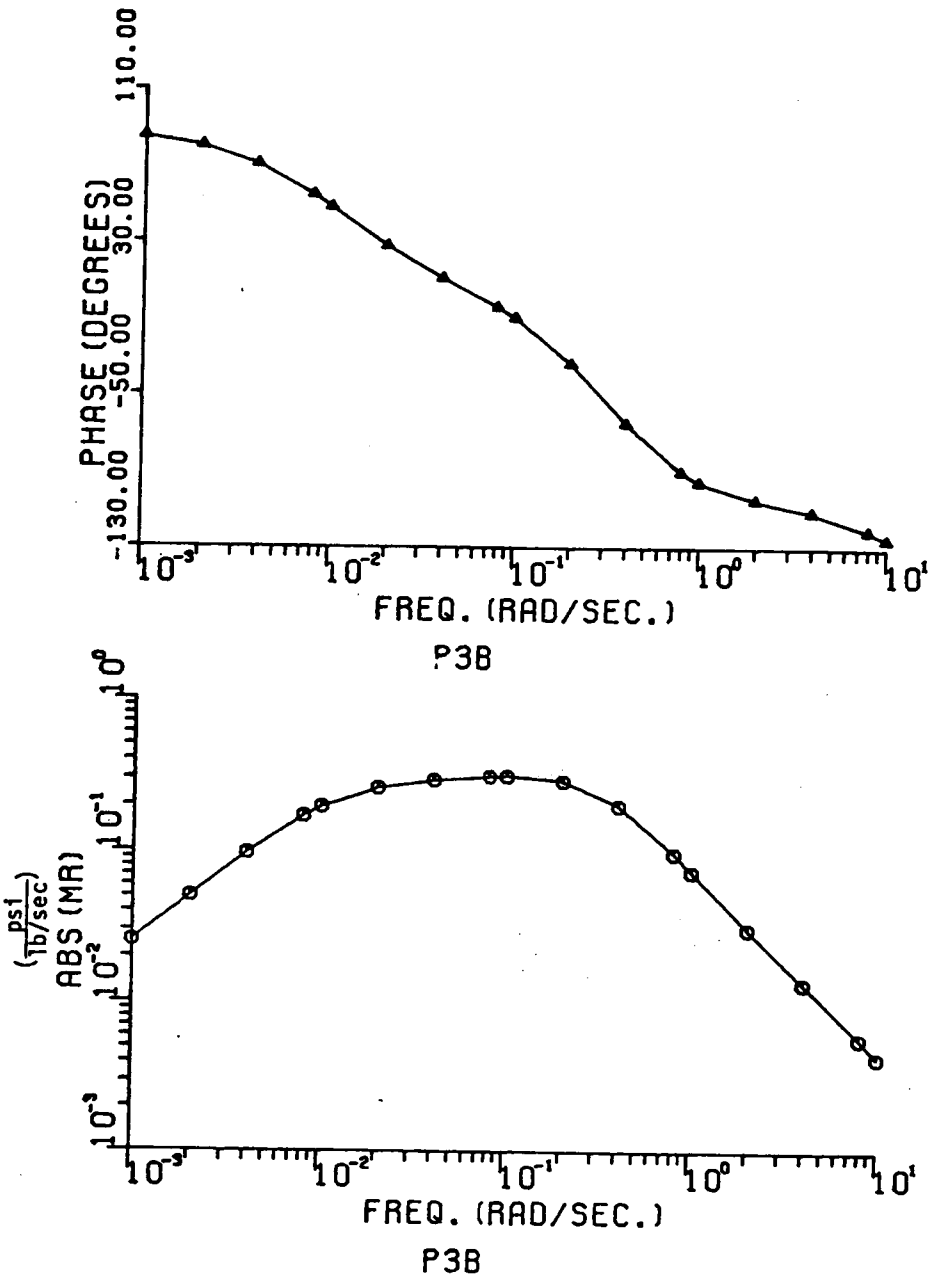


Figure 7. Frequency Response of Main Steam Pressure to Helium Flow (CFSG).

initially rises and then approaches the original value. This is because there is no increase in feedwater flow to sustain the rise. The main steam temperature (TS4) increases significantly (1.44°F), whereas the temperature rise in the helium outlet node is relatively low (0.63°F). The steady values of each output in time response after 300 sec are close to the magnitude of the frequency response at low frequency (0.004 rad/sec) just as it should be.

The response curves of the outputs are almost monotonic and settle down within 165 seconds (0.006 rad/sec in frequency domain). The time lag is primarily due to the thermal capacitance of the metal, water/steam mass and the thermal resistance from the primary to the secondary coolant.

Discussion of Results for Run No. 2 (Figures 8 to 11)

Run No. 2 shows the CPSG model time response and frequency response for a 1 lb/sec increase in helium flow rate. The system responses for "P3B" and "TG1B" are similar to those of Run No. 1 (CFSG). There is a large difference in the early transient of "TS4" response. For the CPSG model, the fast rise of main steam pressure (P3B) reduces the feedwater flow rate which makes the response of "TS4" faster than for the CFSG model in Run No. 1.

Discussion of Results for Run No. 3 (Figures 12 to 15)

Run No. 3 shows the CFSG model time response and frequency response for a 1°F increase in helium inlet temperature. Increased temperature of the primary helium coolant increases the rate of

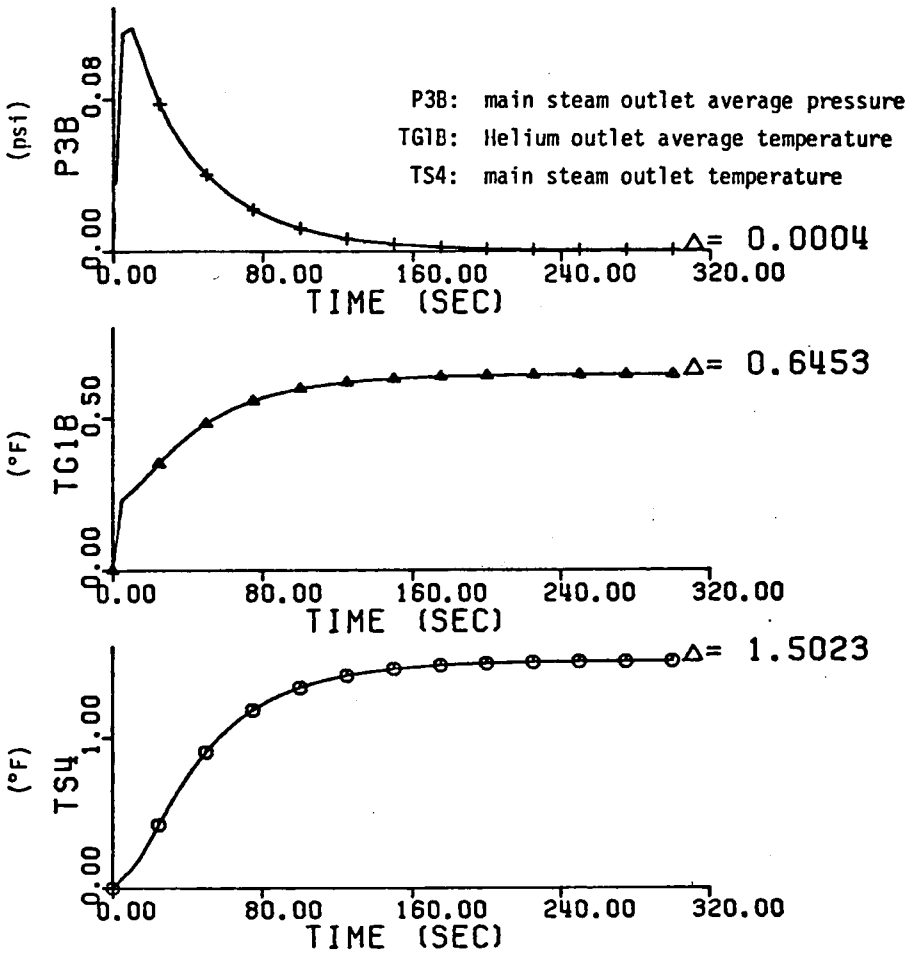


Figure 8. CPSG Time Response to a 1 lb/sec Step Increase of Helium Flow.

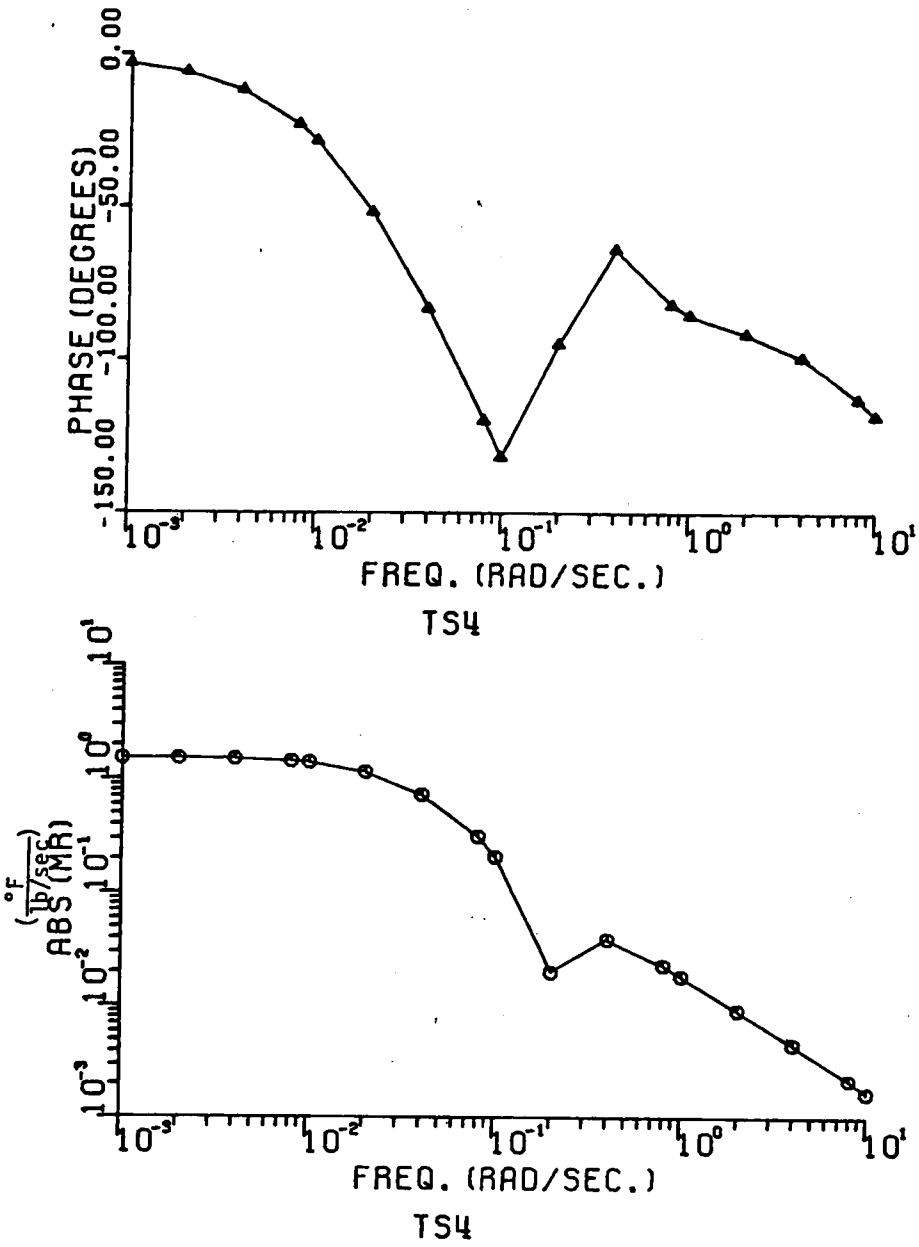


Figure 9. Frequency Response of Main Steam Temperature to Helium Flow (CPSG).

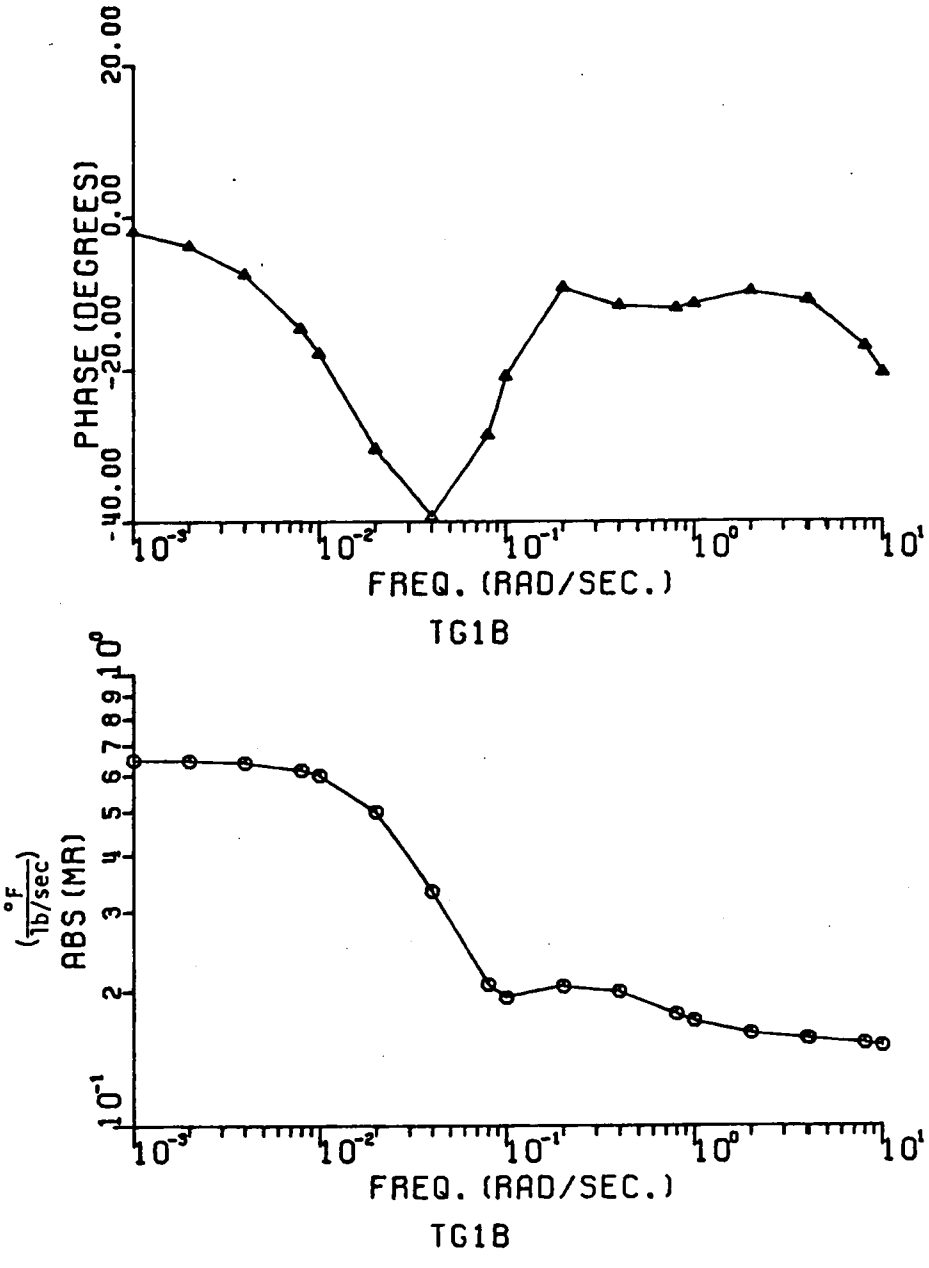


Figure 10. Frequency Response of Helium Outlet Temperature to Helium Flow (CPSG).

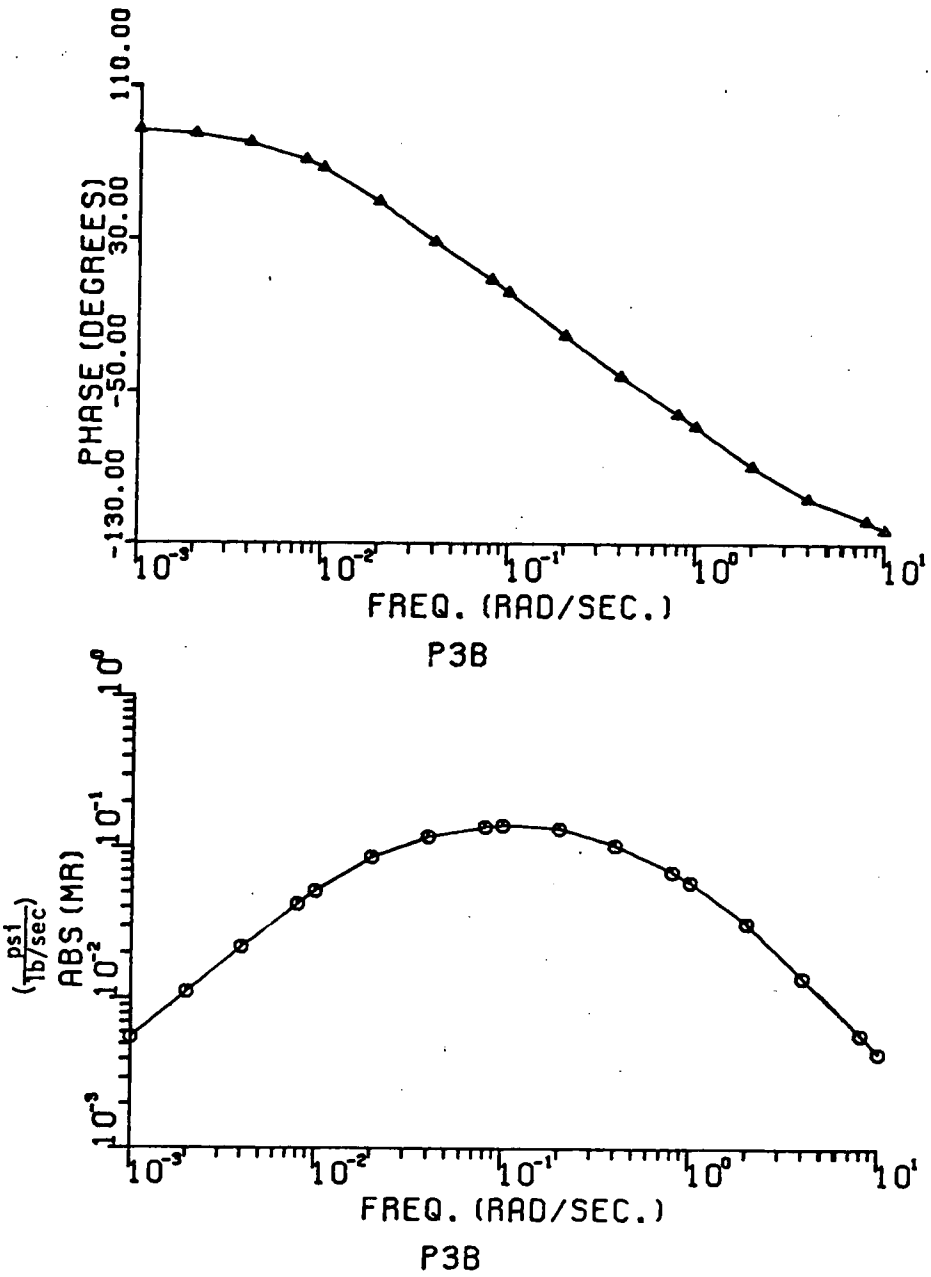


Figure 11. Frequency Response of Main Steam Pressure to Helium Flow (CPSG).

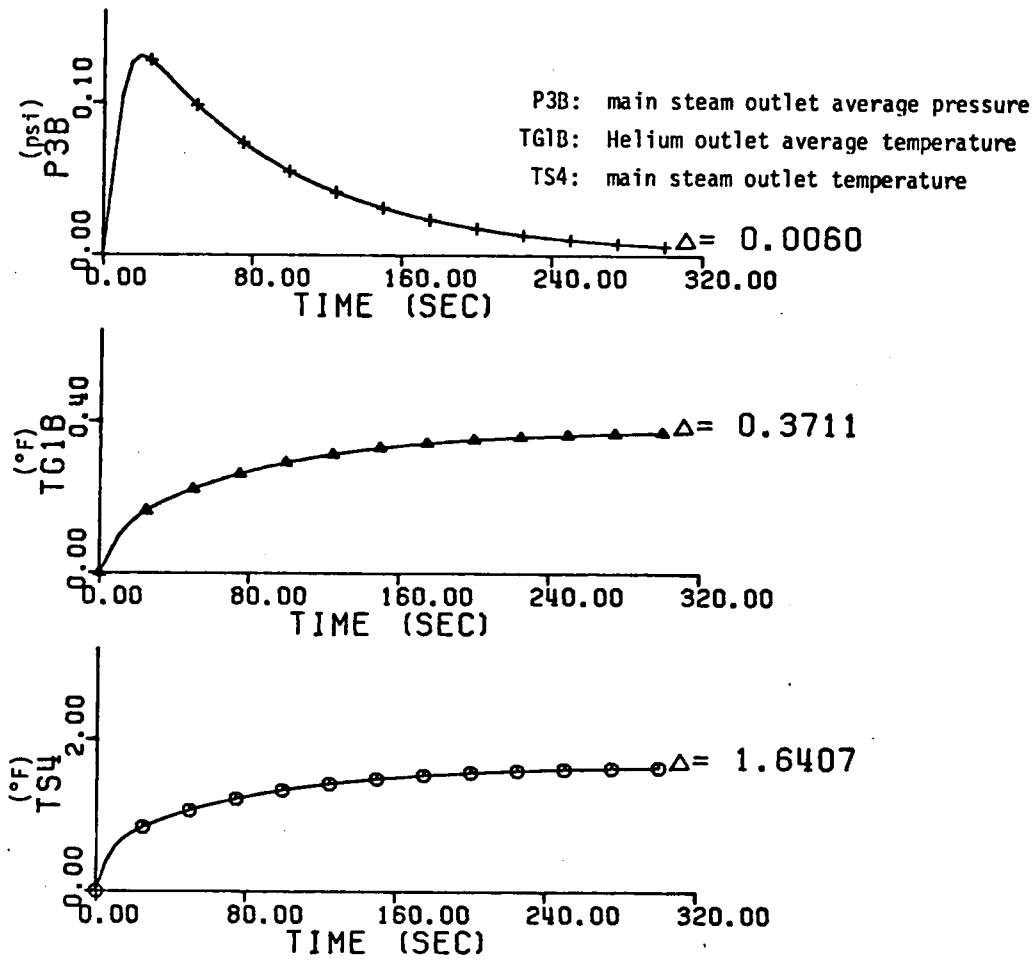


Figure 12. CFSG Time Response to a 1°F Step Increase of Helium Inlet Temperature.

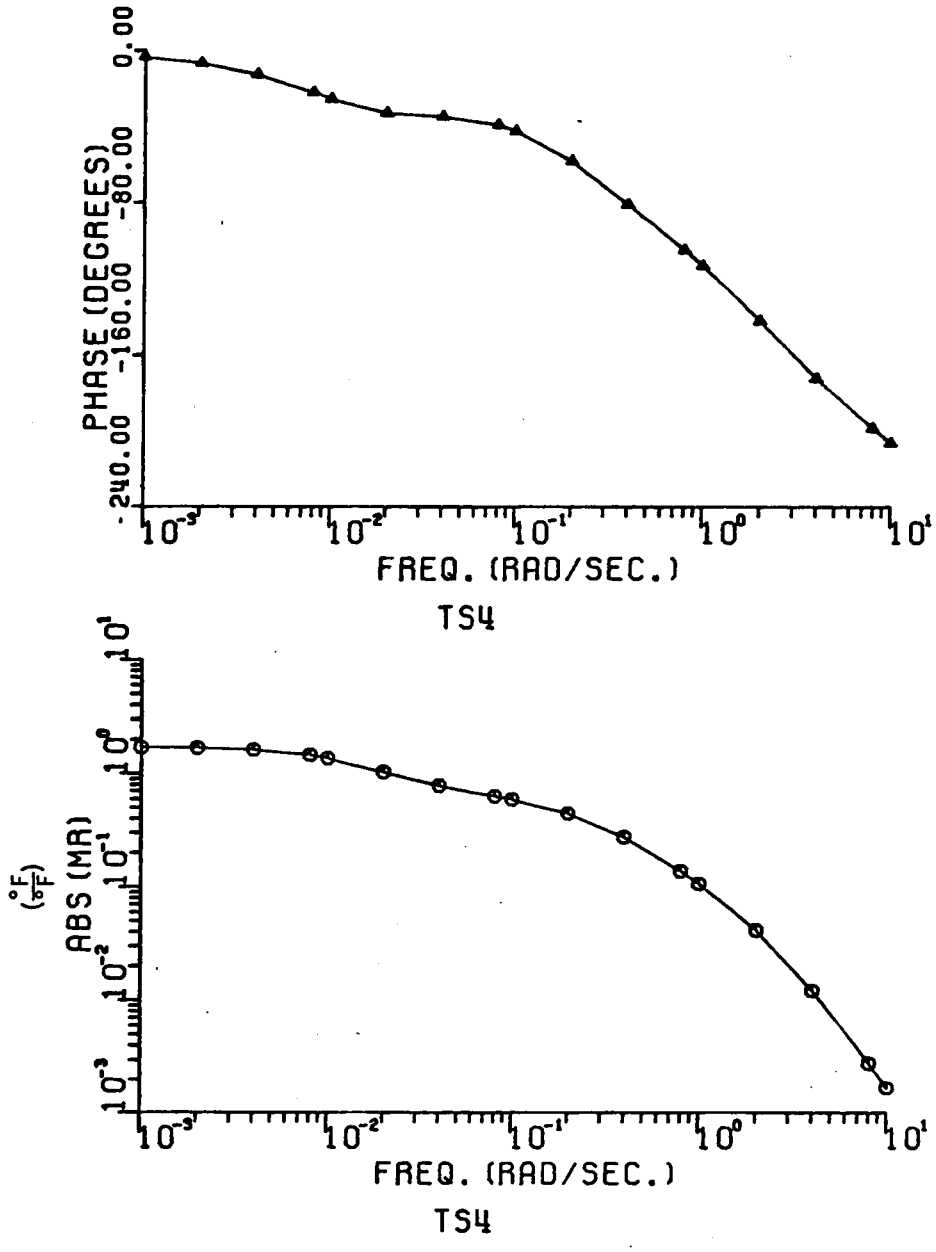


Figure 13. Frequency Response of Main Steam Temperature to Helium Inlet Temperature (CFSG).

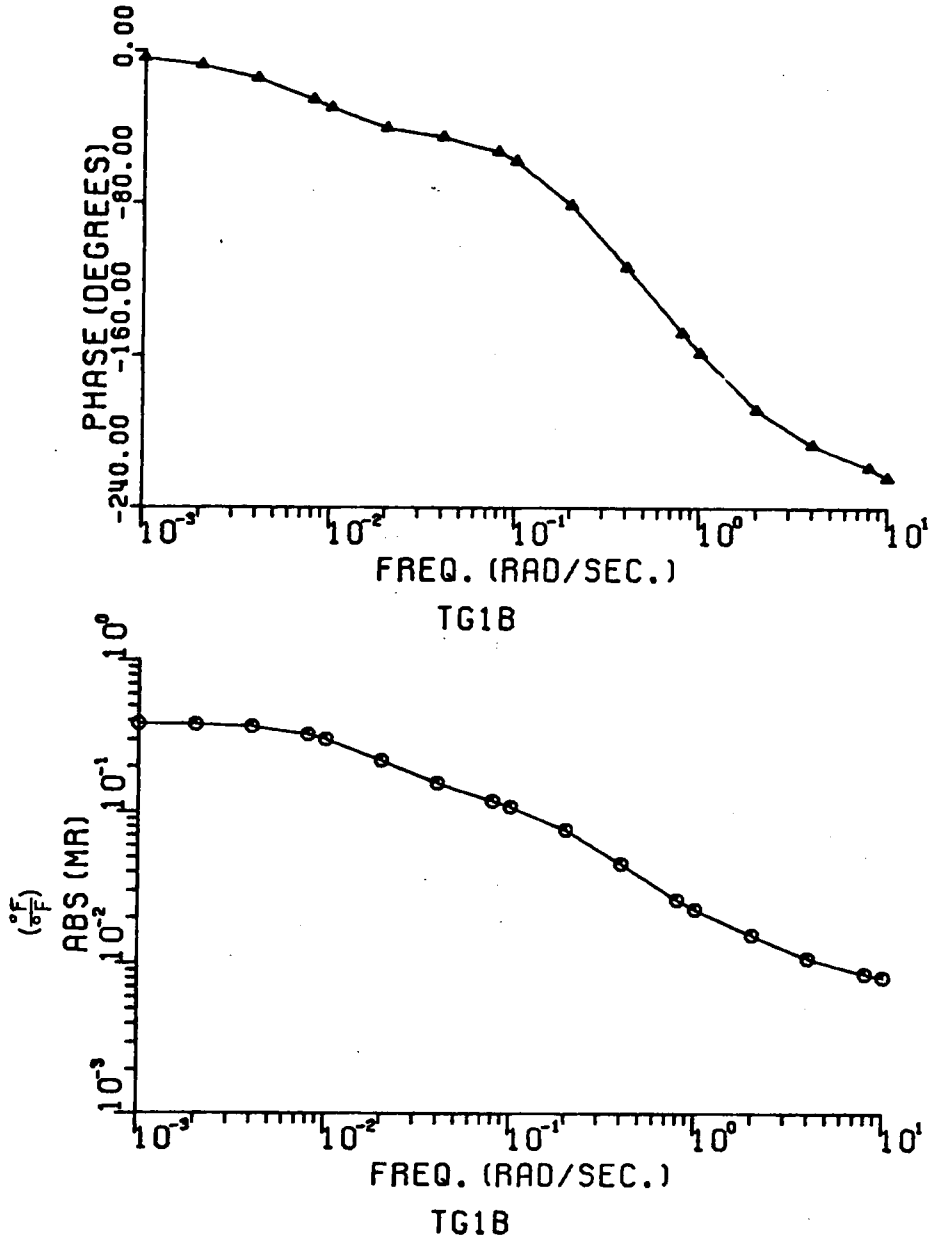


Figure 14. Frequency Response of Helium Outlet Temperature to Helium Inlet Temperature (CFSG).

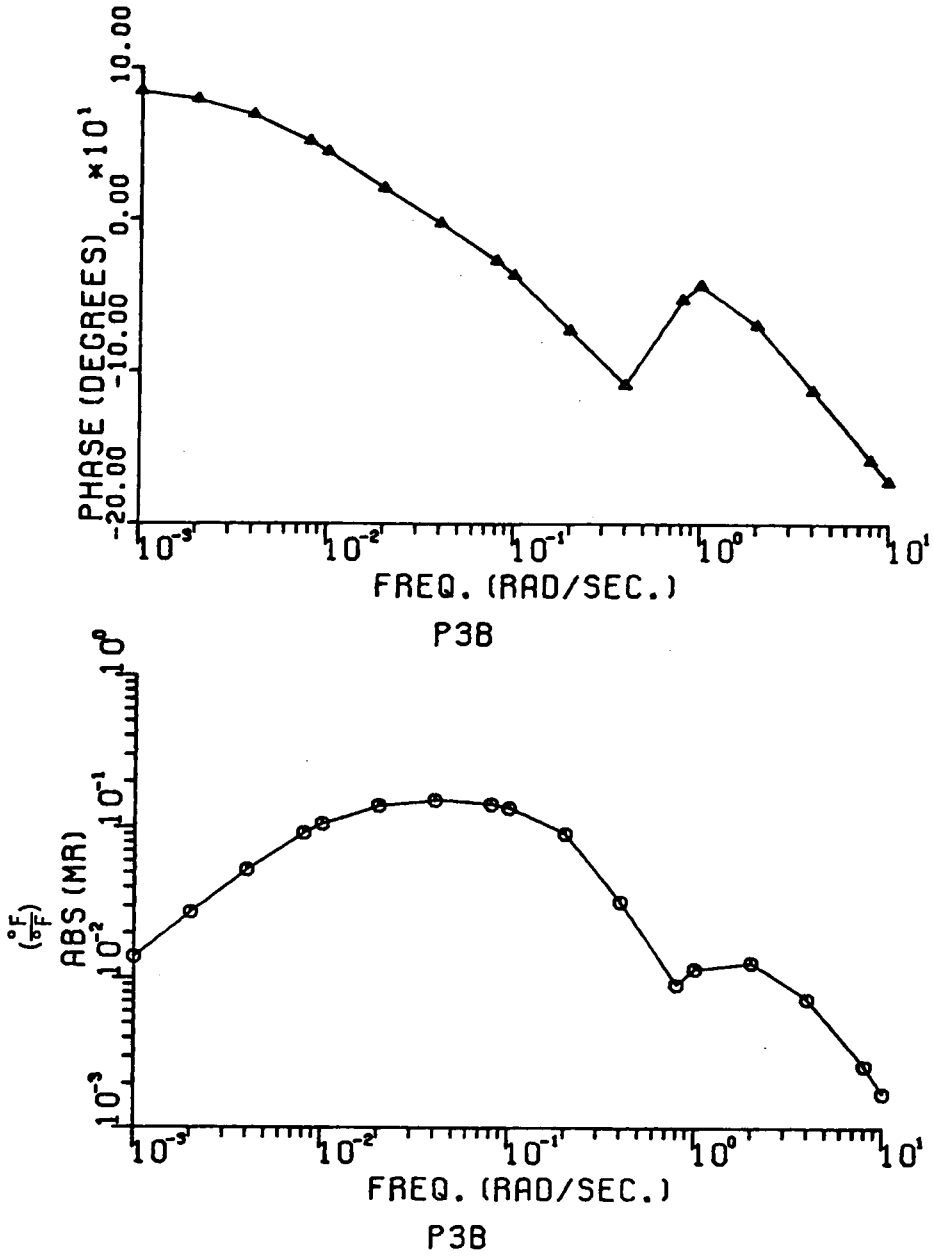


Figure 15. Frequency Response of Main Steam Pressure to Helium Inlet Temperature.

transfer of thermal energy from the primary to the secondary coolant. "P3B" increases initially, then returns to the original value due to the constant feedwater flow. All the temperature nodes increased following the increase of helium inlet temperature.

Discussion of Results for Run No. 4 (Figures 16 to 19)

Run No. 4 shows the CPSG model time response and frequency response for a 1°F increase in helium inlet temperature. The system transient responses for this run are similar to those of Run No. 3.

Discussion of Results for Run No. 5 (Figures 20 to 23)

Run No. 5 shows the CFSG time response and frequency response for a 1 lb/sec increase in feedwater flow rate. For constant helium flow rate and inlet temperature, the temperature in the secondary coolant circuit drops (-2.74°F) following the increased feedwater flow rate. The average helium temperature in the outlet node also drops (-0.68°F). For constant outlet steam header pressure, the main steam pressure increases by 0.71 psi in order to sustain the increase in the feedwater flow rate.

In the above discussions, it is shown that the revised linear, 3 node moving boundary steam generator model which was developed in this study provides reasonable results for the frequency response and time response. This model will be used in the overall Fort St. Vrain system identification work.

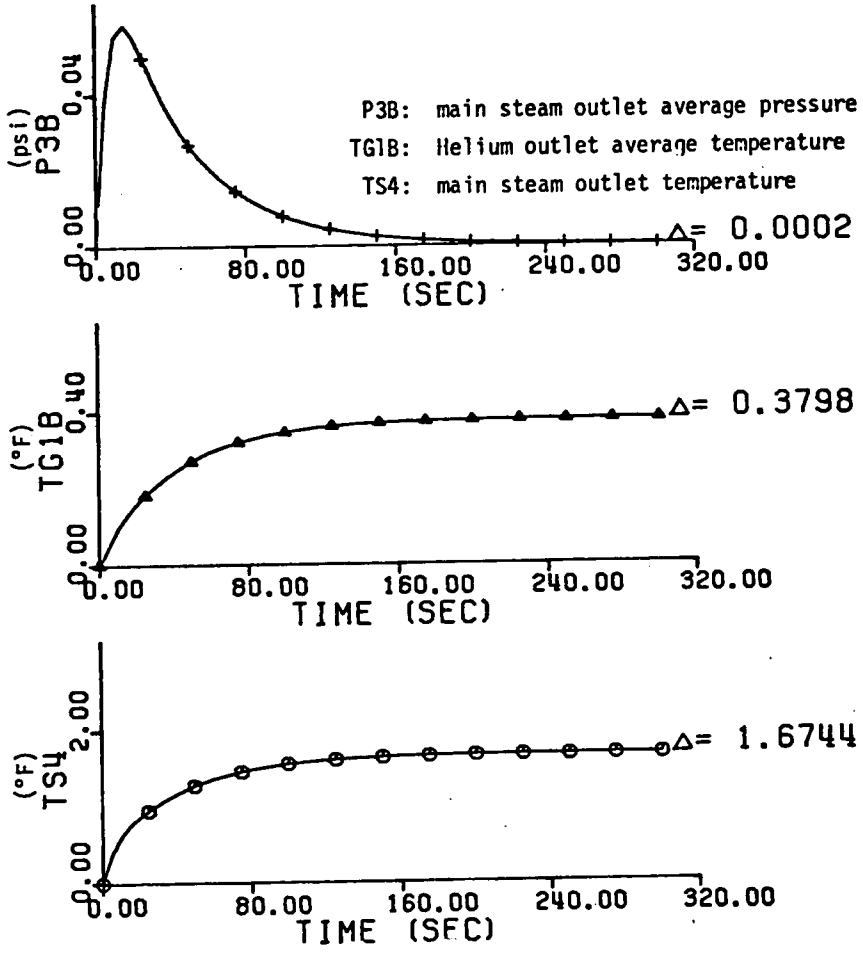


Figure 16. CPSG Time Response to a 1°F Steam Increase of Helium Inlet Temperature.

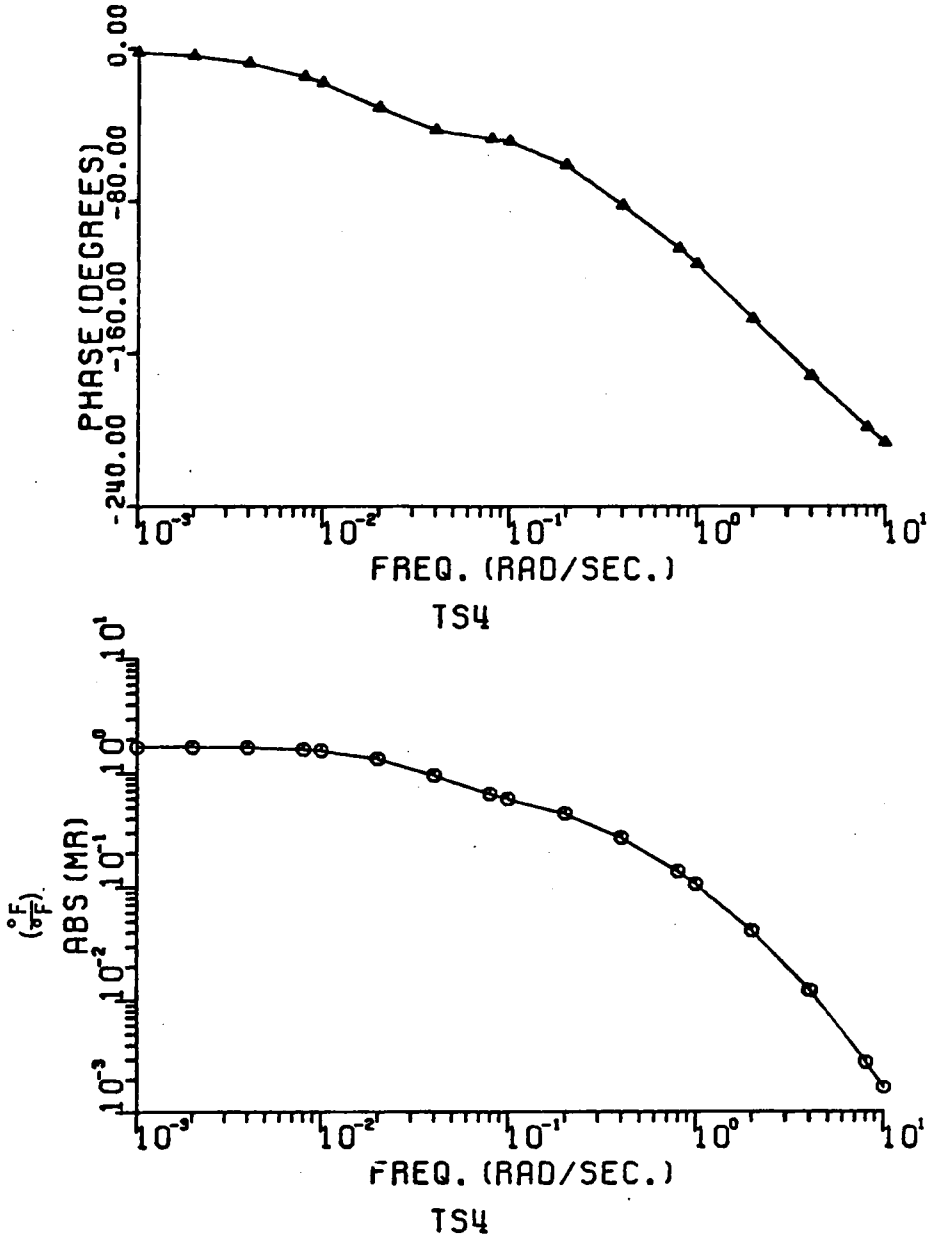


Figure 17. Frequency Response of Main Steam Temperature to Helium Inlet Temperature (CPSG).

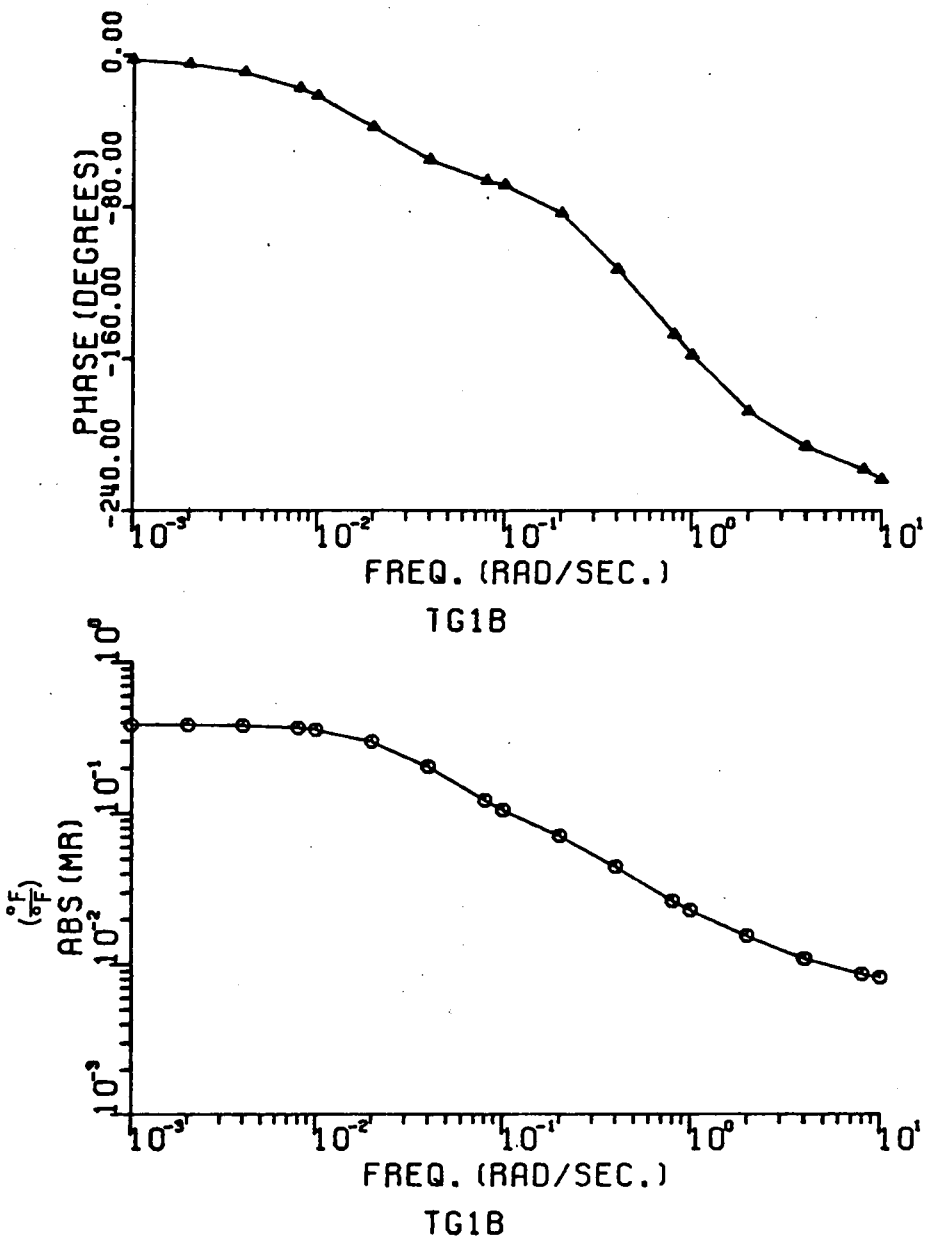


Figure 18. Frequency Response of Helium Outlet Temperature to Helium Inlet Temperature.

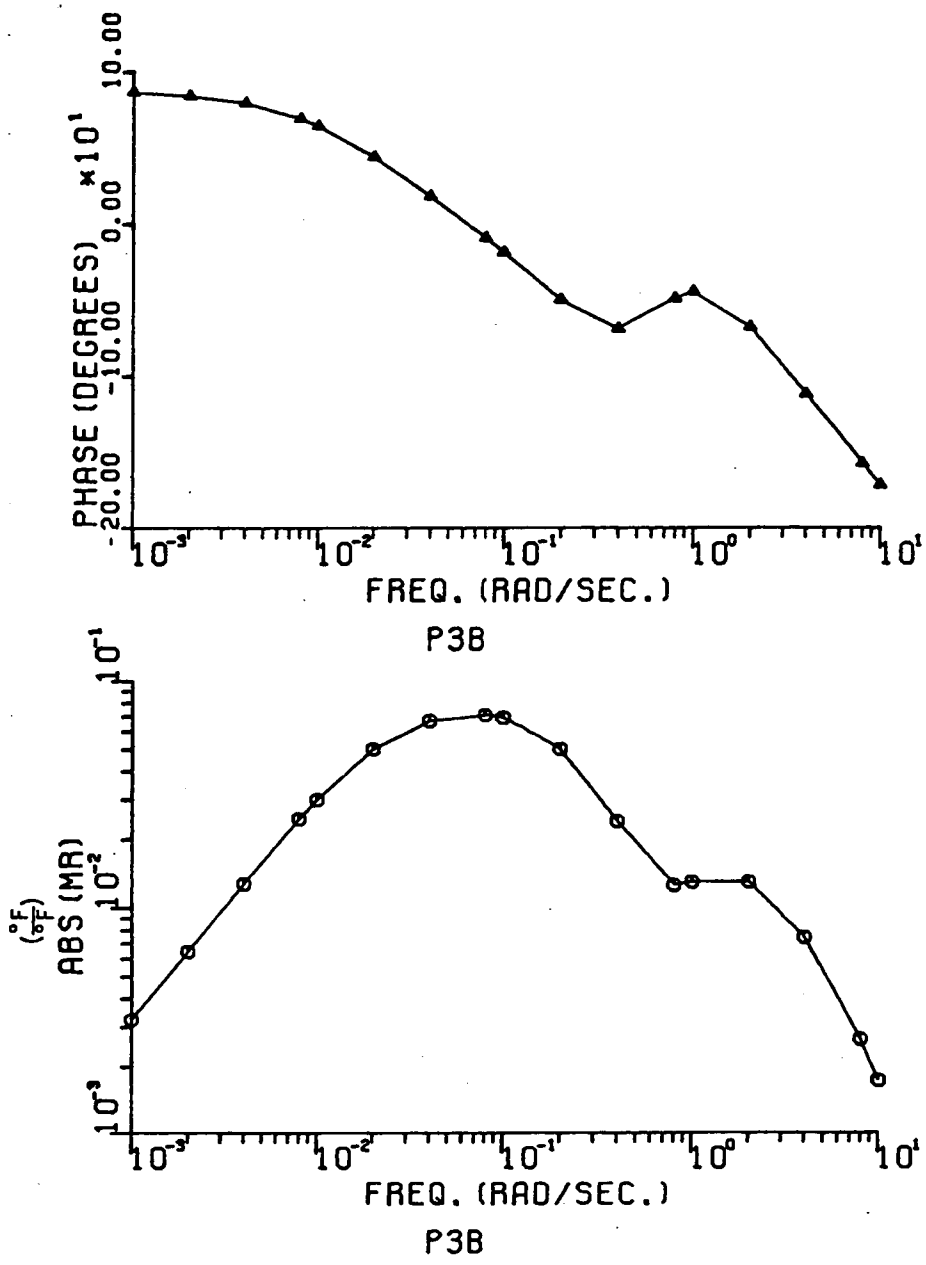


Figure 19. Frequency Response of Main Steam Pressure to Helium Inlet Temperature (CPSG).

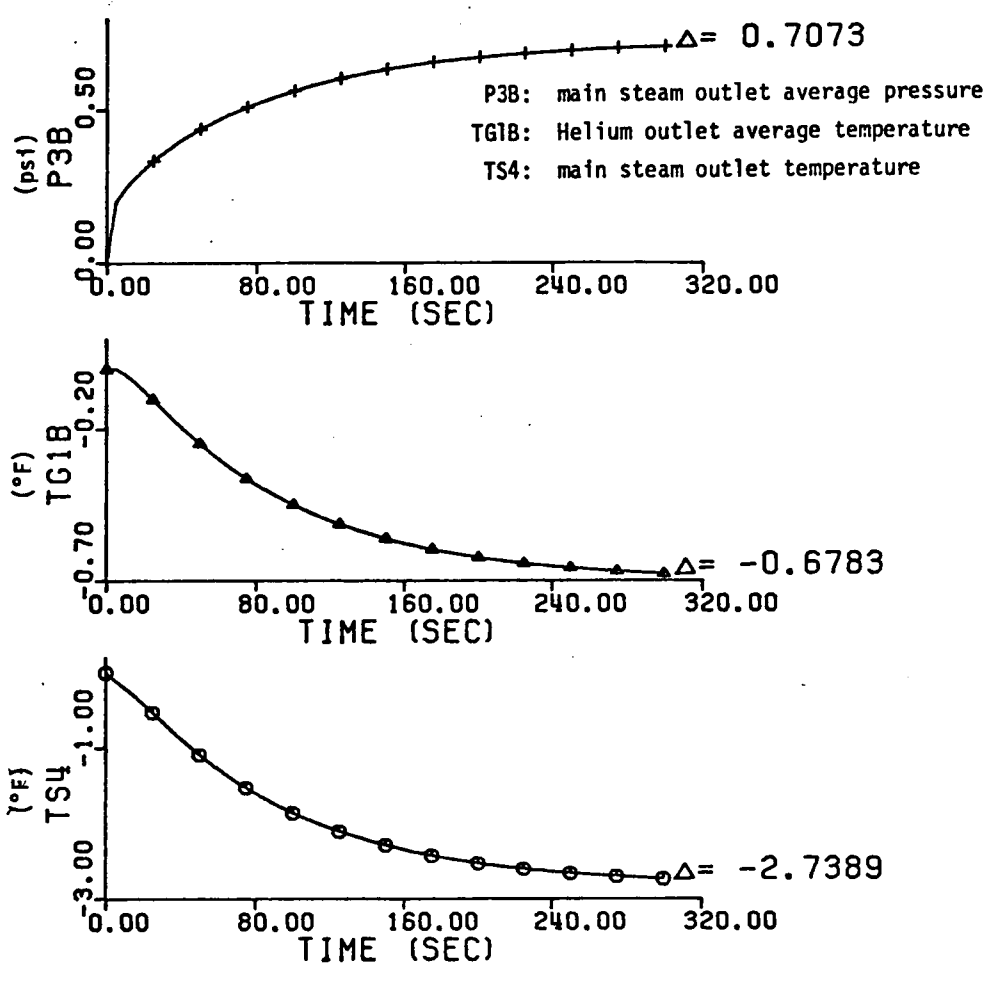


Figure 20. CFSG Time Response to a 1 lb/sec Step Increase of Feedwater Flow.

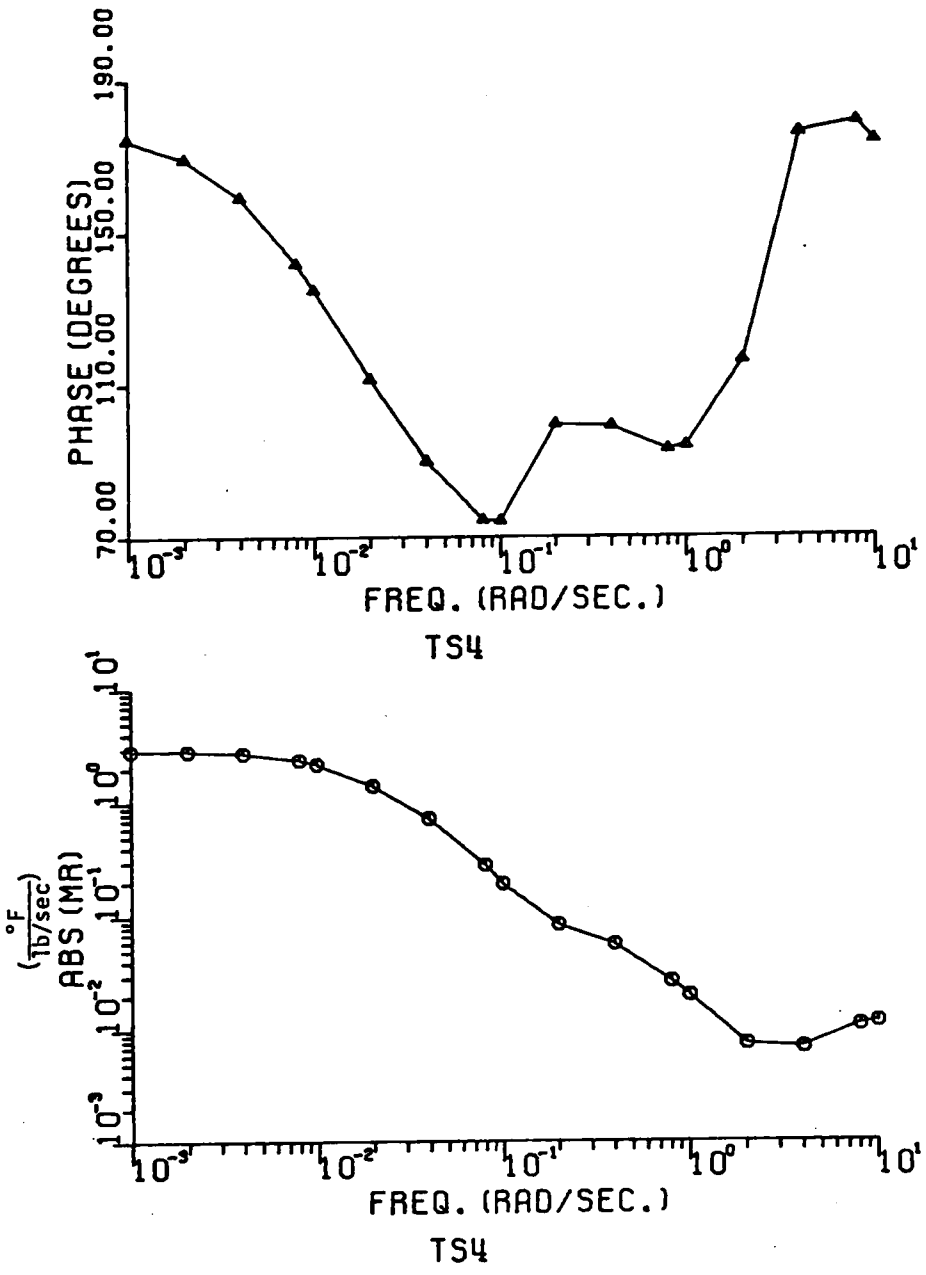


Figure 21. Frequency Response of Main Steam Temperature to Feedwater Flow (CFSG).

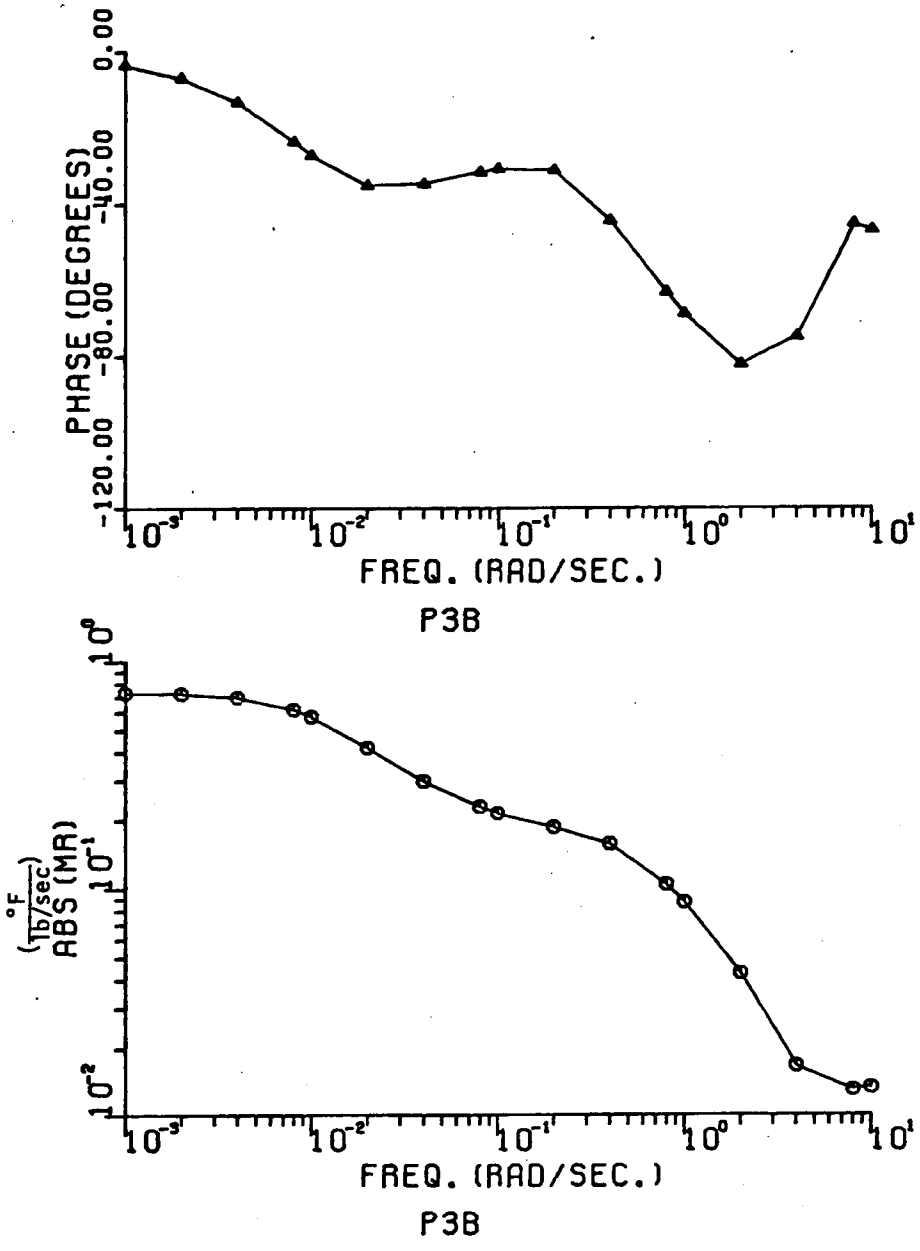


Figure 22. Frequency Response of Helium Outlet Temperature to Feedwater Flow (CFSG).

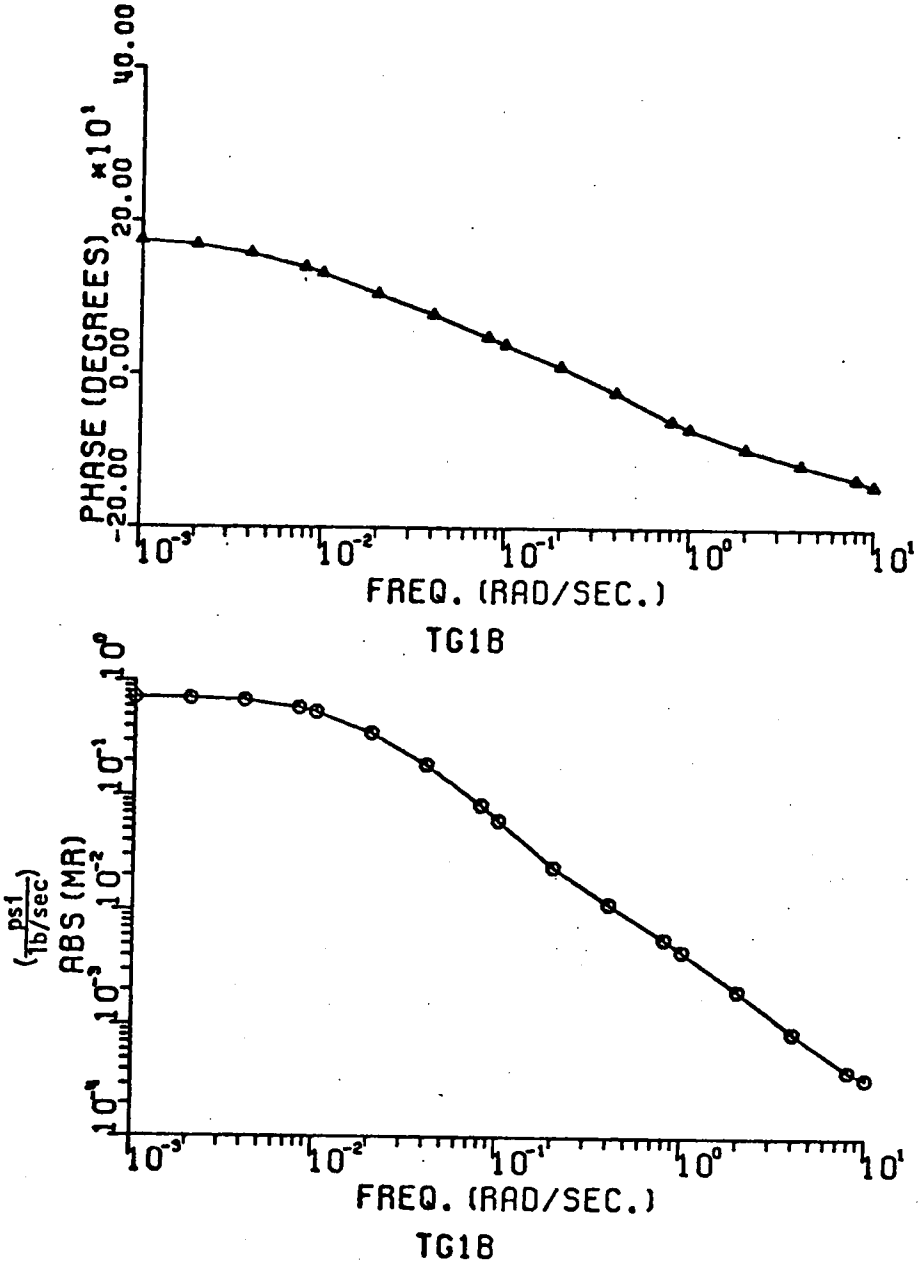


Figure 23. Frequency Response of Main Steam Pressure to Feedwater Flow (CFSG).

CHAPTER 3

A METHOD FOR AUTOMATIC IDENTIFICATION OF PARAMETERS IN LARGE DYNAMIC SYSTEM

3.1 Introduction

In order to develop a strategy for changing the system parameters in such a manner as to decrease the error in model predictions, it is necessary to relate some error function to the parameters. In this work, the error function which is minimized is

$$E = \sum_{\ell=1}^{N} \left(\frac{R_{p\ell} - R_{c\ell}}{\sigma_{R\ell}}\right)^2 + \sum_{\ell=1}^{N} \left(\frac{I_{P\ell} - I_{c\ell}}{\sigma_{I\ell}}\right)^2 \qquad (3.1)$$

where

N = the total number of frequency observation points,

$R_{p\ell}$ (or $I_{p\ell}$) = the real (or imaginary) part of the experimental frequency response from the plant at the ℓth frequency

$R_{c\ell}$ (or $I_{c\ell}$) = the real (or imaginary) part of the model's frequency response at the ℓth frequency

$\sigma_{R\ell}$ (or $\sigma_{I\ell}$) = standard deviation of the real (or imaginary) part of experimental frequency due to the noise contamination.

The reason for the division by the standard deviation, $\sigma_{R\ell}$ or $\sigma_{I\ell}$, is to give more weight to the components of the error function in which the noise contamination is small.

(Note: Another form of error function which uses the differences in gain and phase will be discussed in Appendix A.)

By using the first order approximation, we get from Equation (3.1) a relation between parameter changes and error function changes:

$$E - E_o = \Delta E = \sum_{i}^{Np} \frac{\partial E}{\partial P_i} \delta P_i = \bar{\nabla} E \cdot \delta \bar{P} \tag{3.2}$$

where

E_o = the value of the error function for parameter values at the previous step

Np = the number of parameters to be adjusted

P_i = ith parameter in the system to be adjusted

$\bar{\nabla}$ = gradient operator in parameter space

$$\frac{\partial E}{\partial P_i} = -2 \sum_{\ell=1}^{N} \left[\left(\frac{R_{p\ell} - R_{c\ell}}{\sigma_{R\ell}^2} \right) \frac{\partial R_{c\ell}}{\partial P_i} + \left(\frac{I_{P\ell} - I_{c\ell}}{\sigma_{I\ell}^2} \right) \frac{\partial I_{c\ell}}{\partial P_i} \right]$$

$$(i = 1, 2, \ldots, Np). \tag{3.3}$$

The quantities $R_{p\ell}$ and $I_{p\ell}$ may be calculated from the test data by a code such as HFFT, (a description of the HFFT code is in Appendix B) and theoretical estimates can be calculated by the code PARAPE (described in Section 3.3 and Appendix D) from the reference theoretical model. The quantities $\sigma_{R\ell}$ and $\sigma_{I\ell}$ can be obtained from the actual plant data using the HFFT code.

The quantities $R_{c\ell}$, $I_{c\ell}$, $\frac{\partial R_{c\ell}}{\partial P_i}$, and $\frac{\partial I_{c\ell}}{\partial P_i}$ are calculated from the theoretical model using initial values of the parameters (P_i), differential system A matrix, algebraic system B matrix, and the proper forcing vector in the PARAPE code (see Equation (1.2)).

There are quite a few methods for computing the minimum of an error function of several parameters. The direct search methods, such as the random search method,[11] the method of Rosenbrock,[12] and the simplex method[13] are based on a sequential examination of trial solutions which use simple comparisons to give an indication for a further searching procedure. The information which must be provided is the function value at each selected point. In general, they do not give a rapid rate of convergence.

More efficient techniques can be devised by utilizing additional information, such as the gradient, of the function to be optimized. A class of such methods in which the solution is found by solving a sequence of one-dimensional problems are called descent methods. Since little additional calculation is required to determine the gradients of the function used in this work (see Section 3.3), we will focus on the descent methods in the following discussion. Two of the most popular descent methods: (1) the method of steepest descent and (2) the method of conjugate gradients, will be discussed briefly in Section 3.2.

3.2 Descent Methods-the Method of Steepest Descent and the Method of Conjugate Gradients[5]

In order to develop the concept of descent methods, it is useful to consider the following simple relation between the error function and the parameters

$$E(\bar{P}) = a + \bar{b}^T \bar{P} + \frac{1}{2} \bar{P}^T J \bar{P} \qquad (3.4)$$

where

a = constant

b = constant (Np x 1) vector

J = constant positive definite (Np x Np) matrix.

Let $\bar{\xi}$ be the parameter vector which will minimize E. The descent method is an iterative procedure to find the optimized vector, $\bar{\xi}$, starting from an initial parameter vector, P_1. The parameters are adjusted according to:

$$\bar{P}_{i+1} = \bar{P}_i + \lambda_i \bar{V}_i \tag{3.5}$$

where

$\bar{P}_i$ = the parameter vector estimated at the ith iteration

$\bar{V}_i$ = a descent vector which is determined by the minimization strategy used

λ_i = the distance in the $\bar{V}_i$ direction that minimizes E.

It is necessary to find the value of λ_i that optimizes the parameter estimate. By substituting Equation (3.5) into (3.4), we have

$$E(\bar{P}_{i+1}) = a + \bar{b}^T(\bar{P}_i + \lambda_i \bar{V}_i) + \frac{1}{2}(\bar{P}_i + \lambda_i \bar{V}_i)^T J$$

$$(\bar{P}_i + \lambda_i \bar{V}_i)$$

and

$$\frac{\partial E(\bar{P}_{i+1})}{\partial \lambda_i} = \bar{V}_i^T \bar{b} + \bar{V}_i^T J (\bar{P}_i + \lambda_i \bar{V}_i)$$

$$= \bar{V}_i^T \bar{g}_i + \lambda_i \bar{V}_i^T J \bar{V}_i \tag{3.6}$$

where

$$\bar{g}_i = \bar{b} + J\,\bar{P}_i. \tag{3.7}$$

By setting Equation (3.6) equal to zero, we obtain:

$$\lambda_i = \frac{-\bar{V}_i^T\,\bar{g}_i}{\bar{V}_i^T\,J\,\bar{V}_i}. \tag{3.8}$$

Also from Equation (3.5), (3.7), and (3.8), we have

$$\bar{V}_i^T\,\bar{g}_{i+1} = \bar{V}_i^T\,(\bar{b} + J\,\bar{P}_{i+i})$$

$$= \bar{V}_i^T\,(\bar{g}_i + \lambda_i\,J\,\bar{V}_i) = 0. \tag{3.9}$$

Equation (3.9) can be explained geometrically. The minimization scheme proceeds in the direction $\bar{V}_i$ to lower and lower level surfaces until the point $\bar{P}_{i+1}$ is reached. As E cannot be further reduced in this direction, $\bar{V}_i$ must lie in the tangent plane to the level surface through $\bar{P}_{i+1}$. The situation is sketched in Figure 24.

So far we have said nothing about the choice of the descent direction vector, $\bar{V}_i$. Numerous methods for selecting $\bar{V}_i$ will eventually find the optimized parameter vector, $\bar{\xi}$. But, the strategy in choosing $\bar{V}_i$ will affect the speed and efficiency of the method. If we choose $\bar{V}_i$ to lie along the direction of steepest descent ($-\bar{\nabla}E = -\bar{g}_i$), this is the method of steepest descent. Then, from Equation (3.5), (3.7), and (3.8), we can iteratively generate a sequence of $\bar{P}_i$ which will converge to the optimized parameter

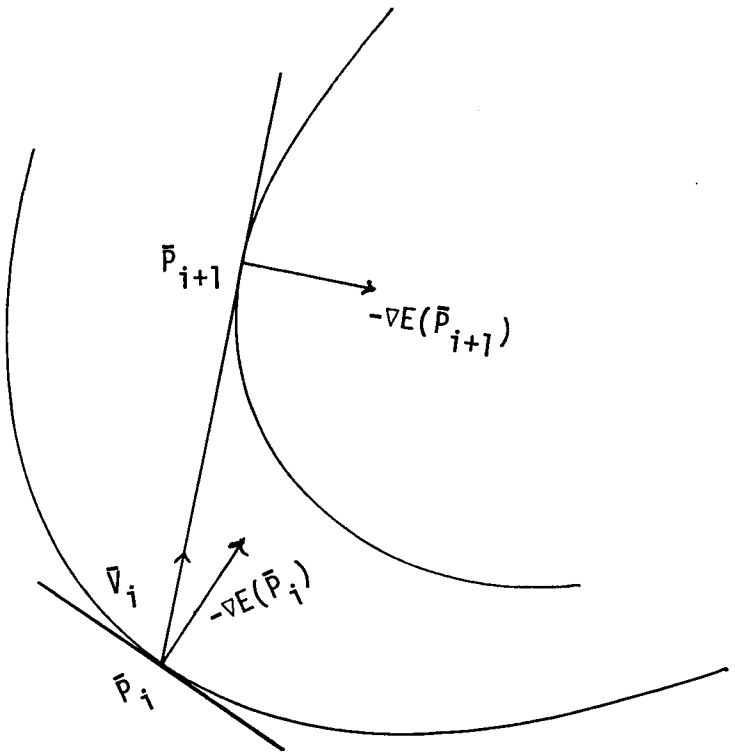


Figure 24. The Descent Vector $\bar{V}_i$ Lies in the Tangent Plane to the Level Surface through $\bar{P}_{i+1}$.

vector, $\bar{\xi}$. This method often converges extremely slowly in practice. The reason can be seen qualitively from Figure 25, part a, for the two parameter case. In Figure 25, part a, the ellipses are elongated, and the line of steepest descent may go nowhere near the optimized vector, $\bar{\xi}$.

A better strategy by which the $\bar{V}_i$ could be chosen is the conjugate direction, $\bar{d}_i$. By definition, if two directions $\bar{d}_i$ and $\bar{d}_s$ are conjugate with respect to the matrix, J, then,

$$\bar{d}_i^T \, J \, \bar{d}_s = 0. \tag{3.10}$$

If $\bar{V}_i$ in Equation (3.5) is replaced by $\bar{d}_i$, the iteration formula becomes:

$$\bar{P}_{i+1} = \bar{P}_i + \lambda_i \, \bar{d}_i \tag{3.11}$$

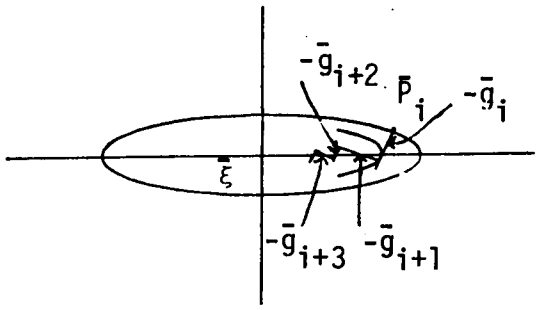
and from Equation (3.9), we have

$$\bar{g}_{i+1}^T \, \bar{d}_i = 0. \tag{3.12}$$

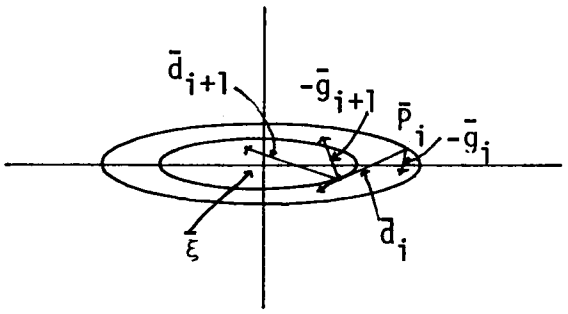
Let us assume that at the (i+1)th stage of the iteration, we have reached the point

$$\bar{P}_{i+1} = \bar{P}_1 + \sum_{k=2}^{i} \lambda_k \, \bar{d}_k$$

$$= \bar{P}_{s+1} + \sum_{k=s+2}^{i} \lambda_k \, \bar{d}_k \quad (\text{for } s = 1, 2, \ldots, i). \tag{3.13}$$



(a) The Method of Steepest Descent.



(b) The Method of Conjugate Gradients.

Figure 25. Descent Methods when Ellipses are Elongated.

Equations (3.7) and (3.13) give

$$\bar{g}_{i+1} = \bar{b} + J\,\bar{p}_{i+1}$$

$$= \bar{b} + J\,(\bar{p}_{s+1} + \sum_{k=s+2}^{i} \lambda_k\,\bar{d}_k)$$

$$= \bar{g}_{s+1} + \sum_{k=s+2}^{i} \lambda_k\,\bar{d}_k$$

so that,

$$\bar{d}_s^T\,\bar{g}_{i+1} = \bar{d}_s\,\bar{g}_{s+1} + \sum_{k=s+2}^{i} \lambda_k\,\bar{d}_s^T\,J\,\bar{d}_k$$

$$= 0 \quad \text{(by Equations (3.12) and (3.10))}. \tag{3.14}$$

Equation (3.14) says that if $\bar{d}_1, \bar{d}_2, \ldots, \bar{d}_{Np}$ are a set of descent vectors mutually conjugate with respect to J, then the minimum of E in Equation (3.4) can be found at the Np th step. For after the Npth step $\bar{g}_{Np+1}$ is orthogonal to Np linearly independent vectors, $\bar{d}_i$, so that it must vanish identically. (Note: $\bar{g}$ is a vector with Np components.)

Kowalik and Osborne[5] showed that by using Equations (3.10), (3.11), and (3.14), the conjugate directions can be generated iteratively with the relation of the following form

$$\bar{d}_{i+1} = -\bar{g}_{i+1} + \alpha_{i+1}\,\bar{d}_i. \tag{3.15}$$

The constant, α_{i+1}, can be obtained by left-multipling Equation (3.15) with $\bar{d}_i^T$

$$\alpha_{i+1} = \frac{\bar{d}_i^T J \bar{g}_{i+1}}{\bar{d}_i^T J \bar{d}_i}$$

$$= -\frac{\bar{d}_i^T J \bar{g}_{i+1}}{\bar{d}_i^T J \bar{g}_i} \quad \text{(by Equations (3.15) and (3.10))}$$

$$= -\frac{(\bar{P}_{i+1} - \bar{P}_i)^T J \bar{g}_{i+1}}{(\bar{P}_{i+1} - \bar{P}_i)^T J \bar{g}_i} \quad \text{(by Equation (3.11))}$$

$$= -\frac{(\bar{g}_{i+1} - \bar{g}_i)^T \bar{g}_{i+1}}{(\bar{g}_{i+1} - \bar{g}_i)^T \bar{g}_i} \quad \text{(by Equation (3.7))}$$

$$= \frac{\bar{g}_{i+1}^T \bar{g}_{i+1}}{\bar{g}_i^T \bar{g}_i}$$

$$= \frac{\text{the inner product of the gradient vector at current iteration}}{\text{the inner product of the gradient vector at previous iteration}}$$

The method of conjugate gradients is qualitively illustrated in Figure 25, part b.

The conjugate gradient method can be applied to a general function provided we can (a) find the minimum of this function along a line and (b) evaluate the gradient vector at a point. The use of this method for general functions was suggested by Fletcher and Reeves.[14] The algorithm is summarized in the following:

(1) Let vector $\bar{P}_1$ = initial values of parameter.

Compute $\bar{g}_1 = \bar{\nabla}E(\bar{P}_1)$.

Set $\bar{d}_1 = -\bar{g}_1$, this is the direction of steepest descent.

(2) For k = 2, 3, . . ., Np + 2 iterations

a. Set $\bar{P}_k = \bar{P}_{k-1} + \lambda_{k-1} \bar{d}_{k-1}$, where

b. λ_{k-1} minimizes $q_{k-1}(\lambda) = E(\bar{P}_{k-1} + \lambda_{k-1} \bar{d}_{k-1})$,

c. Compute $\bar{g}_k = \bar{\nabla} E(\bar{P}_k)$.

d. Unless k = Np + 2, let next conjugate direction be

$$\bar{d}_k = -\bar{g}_k + \frac{\bar{g}_k^T \bar{g}_k}{\bar{g}_{k-1}^T \bar{g}_{k-1}} \bar{d}_{k-1}$$

and repeat (a).

(3) Replace $\bar{P}_1$ by $\bar{P}_{Np+2}$ and restart the iteration.

(4) The criteria to stop the procedure are:

a. If any $|\bar{g}_k|$ vanishes, the iteration must stop. This is done both to avoid division by zero in the next iteration and because this is the formal requirement for $\bar{P}$ to be at a minimum.

b. If $E(P_k)$ is less than the pre-specified value.

c. If the number of iterations exceeds a pre-specified number.

3.3 The Method for Calculating the Frequency Response and Its Sensitivity to Parameter Changes

It is assumed that the nuclear system to be investigated can be described by a system of linear differential equations with constant coefficients as Equation (1.2). The equation is repeated as follows:

$$A\dot{\bar{x}} = B\bar{x} + \bar{f}g \qquad (3.16)$$

upon Laplace transforming Equation (3.16) and rearranging the following is obtained:

$$sA\ \bar{X}(s) = B\ \bar{X}(s) + \bar{f}g(s) \tag{3.17}$$

$$\bar{G}(s) = \frac{\bar{X}(s)}{g(s)} = (sA - B)^{-1}\ \bar{f} \tag{3.18}$$

where

s = Laplace transform variable

$\bar{X}(s)$ = the transformed state variable (nx1) vector

$\bar{G}(s)$ = the transfer function, which relates the output to its input (nx1) vector.

The frequency response $\bar{G}(s)$, at a particular angular frequency ω_ℓ, is obtained by replacing s by $j\omega_\ell$ ($j = \sqrt{-1}$).

The system coefficients a_{ij} and b_{ij} are algebraically related to the parameters, P_i. From this algebraic relation, we can get the frequency response $\bar{G}(s)$ sensitivity with respect to parameters as follows:

$$\frac{\partial \bar{G}(s)}{\partial P_i} = \sum_{j=1}^{n} \sum_{m=1}^{n} \left[\frac{\partial \bar{G}(s)}{\partial a_{jm}} \frac{\partial a_{jm}}{\partial P_i} + \frac{\partial \bar{G}(s)}{\partial b_{jm}} \frac{\partial b_{jm}}{\partial P_i}\right] \tag{3.19}$$

where the sensitivities $\frac{\partial \bar{G}(s)}{\partial a_{jm}}$ and $\frac{\partial \bar{G}(s)}{\partial b_{jm}}$ are obtained from Equation (3.17) by differentiating with respect to a_{jm} and b_{jm}, respectively. The results are as follows:

$$\frac{\partial \bar{G}(s)}{\partial a_{jm}} = -s(sA - B)^{-1} \frac{\partial A}{\partial a_{jm}} \bar{G}(s) \tag{3.20}$$

$$\frac{\partial \bar{G}(s)}{\partial b_{jm}} = (sA - B)^{-1} \frac{\partial B}{\partial b_{jm}} \bar{G}(s). \tag{3.21}$$

Thus, little additional calculation is required to determine the sensitivities since the inverse of the matrix $(sA - B)^{-1}$ has already been determined in the calculation of the frequency response, $\bar{G}(s)$, and the frequency response vector is available.

In the PARAPE code, the algebraic relation between the a_{jm} and b_{jm} coefficients and the parameters, P_i, is handled by a device called the algebra table.[15] In the algebra table, the user specifies coefficients which relate appropriate elements of A and B to the parameters, P_i, as follows:

$$S = F_1 P_1^{t_{11}} P_2^{t_{12}} \ldots + F_2 P_1^{t_{21}} P_2^{t_{22}} \ldots + \ldots$$

where

$S = a_{jm}$ or b_{jm} as the case may be

F = a constant

t = a constant power

This may also be written

$$S = \sum_{q=1}^{M} F_q \prod_{k=1}^{Np} P_k^{t_{qk}} \tag{3.22}$$

where

M = number of terms.

The general rule for differentiating terms of this type leads to:

$$\frac{\partial S}{\partial P_i} = \sum_{q=1}^{M} F_q \, t_{qi} \, P_i^{-1} \, \delta_i^q \prod_{k=1}^{Np} P_k^{t_{qk}} \tag{3.23}$$

where

$\delta_i^q = 1$, if P_i appears in the qth term and

$= 0$, if P_i does not appear in the qth term.

The PARAPE code uses the relationships between S and P_i as shown in Equations (3.22) and (3.23) to calculate the quantities $\frac{\partial a_{jm}}{\partial P_i}$ and $\frac{\partial b_{jm}}{\partial P_i}$ which are needed in Equation (3.19).

The quantities $R_{c\ell}$, $I_{c\ell}$, $\frac{\partial R_{c\ell}}{\partial P_i}$, and $\frac{\partial I_{c\ell}}{\partial P_i}$ shown in Equations (3.1) and (3.3) can be related to $\bar{G}(s)$ and $\frac{\partial \bar{G}(s)}{\partial P_i}$ as follows:

a. Select the state variable, X_d. which will be measured in the test.

b. Select the frequencies, ω_ℓ ($\ell = 1, 2, \ldots N$).

c. Replace s by $j\omega_\ell$ in Equations (3.18) and (3.19).

d. Then, we have the following relations

$$R_{c\ell} = \text{Real } [G_d(j\omega_\ell)] \tag{3.24a}$$

$$I_{c\ell} = \text{Imaginary } [G_d(j\omega_\ell)] \tag{3.24b}$$

$$\frac{\partial R_{c\ell}}{\partial P_i} = \text{Real } [\frac{\partial G_d(j\omega_\ell)}{\partial P_i}] \tag{3.24c}$$

$$\frac{\partial I_{c\ell}}{\partial P_i} = \text{Imaginary } [\frac{\partial G_d(j\omega_\ell)}{\partial P_i}]. \tag{3.24d}$$

3.4 The Application of the Partitioned Matrix Technique in the Optimization Scheme

The most time-consuming steps in each iteration of the parameter optimization is the calculation of the error function, E, in Equation (3.1) and the gradient, $\frac{\partial E}{\partial P_i}$, in Equation (3.3) for every new parameter

vector. It is necessary to invert a large complex matrix, $(j\omega_{\ell} A - B)$, in Equation (3.18) for each step to find the minimum along each new descent direction.

The number of multiplications and additions required to invert a matrix by standard computer subroutines is of order $(n)^3$.[16] Normally, the order of the system ranges from 10 up to 100. The amount of work to complete the optimization procedure is approximately equal to the number of frequency points x number of descent directions x number of steps in finding minimum along each descent direction $x\ n^3$.

In practice, only a few important design parameters (such as temperature coefficients, void coefficients, pressure coefficients and heat transfer coefficients) need to be adjusted in order to fit the response from the model to experimental results. The rest of the parameters in the system either have no significant effect on the measured state variable or can be accurately estimated. In effect one wishes to "fit" the theoretical model as closely as possible to the actual system response. The system has only a few variables which can be measured. It is not possible to adjust all the elements in the system matrix at the same time. It is best to adjust a few parameters which are sensitive to the input and output. In this case, then we can shift all the elements of matrices A and B which relate to the parameters under study to the upper-left corner of the matrix. Only the small sub-matrix which involves the

adjustable parameters must be inverted in each step. If the order of the sub-matrix is reduced by half, one-eighth as much computer time will be needed to invert the resultant matrix.

The Partitioned Matrix Algorithm

From the algebra table, the elements of matrix A and B which relate to the parameters can be identified. Then, by elementary column/row exchange operations, the elements of matrices A and B which contain the parameters can be shifted to the upper left corner. It will be proven in Appendix C that the system response is not affected by these operations in any way.

After these elementary column/row exchange operations are applied to Equation (3.17), the following partitioned matrix equation will be obtained:

$$s\begin{bmatrix} A_{11} & A_{12} \\ A_{21} & A_{22} \end{bmatrix}\begin{bmatrix} \bar{X}_1 \\ \bar{X}_2 \end{bmatrix} = \begin{bmatrix} B_{11} & B_{12} \\ B_{21} & B_{22} \end{bmatrix}\begin{bmatrix} \bar{X}_{11} \\ \bar{X}_{21} \end{bmatrix} + \begin{bmatrix} \bar{f}_1 \\ \bar{f}_2 \end{bmatrix} g \qquad (3.25)$$

(Note: $\bar{X}_1$, $\bar{X}_2$, and g are functions of s.)

Let IDIM be the dimension of A_{11} and B_{11}.

$s = j\omega$

$\bar{X}_1$ = the final state variables shifted into first IDIM rows of state variable vector $\bar{X}$. (It includes the measured state variables.)

$\bar{X}_2$ = the rest of state variable which are not in $\bar{X}_1$.

A_{11} (or B_{11}) = the sub-matrices which contain all the elements of A (or B) with the parameter. Dimension (IDIM x IDIM).

MN = n - IDIM

A_{12} (or B_{12}) = the system partitioned submatrix with Dimension (IDIM x MN)

A_{21} (or B_{21}) = the system partitioned submatrix with Dimension (MN x IDIM)

A_{22} (or B_{22}) = the system partitioned submatrix with Dimension (MN x IDIM)

$\bar{f}_1$ = the forcing terms corresponding to $\bar{X}_1$ (IDIM x 1) vector.

$\bar{f}_2$ = the forcing terms corresponding to $\bar{X}_2$ (MN x 1) vector.

By simple matrix operations, Equation (3.25) gives

$$sA_{11}\,\bar{X}_1 + sA_{12}\,\bar{X}_2 = B_{11}\,\bar{X}_1 + B_{12}\,\bar{X}_2 + \bar{f}_1\,g \qquad (3.26)$$

$$sA_{21}\,\bar{X}_1 + sA_{22}\,\bar{X}_2 = B_{21}\,\bar{X}_1 + B_{22}\,\bar{X}_2 + f_2\,g. \qquad (3.27)$$

Solve Equation (3.27) for $\bar{X}_2$, to obtain:

$$\bar{X}_2 = C^{-1}\,D\,\bar{X}_1 + C^{-1}\,\bar{f}_2\,g \qquad (3.28)$$

where

$C = sA_{22} - B_{22}$

$D = -sA_{21} + B_{21}$.

Normally, the matrix C is non-singular. In order to eliminate the possibility that C is a singular matrix, a simple subroutine can be included which will check the rows and columns of C and the subroutine will shift the row (or column) that all the elements are zeros to the upper-left corner of C. The program will increase the

dimension of sub-matrix A_{11} and B_{11} to include the shifted row (or column) accordingly (see Chapter 4, page 121, for an example).

Substitute $\bar{X}_2$ in Equation (3.21) by the solution in Equation (3.28) and rearrange to obtain

$$\bar{G}_1(s) = \frac{\bar{X}_1}{g} = [s(A_{11} + H) - (B_{11} + F)]^{-1} \bar{h} \tag{3.29}$$

where

$$H = A_{12} C^{-1} D \qquad \text{(IDIM x IDIM) matrix} \tag{3.30}$$

$$F = B_{12} C^{-1} D \qquad \text{(IDIM x IDIM) matrix} \tag{3.31}$$

$$\bar{h} = \bar{f}_1 + B_{12} C^{-1} \bar{f}_2 - sA_{12} C^{-1} \bar{f}_2 \qquad \text{(IDIM x 1) vector.} \tag{3.32}$$

(Because C^{-1} and D are functions of s, so are H, F, and $\bar{h}$). By differentiating Equation (3.29) with respect to a_{11jm} and b_{11jm}, respectively, we have the following equations:

$$\frac{\partial \bar{G}_1(s)}{\partial a_{11jm}} = - [s(A_{11} + H) - (B_{11} + F)]^{-1} s(\frac{\partial A_{11}}{\partial a_{11jm}}) \bar{G}_1(s) \tag{3.33}$$

$$\frac{\partial \bar{G}_1(s)}{\partial b_{11jm}} = [s(A_{11} + H) - (B_{11} + F)]^{-1} (\frac{\partial B_{11}}{\partial b_{11jm}}) \bar{G}_1(s). \tag{3.34}$$

Thus, just like the case without partitioning, little additional calculation is required to calculate the sensitivities.

The quantities $R_{c\ell}$, $I_{c\ell}$, $\frac{\partial R_{c\ell}}{\partial P_i}$, and $\frac{\partial I_{c\ell}}{\partial P_i}$ which are required for the calculation of the error function, E, and gradient, $\bar{\nabla}E$, in the optimization algorithm can be obtained from Equations (3.29), (3.33), and (3.34) by the procedure described in Section 3.3, page

Only at the initial step do we have to invert the matrix C with dimension MN for the calculation of matrices H, F, and h in Equations (3.30), (3.31), and (3.32). It is clear from Equations (3.29), (3.33), and (3.34) that for the following steps in the optimization scheme, the matrix which has to be inverted is the complex matrix, $[s(A_{11} + H) - (B_{11} + F)]$, with dimension IDIM. The matrices A_{11} and B_{11} are the partitioned matrices with the parameters under study only. Since the dimension (IDIM) of the resultant sub-matrix is much smaller than the dimension (n) of the original system matrix, a significant computer time will be saved in the optimization. As will be demonstrated in the following chapters, this new algorithm makes the application practical for large linear dynamic system models.

3.5 Identifiability of the Parameters

It is very important to be able to estimate the identifiability of selected parameters prior to an experiment. Identifiability depends on questions of uniqueness, sensitivity and separability.

The uniqueness question deals with the mathematical possibility of determining parameters assuming perfectly accurate experimental data. For the case of a single input and a single output, established uniqueness criteria for identification of elements in the coefficient matrix (B of Equation (3.16)) with system models in which the A matrix of Equation (3.16) is the identity matrix. He found

a. Any (2n-1) coefficients can be determined uniquely if the initial guesses on these adjustable elements are close to the correct values.

b. Any two diagonal elements and (n-1) off-diagonal elements from any single row or column can be determined uniquely, regardless of the error in the initial guesses on these adjustable parameters.

Because of practical difficulties due to measurement inaccuracies, these rules only have limited usefulness. The problem of identifiability will be dealt with by considering the sensitivity and separability questions in the following.

As shown in Section 3.2, page 68, the minimum of the error function, E, is given by

$$\frac{\partial E}{\partial P_k} = 0 \qquad (k = 1, 2, \ldots, Np).$$

Changes in E can be related to changes in the parameters by expanding in a Taylor series as follows:

$$\Delta E = \sum_{k=1}^{Np} \frac{\partial E}{\partial P_k} \Delta P_k + \sum_{k=1}^{Np} \sum_{j=1}^{Np} \frac{\partial^2 E}{\partial P_k \partial P_j} \Delta P_k \Delta P_j$$

$$+ \text{higher order terms.}$$

If we neglect the higher order terms, then at the point where E is a minimum ($\frac{\partial E}{\partial P_k} = 0$), we obtain

$$\Delta E = \sum_{k=1}^{Np} \sum_{j=1}^{Np} \frac{\partial^2 E}{\partial P_k \partial P_j} \Delta P_k \Delta P_j = \Delta \bar{P}^T J \Delta \bar{P}. \tag{3.35}$$

Differentiate Equation (3.1) with respect to P_k and P_j, we have:

$$J_{kj} = \frac{\partial^2 E}{\partial P_k \partial P_j} = -2 \sum_{\ell=1}^{N} \left[\frac{(R_{p\ell} - R_{c\ell})}{\sigma_{k\ell}^2} \frac{\partial^2 R_{c\ell}}{\partial P_k \partial P_j} - \frac{1}{\sigma_{R\ell}^2} \frac{\partial R_{c\ell}}{\partial P_k} \frac{\partial R_{c\ell}}{\partial P_j}\right]$$

$$- 2 \sum_{\ell=1}^{N} \left[\frac{(I_{P\ell} - I_{c\ell})}{\sigma_{I\ell}^2} \frac{\partial^2 I_{c\ell}}{\partial P_k \partial P_j} - \frac{1}{\sigma_{I\ell}^2} \frac{\partial I_{c\ell}}{\partial P_k} \frac{\partial I_{c\ell}}{\partial P_j}\right]. \tag{3.36}$$

The first term inside the square bracket may be ignored since $(R_{P\ell} - R_{c\ell})$ and $(I_{P\ell} - I_{c\ell})$ will be small near the optimized parameter vector. This approximation is quite valid for many practitional cases. So,

$$J_{kj} = 2 \sum_{\ell=1}^{N} \left(\frac{1}{\sigma_{R\ell}^2} \frac{\partial R_{c\ell}}{\partial P_k} \frac{\partial R_{c\ell}}{\partial P_j} + \frac{1}{\sigma_{I\ell}^2} \frac{\partial I_{c\ell}}{\partial P_k} \frac{\partial I_{c\ell}}{\partial P_j}\right)$$

$$= \sum_{\ell=1}^{N} \left(\frac{\partial^2 E}{\partial P_k \partial P_j}\right)_{\ell} = \sum_{\ell=1}^{N} J_{kj\ell}. \tag{3.37}$$

There are no additional computations beyond those previously described to provide J_{kj}. All of the quantities in Equation (3.37) are known during the optimization steps.

When j equals k, J_{kk}, represents the curvature of the error function along the parameter P_k at the minimum. (For the curvature of the error function based on gain and phase angle, see Appendix A.) If the surface is steep, the curvature is large, and the accuracy with which the parameter is estimated will be improved. This is because a small variation of the parameter in Equation (3.3) away from the optimum value will lead to a large variation of the error function. On the other hand, if the surface is shallow, the curvature is small and the accuracy with which the parameter is estimated will be low. In this way, the calculation of the curvature at the minimum could provide useful information for investigating the goodness of parameter estimates.

It is useful to demonstrate these concepts using a two parameter example. In that case, Equation (3.35) gives:

$$\Delta E = \Delta \bar{P}^T \begin{bmatrix} J_{11} & J_{12} \\ J_{21} & J_{22} \end{bmatrix} \Delta \bar{P} \qquad \text{(Note: } J_{12} = J_{21}\text{)}$$

or

$$\Delta E = J_{11}\, \Delta P_1^{\,2} + 2\, J_{12}\, \Delta P_1\, \Delta P_2 + J_{22}\, \Delta P_2^{\,2}. \tag{3.38}$$

This shows that Equation (3.38) is a quadratic curve centered at the origin. The level surfaces (ellipses) of Equation (3.38) for various values of ΔE are shown in Figure 26. Notice that if J_{11} equals to J_{22}, the level surfaces are circles. In Figure 26, the ellipse with a dashed line is the level surfaces with ΔE equal to unity. $\overline{OP}$ and $\overline{OQ}$ are the axes of the ellipse. This

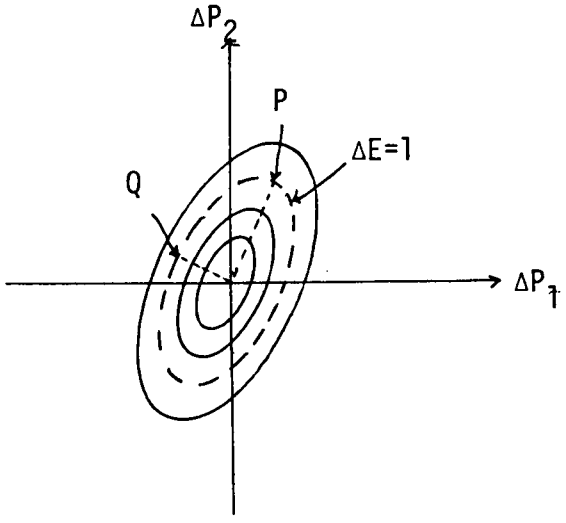


Figure 26. Level Surfaces for Different Values of ΔE.

contour map provides us with a pictorial presentation the accuracy with which the parameters can be determined. The off-diagonal element, J_{12}, gives the rate of change of the slope of the level surface (in a direction parallel to the P_2 direction) with respect to a change in P_1 direction.

If we know the rotation angle, θ, and the axes of the ellipse, then we can easily plot the level surfaces. A convenient procedure to get these important constants (for ΔE equal to unity) involves transforming the equation to a new set of perpendicular axes (R_1, R_2) rotated through an angle θ with respect to the old (P_1, P_2) axes, and such that the resulting equation has no cross terms in R_1 R_2. Let the orthonormal matrix, S, represent the transformation such that $K = S^T J S$ is the diagonal matrix. From standard references[16] we know that orthonormal matrix is given by

$$S = \begin{bmatrix} \cos\theta & -\sin\theta \\ \sin\theta & \cos\theta \end{bmatrix} \tag{3.39}$$

where

$$\theta = \frac{1}{2} \tan^{-1} \left(\frac{2 J_{12}}{J_{11} - J_{22}}\right). \tag{3.40}$$

Then, after the S transformation in the new axes (R_1, R_2) we have

$$1 = K_{11} \Delta R_1^2 + K_{22} \Delta R_2^2 \qquad (\text{for } \Delta E = 1) \tag{3.41}$$

and the axes of the ellipse are

$$\overline{OP} = \frac{1}{\sqrt{K_{11}}} \quad \text{and} \quad \overline{OQ} = \frac{1}{\sqrt{K_{22}}} \tag{3.42}$$

So, from the matrix, J, we can get the rotation angle, θ, and the axes of all ellipse by following the above procedures (from Equation

(3.38) to Equation (3.42)). Some particular cases for the matrix, J, will be discussed in the following.

Case a. Let $J_{12} = 0$, and $J_{11} > J_{22}$. For this case, the rotation angle is zero, and $\overline{OP}$ is smaller than $\overline{OQ}$. Figure 27 part a, shows that the parameter, P_1, can be better estimated (as compared to P_2), since a small variation of P_1 away from origin will cause a large variation of the error function.

Case b. Let $J_{12} = 0$ and $J_{11} < J_{22}$. For this case, the rotation angle is still zero, and $\overline{OP}$ is larger than $\overline{OQ}$ (see Figure 27, part b). So the parameter P_2 can be better estimated.

Case c. Let $J_{12} \neq 0$. Then, the rotation angle is not zero. Figure 27, part c, shows the possible situations for this case. For the ellipse with a solid line, the parameter P_1 can be better estimated. It is because that the rotation angle, θ_1, is larger than 45°, and the projection of the major axis on P_1 axes is smaller than the projection on P_2 axis. This means that, for the same amount of change of a parameter, P_1 will cause more variation in the error function than P_2. But, for the ellipse with a dashed line ($\theta_2 < 45°$), P_2 can be estimated.

The work on identifiability in this dissertation is closely related to results that have been obtained in research on stochastic processes. The accuracy obtainable from various estimators in stochastic processes is usually expressed in terms of the variance and covariance of the estimated parameters. Maximum likelihood estimation is one of the estimation methods developed for stochastic processes. The

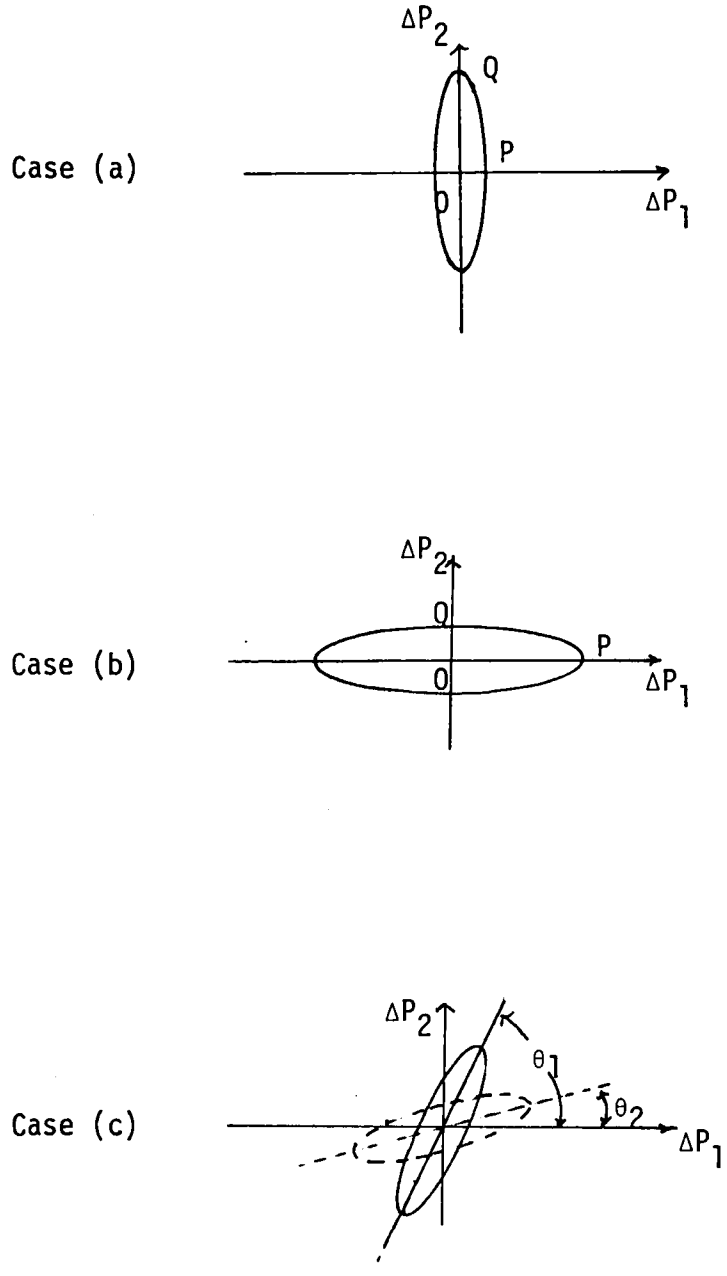


Figure 27. The Ellipses for Different Matrices, J.

identifiability question in maximum likelihood estimation is usually attached using the Fisher information matrix. The relation between the Fisher information matrix (generated from the maximum likelihood function) and the matrix, J, in Equation (3.35) will be briefly discussed in the following.

Maximum likelihood estimation is well described in the liter atures.[18] Before the measurement, we know that the random samples of $\bar{y}$ have the joint probability function, $\rho(\bar{y}; \bar{\xi})$ and $\bar{y}$ depends on the parameter, $\bar{\xi}$. (See Equation (3.43) for an example of the probability function form with a Gaussian distribution.) After the measurement, the functional relationship between the observed output, $\bar{G}_p = (G_{P1}, G_{P2}, \ldots G_{PN})$, and the estimated parameter, $\bar{P}$, is the same as given by the joint probability function. We write this dependence as $L(\bar{G}_p; \bar{P})$, where L is called likelihood function. The observed output values are given by the measurement, and the likelihood function is a function of the parameter vector, $\bar{P}$, only. The maximum likelihood estimates $\bar{P}$ of $\bar{\xi}$ are the parameters for which the likelihood function is maximized.

Let us take a one parameter case as an example. Let ξ be a parameter to be estimated and assume additive noise, n_ℓ, which has a Gaussian distribution such that the probability density function for the noise is:

$$\rho(n) = \frac{1}{(2\pi)^{1/2}\sigma} \exp\left[-\frac{n^2}{2\sigma^2}\right] \tag{3.43}$$

and

$$E[n] = 0, \quad E[n^2] = \sigma^2$$

where

E = expectation operator.

The observed output values are:

$$G_{P\ell} = f(\xi) + n_{\ell} \quad (\text{for } \ell = 1, 2, \ldots, N) \tag{3.44}$$

and let the output values from the model be given by

$$G_{C\ell} = f(P). \tag{3.45}$$

This leads to a likelihood function:

$$L(\bar{G}_p, P) = \prod_{\ell=1}^{N} \rho(G_{p\ell}, P)$$

$$= \frac{1}{(2\pi)^{N/2}\ \sigma^N} \prod_{\ell=1}^{N} \exp \frac{-[G_{p\ell} - f(P)]^2}{2\sigma^2}. \tag{3.46}$$

So the maximum likelihood estimate, P, of ξ is the value of P which will maximize Equation (3.46). Since the logarithmic function is monotonic, the maximum of $\ln L(\bar{G}_p, P)$ and the maximum of $L(\bar{G}_p, P)$ occur at the same value of P. By taking the logarithm of Equation (3.46), we have

$$\ln L(\bar{G}_p, P) = \text{constant} - \frac{1}{2\sigma^2} \sum_{\ell=1}^{N} [G_{P\ell} - f(P)]^2$$

$$= \text{constant} - \frac{1}{2\sigma^2} \sum_{\ell=1}^{N} (G_{P\ell} - G_{C\ell})^2. \tag{3.47}$$

The error function used in this dissertation has the same form as the second term at the right-hand side of Equation (3.47). Since the parameter P which minimizes E will maximize ln L, too, ln L and E provide the same information to indicate how well the parameter is estimated.

The so-called Fisher information matrix is defined as follows:

$$J = E[(\frac{\partial \ln L}{\partial \bar{P}})\ (\frac{\partial \ln L}{\partial \bar{P}})^T] = - E[\frac{\partial^2 \ln L}{\partial \bar{P} \partial \bar{P}^T}]. \tag{3.48}$$

By the Cramer-Rao inequality,[17,19] the covariance matrix (or uncertainty matrix) of the parameters has the following relationship:

$$\text{Cov}\ (\bar{P}) \geq J^{-1} \tag{3.49}$$

where the inverse of J is called the minimum variance bound matrix.

So the minimum achievable error (or the maximum achievable accuracy) of the kth parameter from this estimator is equal to the kth diagonal elements of the inverse of the Fisher information matrix, J. Notice that the matrix J in Equation (3.35) has the same form and meaning as the Fisher information matrix J in Equation (3.48).

The above discussion shows that to have a better estimation of the kth parameter, P_k, the curvature, J_{kk}, has to be as large as possible. As shown in Equation (3.37), J_{kk} is the summation of $J_{kk\ell}$ over the test frequencies. In order to find out whether the frequency range covered in a test includes sufficiently large values of $J_{kk\ell}$, it would be worthwhile to carry out a theoretical computation of $J_{kk\ell}$ over a wide frequency range. The extended frequency range which includes the frequency range of a test can be specified by the PARAPE code user. The optimized parameter values which are obtained by running the PARAPE code will be used in the theoretical model to calculate $J_{kk\ell}$ (for k = 1, 2, . . ., Np) over the extended frequencies. If the relatively larger values of $J_{kk\ell}$ do not appear

in the test frequency range, it suggests that the dynamic test should be redesigned to cover the frequencies where the large values appeared to provide the maximum information for the parameter identification. This will be illustrated in the demonstration problems in the following chapters.

CHAPTER 4

DEMONSTRATION OF THE METHOD-CASE STUDY I: OCONEE I NUCLEAR SYSTEM

4.1 Introduction

It is very important to check the validity of theoretical models which are derived from first principles. For that purpose, one must compare the response predicted by the theoretical model to that obtained from experiments on the plant. It is well known[20] that experimental data obtained from dynamic tests contain the information which can be used to adjust the important design parameters in the model.

Dynamic tests on the Oconee I nuclear power plant were performed by Kerlin and Katz.[21] Power demand perturbations in the form of periodic, binary (two-level) input signals were introduced into the plant control system to induce small control rod motions. The test data were processed by the HFFT computer code into the frequency domain for comparison with the theoretical frequency response.

To demonstrate the efficiency of the method which was developed in Chapter 3, page 76, the PARAPE* code was used for systemmatic adjustment of parameters of the theoretical model to obtain better agreement between theory and experiment.

---

*There are two versions of PARAPE code developed: (1) PARARI: the error function used as Equation (3.1) and (2) PARAGP: the error function used as Equation (A.1).

4.2 The Theoretical Model of the Oconee I System

Oconee I is an 886 MWe (2568 MWt) pressurized water reactor reactor located in northwestern South Carolina. It is owned and operated by Duke Power Company. The fuel is Zircaloy-4 clad UO_2. The reactor coolant, borated water, enters the core at 554°F and leaves at 606°F. There are two primary loops designated, A and B, each with a vertical once-through steam generator (OTSG A and OTSG B) that produce 910 psig , 570°F superheated steam when operating at full load. An electrically heated pressurizer in reactor coolant loop A will accomodate primary water volume changes and maintain the pressure at about 2185 psig. A schematic of the system is shown in Figure 28.

A linearized theoretical model was developed by Katz.[21] The overall model includes the neutronics, core heat transfer, mixing plenums in the core and steam generator (including primary fluid, tube metal, and secondary fluid), piping and pressurizer. The model's coefficients were evaluated using the data in Tables 4.1, 4.2, 4.3, and 4.4. The equations for each component are briefly described below.

Reactor and Core Heat Transfer Model.

A simplified core model (one fuel lump and two coolant lumps) will be used in this study. (For the detailed core model, see reference 21.) The reactor power was modeled using the point kinetics equations with six groups of delayed neutrons and reactivity feedbacks

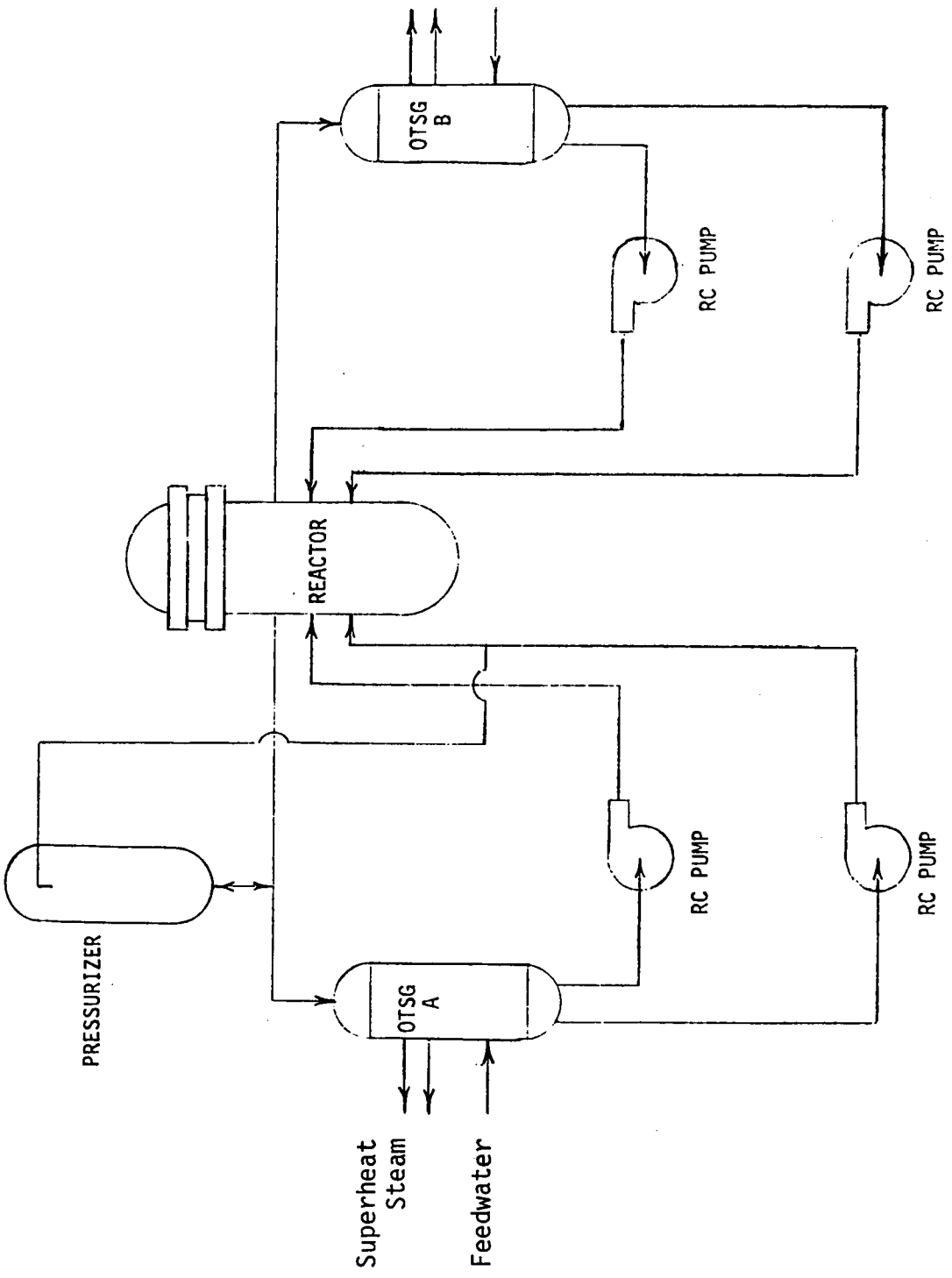


Figure 28. Schematic of Oconee I System.

TABLE 4.1

CORE DESIGN, THERMAL, AND HYDRAULIC DATA
OCONEE I FSAR[26]

REACTOR	
Type	Pressurized Water
Rated Heat Output, MWt	2568
Rated Electric Output, MWe	886
Vessel Coolant Inlet Temp, F	554
Vessel Coolant Outlet Temp, F	603.8
Core Outlet Temp, F	606.2
Operating Pressure, psig	2185
CORE AND FUEL ASSEMBLIES	
Total Number of Fuel Assemblies in Core	177
Number of Fuel Rods per Fuel Assembly	208
Number of Control Pins per Control Rod Cluster Assembly	16
Number of Incore Instrumentation Positions per Fuel Assembly	1
Fuel Rod Outside Diameter, in.	.430
Fuel Rod Pitch, in.	0.568
Fuel Assembly Pitch Spacing, In.	8.587
Unit Cell (Metal/Water) Ratio	0.82
Clad Material	Zircaloy-4

TABLE 4.1 (Continued)

FUEL	
Material	UO_2
Form	Dished-end, cylindrical pellets
Diameter, in.	0.370
Active Length, in.	144
Density, percent of theoretical-	
Unit I, Core 1	93.5
HEAT TRANSFER AND FLUID FLOW AT RATED POWER	
Total Heat Transfer Surface in Core, ft^2	49,734
Average Heat flux, Btu/hr-ft^2	171,470
Maximum Heat Flux, Btu/hr-ft^2	543,440
Average Power Density in Core, kw/ℓ	83.38
Average Thermal Output, kw/ft of fuel rod	5.656
Maximum Thermal Output, kw/ft of fuel rod	17.63
Maximum Clad Surface Temp, F	654
Average Core Fuel Temp, F	1,540
Maximum Fuel Central Temp at Hot Spot, F	4,250

TABLE 4.1 (Continued)

Total Reactor Coolant Flow, lb/hr	131.32×10^6
Core Flow Area (effective for heat transfer), ft^2	49.19
Core Coolant Average Velocity, fps	15.73
Coolant Outlet Temp at Hot Channel, F	647.1

TABLE 4.2

NUCLEAR DESIGN DATA OCONEE I FSAR[26]

FUEL ELEMENT VOLUME FRACTIONS	
Fuel	0.303
Moderator	0.580
Zircaloy	0.102
Stainless Steel	0.003
Void	0.012
	1.000
TOTAL UO_2, metric tons	94.1
CORE DIMENSION, in.	
Equivalent Diameter	128.9
Active Height	144.0
UNIT CELL H_2O TO U ATOMIC RATIO	
Cold	2.85
Hot	2.04
FUEL LOADING, wt percent U-235	
Core Average First Cycle	2.10

TABLE 4.3

REACTOR VESSEL DESIGN DATA OCONEE I FSAR[26]

Design/Operating Pressure, psig	2500/2185
Design/Operating Temperature, °F	650/600
Overall Height of Vessel and Closure Head, ft-in	40-8 3/4
Water Volume, ft^3	4058

TABLE 4.4

STEAM GENERATOR DESIGN DATA OCONEE I FSAR[26]

Item	Data Per Unit
Design Pressure, Reactor Coolant/	
Steam, psig	2500/1050
Design Temperature, Reactor Coolant/	
Steam, °F	650/600
Reactor Coolant Flow, lb/hr	65.66×10^6
Steam Conditions at Full Load,	
Outlet Flow, lb/hr	5.6×10^6
Temperature, °F	570 (35 deg superheat)
Pressure, psig	910
Feedwater Temperature, °F	460
Overall Height, ft-in	72-2 1/2
Shell OD, in	151 1/8
Reactor Coolant, Volume, ft^3	2030
Mass of Metal, lbm	1.88×10^5
Heat Transfer Area (tube OD)	66,234
Superheat (degrees F)	
15 percent power	50
100 percent power	32
Fraction of OTSG devoted to superheating	
15 percent power	.85
100 percent power	.28

due to changes in fuel temperature, coolant temperature, and primary coolant system pressure. The linearized equations are:

$$\frac{d\ \delta P/P_o}{dt} = -\frac{\beta}{\Lambda}\delta P/P_o + \sum_{i=1}^{6} \lambda_i\ \delta\ C_i/P_o + \frac{\alpha_f}{\Lambda}\delta\ T_f$$

$$+ \frac{\alpha_P}{\Lambda}\delta P_p + \frac{\alpha_c}{\Lambda}\delta T_1 + \frac{1}{\Lambda}\delta\rho_{rod} \qquad (4.1)$$

$$\frac{d\ \delta C_i/P_o}{dt} = \frac{\beta_i}{\Lambda}\delta P/P_o - \lambda_i\ \delta C_i/P_o \qquad (i = 1, \ldots, 6) \qquad (4.2)$$

where

δ = deviation of state variable from equilibrium conditions

P = power, MWt

P_o = initial steady state power, MWt

β = total delayed neutron fraction

β_i = delayed neutron fraction for the ith group

λ_i = decay constant for the ith delayed neutron group

C_i = ith precursor concentration

α_f = Doppler coefficient, $\Delta k/k/°F$

α_c = coolant temperature coefficient of reactivity, $\Delta k/k/°F$

α_p = coolant pressure coefficient of reactivity, $\Delta k/k/psi$

T_f = fuel temperature, °F

T_1 = average temperature of coolant in core, °F

P_p = primary system pressure, psi

ρ_{rod} = reactivity due to control rod movement

Λ = neutron generation time, sec.

The core heat transfer model used a Mann's nodal[22] approximation for fuel and coolant temperature nodes as shown in Figure 29. Two well stirred coolant nodes are used for a fuel node to obtain a good approximation of the heat transfer driving force between fuel and coolant. The set of equations is as follows.

$$\frac{d}{dt}\delta T_f = \frac{(hA)_{fc}}{(MC_p)_f}(\delta T_f - \delta T_1) + P_o\frac{(\delta P/P_o)}{(MC_p)_f} \tag{4.3}$$

$$\frac{d}{dt}\delta T_1 = \frac{(hA)_{fc}}{2(MC_p)_c}(\delta T_f - \delta T_1) + \frac{2}{\tau_c}(\delta T_4 - \delta T_1) \tag{4.4}$$

$$\frac{d\delta T_2}{dt} = \frac{(hA)_{fc}}{2(MC_p)_c}(\delta T_f - \delta T_1) + \frac{2}{\tau_c}(\delta T_1 - \delta T_2) \tag{4.5}$$

where

T_4 = temperature of reactor coolant in lower plenum, °F

$(MC_p)_f$ = product of mass and specific heat of fuel, $\frac{MW\ sec}{°F}$

$(MC_p)_c$ = product of mass and specific heat of coolant, $\frac{MW\ sec}{°F}$

τ_c = residence time of coolant in core, sec

$(hA)_{fc}$ = product of effective heat transfer coefficient from fuel to coolant and heat transfer area, $\frac{MW}{°F}$.

Piping and Plenums

The temperature of the reactor coolant in the upper and lower plenums is given by the following well mixed tank models:

$$\frac{d\ \delta T_3}{dt} = \frac{1}{t_3}(\delta T_2 - \delta T_3) \tag{4.6}$$

$$\frac{d\ \delta T_4}{dt} = \frac{1}{t_4}(\delta T_6 - \delta T_4) \tag{4.7}$$

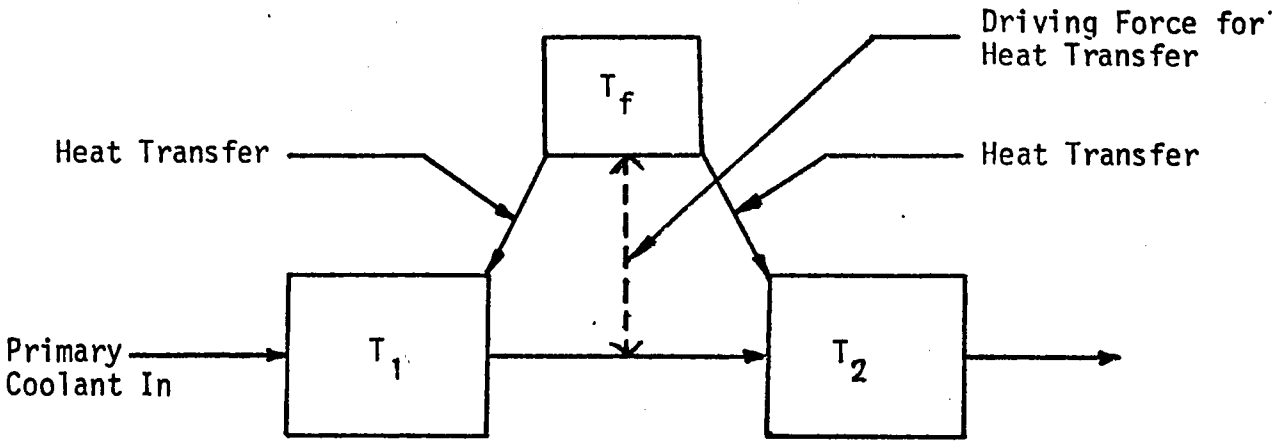


Figure 29. Schematic of Fuel-Coolant Heat Transfer Model.

where

T_3 = temperature of the coolant in upper plenum, °F

T_4 = temperature of the coolant in lower plenum, °F

T_6 = temperature of coolant in cold leg piping, °F

t_3 = coolant residence time in upper plenum, sec

t_4 = coolant residence time in lower plenum, sec.

The equations which describe the temperature of the reactor coolant in hot and cold leg piping are:

$$\frac{d\ \delta T_5}{dt} = \frac{1}{t_5} (\delta T_2 - \delta T_5) \tag{4.8}$$

$$\frac{d\ \delta T_6}{dt} = \frac{1}{t_6} (\delta T_{P4} - \delta T_6) \tag{4.9}$$

where

T_5 = temperature of coolant in hot let piping, °F

T_{P4} = temperature of coolant leaving the steam generator, °F

t_5 = coolant residence time in hot leg piping, sec

t_6 = coolant residence time in cold leg piping, sec.

Steam Generator

The once through steam generator is a vertical, straight-tube- and shell heat exchanger. It is designed to produce superheated steam at constant pressure over the full range of operating power levels. There are four different characteristic heat transfer regions. These four regions are: (1) feedwater heating, (2) nucleate boiling, (3) film boiling, and (4) superheating. The most unique feature of

the steam generator is the part of the high temperature steam in the superheating section will be drawn through the port back into the downcomer annulus to heat the feedwater to saturation. The steam generator design data are listed in Table 4.4.

A moving boundary, lumped model of the once through steam generator (OTSG) was developed by Chen[23] using the following basic assumptions.

1. Constant flow rate on the primary coolant side.
2. One-dimensional flow of the primary and secondary side.
3. Negligible heat conduction in the direction of flow.
4. Constant compressibility factors in the steam region.
5. Average material properties (density, temperature, etc.) are used in each region.
6. Constant Martinelli and Nelson correlation for the frictional pressure drop calculation is used in the two-phase region.
7. Constant orifice coefficients for feedwater entering the downcomer are used.
8. The saturation temperature of the secondary coolant is pressure dependent.

The steam generator model takes one typical tube and divides it into a boiling and superheating section. In each section, the primary water is further divided into two equal well-stirred regions with different average temperatures (T_{pi}), and the tube wall (T_{wi}) section for each region is treated as a single lump. The superheating section of the secondary coolant consists of two equal lumps with

different temperatures (T_{si}). The boiling length X_b is a calculated state variable. Also, included in the model is the rate, W_b, at which steam is drawn back into the downcomer to heat the feedwater to saturation. This rate is determined by the heat energy needed to bring the feedwater up to saturation conditions. Figure 30 shows this division schematically.

The development of the model equations were based on mass, momentum, and energy balances in each section. After rearrangement and mathematical manipulation, the non-linear equations were linearized resulting in a theoretical model with fourteen state variables (see Reference 23 for detailed development).

Pressurizer

The pressurizer model[24] is based on mass, energy, and volume balances and the assumption that saturation conditions always apply for the steam-water mixture in the pressurizer. The rate of change of the pressure, P_p, in the pressurizer can be expressed as follows:

$$\frac{d P_p}{dt} = f (P_p, W_w, q, W_{sp}) \qquad (4.10)$$

where

W_w = mass flow of water into (or out of) the pressurizer

q = rate of heat addition to the pressurizer fluid with electric heaters

W_{sp} = mass flow rate of spray.

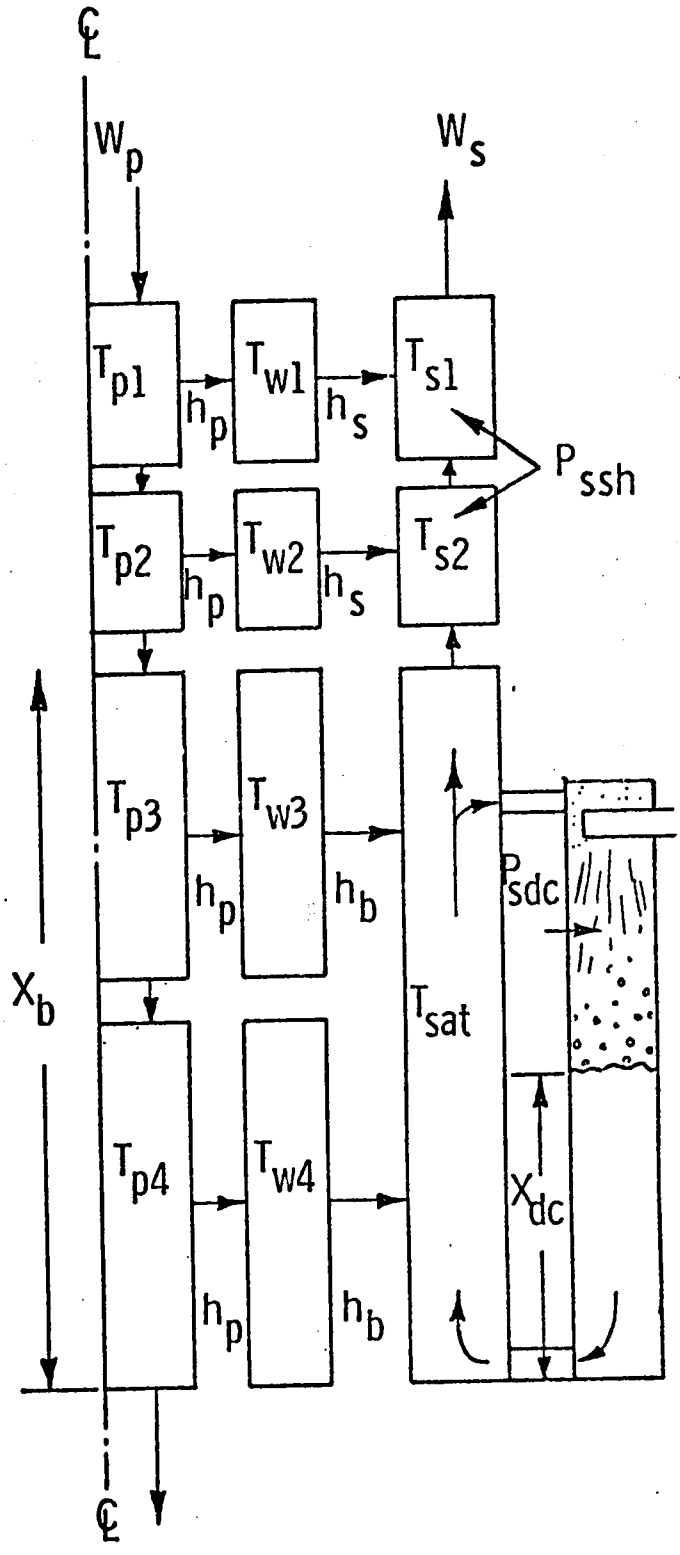


Figure 30. Model of Oconee I Once Through Steam Generator.

The mass change in the pressurizer is obtained by summing the contributions due to expansion (or contraction) of the coolant in each node in the primary loop as follows:

$$\delta M_w = \sum_{i=1}^{6} V_i \gamma_i \delta T_i + \sum_{j=1}^{4} V_{Pj} \gamma_{Pj} \delta T_{Pj}$$

or

$$\delta W_w = \sum_{i=1}^{6} V_i \gamma_i \frac{d\ \delta T_i}{dt} + \sum_{j=1}^{4} V_{Pj} \gamma_{Pj} \frac{d\ \delta T_{Pj}}{dt} \qquad (4.11)$$

where

V_i = Volume of ith primary coolant node

V_{Pj} = Volume of jth primary coolant node in OTSG (see Figure 30)

γ = Slope of coolant density versus temperature curve.

In this case study, the quantities q and W_{sp} are assumed to be at steady state. After mathematical manipulation, the non-linear Equation (4.10) is linearized (see reference 24 for details). Then after Equation (4.10) is linearized and δW from Equation (4.11) is substituted, we obtain a linear differential equation which relates P_p to the other state variables. Coefficients for the pressurizer equation are shown in Table 4.6.

Overall System

The set of differential equations which has been developed to represent the components can be cast into state variable form:

$$A \frac{d\bar{x}}{dt} = B\bar{x} + \bar{f}g$$

where

$$\bar{X} = \begin{bmatrix} X_1 \\ X_2 \\ \cdot \\ \cdot \\ \cdot \\ X_{29} \end{bmatrix} = \begin{bmatrix} \delta P/P_o \\ \delta C_1/P_o \\ \cdot \\ \cdot \\ \cdot \\ \delta C_6/P_o \end{bmatrix} = \text{the state variable vector}$$

A = identity matrix

B = matrix of constant coefficients which are calculated by using reference parameters values

$$\bar{f} = \begin{bmatrix} \delta f_1 \\ \delta f_2 \\ \cdot \\ \cdot \\ \cdot \\ \delta f_{29} \end{bmatrix} = \begin{bmatrix} \delta \rho_{rod} \\ 0 \\ \cdot \\ \cdot \\ \cdot \\ 0 \end{bmatrix} = \text{the forcing vector.}$$

For the reactivity perturbation case, only the first element of the forcing vector is non-zero. The indices of the state variables of the model are listed in Table 4.5 and the values of non-zero elements of the B matrix, b_{ij}, is given in Table 4.6. The frequency response was computed using the SFR-3 code,[15] and the results are plotted in Figure 31.

4.3 Experimental Results[21]

A pseudo binary input signal with 127 bits and a bit time of 1 sec was used in the test to obtain the transfer function between the reactivity and power level for Oconee I. The power variation

TABLE 4.5

STATE VARIABLE INDEX FOR OCONEE I SYSTEM

Number	State Variable	Definition
1	P	Power
2	C_1	1st precursor concentration
3	T_f	Fuel temperature
4, 5	T_1, T_2	Reactor coolant temperature
6	T_3	Temperature of coolant in upper plenum
7	T_5	Temperature of coolant in hot leg piping
8	T_6	Temperature of coolant in cold leg piping
9	T_4	Temperature of coolant in lower plenum
10	P_p	Pressurizer pressure
11-14	T_{P1}-T_{P4}	Primary coolant temperatures
15-18	T_{w1}-T_{w4}	Tube wall temperatures
19, 20	T_{s_1}, T_{s_2}	Steam temperatures
21	X_b	Boiling length
22	P_{ssh}	Superheated steam pressure
23	X_{dc}	Downcomer column height
24	P_{sdc}	Downcomer fluid pressure
25-29	C_2-C_6	2nd to 6th precursor concentrations

TABLE 4.6

OCONEE I SYSTEM COEFFICIENT MATRIX

I	J	Value	I	J	Value
1	1	-2.76000E 02	1	2	1.25000E-02
1	3	-4.40000E-01	1	4	-8.00000E-01
1	25	3.08000E-02	1	26	1.14000E-01
1	27	3.07000E-01	1	28	1.19000E 00
1	29	3.19000E 00	2	1	8.36000E 00
2	2	-1.25000E-02	3	1	1.88890E 02
3	3	-2.00900E-01	3	4	2.00900E-01
4	3	6.30000E-02	4	4	-2.69500E 00
4	9	2.63200E 00	5	3	6.30000E-02
5	4	2.56900E 00	5	5	-2.63200E 00
6	5	4.80200E-01	6	6	-4.80200E-01
7	6	9.00000E-01	7	7	-9.00000E-01
8	8	-8.37000E-01	8	14	8.37000E-01
9	8	4.80200E-01	9	9	-4.80200E-01
10	3	1.81100E-02	10	4	-2.13600E-02
10	5	1.17960E-01	10	6	1.58650E-02
10	7	8.56900E-01	10	8	-1.92000E-03
10	9	1.14360E-01	10	10	-1.19300E-06
10	11	-6.56100E-01	10	12	-1.63800E 00
10	13	-6.55900E-01	10	14	-7.73800E-01
10	15	6.56100E-01	10	16	6.56100E-01
10	17	4.45130E-01	10	18	4.45150E-01
10	21	-4.59300E-01	10	22	-8.74400E-01
10	23	2.94370E-01	10	24	9.26180E-01
11	7	2.34400E 00	11	11	-3.36700E 00
11	15	1.02300E 00	11	21	1.46100E-01
12	11	2.34400E 00	12	12	-3.36700E 00
12	16	1.02300E 00	12	17	-2.14200E-02
12	18	-2.14200E-02	12	21	2.37200E-01
12	22	-8.87900E-02	12	23	2.98900E-02
12	24	9.40199E-02	13	12	8.12300E-01
13	13	-1.83500E 00	13	17	7.88200E-01
13	18	-2.34900E-01	13	21	-7.23500E-01
13	22	-9.73300E-01	13	23	3.27700E-01
13	24	1.03100E 00	14	13	8.12300E-01
14	14	-1.83500E 00	14	17	-7.27100E-02
14	18	9.50400E-01	14	21	-3.75900E-01
14	22	-3.01300E-01	14	23	1.01400E-01
14	24	3.19100E-01	15	11	4.44000E 00
15	15	-4.91000E 00	15	17	-2.13900E-02
15	18	-2.13900E-02	15	19	4.69900E-01
15	21	-2.11800E-02	15	22	-8.86199E-02
15	23	2.98300E-02	15	24	9.38500E-02

TABLE 4.6 (Continued)

I	J	Value	I	J	Value
16	12	4.44000E 00	16	16	-4.91000E 00
16	17	-5.80300E-01	16	18	-5.80300E-01
16	20	4.69900E-01	16	21	-5.74800E-01
16	22	-2.40500E 00	16	23	8.09500E-01
16	24	2.54700E 00	17	13	4.44000E 00
17	17	-8.86300E 00	17	18	-1.84800E-01
17	21	-1.90000E-01	17	22	-3.46900E-01
17	23	7.96100E-01	17	24	9.31500E-01
18	14	4.44000E 00	18	17	8.83500E-03
18	18	-8.66900E 00	18	21	1.81200E-03
18	22	4.55700E-01	18	23	2.59500E-02
18	24	8.16369E-02	19	15	2.39500E 00
19	16	1.15000E-01	19	17	2.16800E 00
19	18	2.16800E 00	19	19	-4.96400E 00
19	20	2.31200E 00	19	21	-2.00300E 00
19	22	-1.91100E 01	19	23	2.22000E 00
19	24	1.84300E 01	20	15	1.15000E-01
20	16	2.39500E 00	20	17	6.39900E-01
20	18	6.39900E-01	20	19	-2.38300E-01
20	20	-5.22000E 00	20	21	-5.61700E 00
20	22	-2.06700E 01	20	23	2.24400E 00
20	24	2.07500E 01	21	17	-1.94400E-01
21	18	-1.94400E-01	21	21	-1.92500E-01
21	22	-8.05400E-01	21	23	2.71100E-01
21	24	8.52900E-01	22	15	1.12500E 00
22	16	1.12500E 00	22	17	2.84600E 01
22	18	2.84600E 01	22	19	-2.33100E 00
22	20	-1.30300E 00	22	21	1.64100E 01
22	22	-2.11100E 02	22	23	2.19500E 01
22	24	2.02900E 02	23	17	3.14300E-02
23	18	3.14300E-02	23	20	-3.03900E-04
23	21	4.01400E-02	23	22	3.55500E-01
23	23	-1.15300E-01	23	24	-3.62800E-01
24	17	2.56000E 00	24	18	2.56000E 00
24	20	6.49600E-01	24	21	3.29300E 00
24	22	3.84100E 02	24	23	-1.32100E 01
24	24	-3.85600E 02	25	1	5.65600E 01
25	25	-3.08000E-02	26	1	5.23600E 01
26	26	-1.14000E-01	27	1	1.09080E 02
27	27	-3.07000E-01	28	1	3.70000E 01
28	28	-1.19000E 00	29	1	1.25600E 01
29	29	-3.19000E 00			

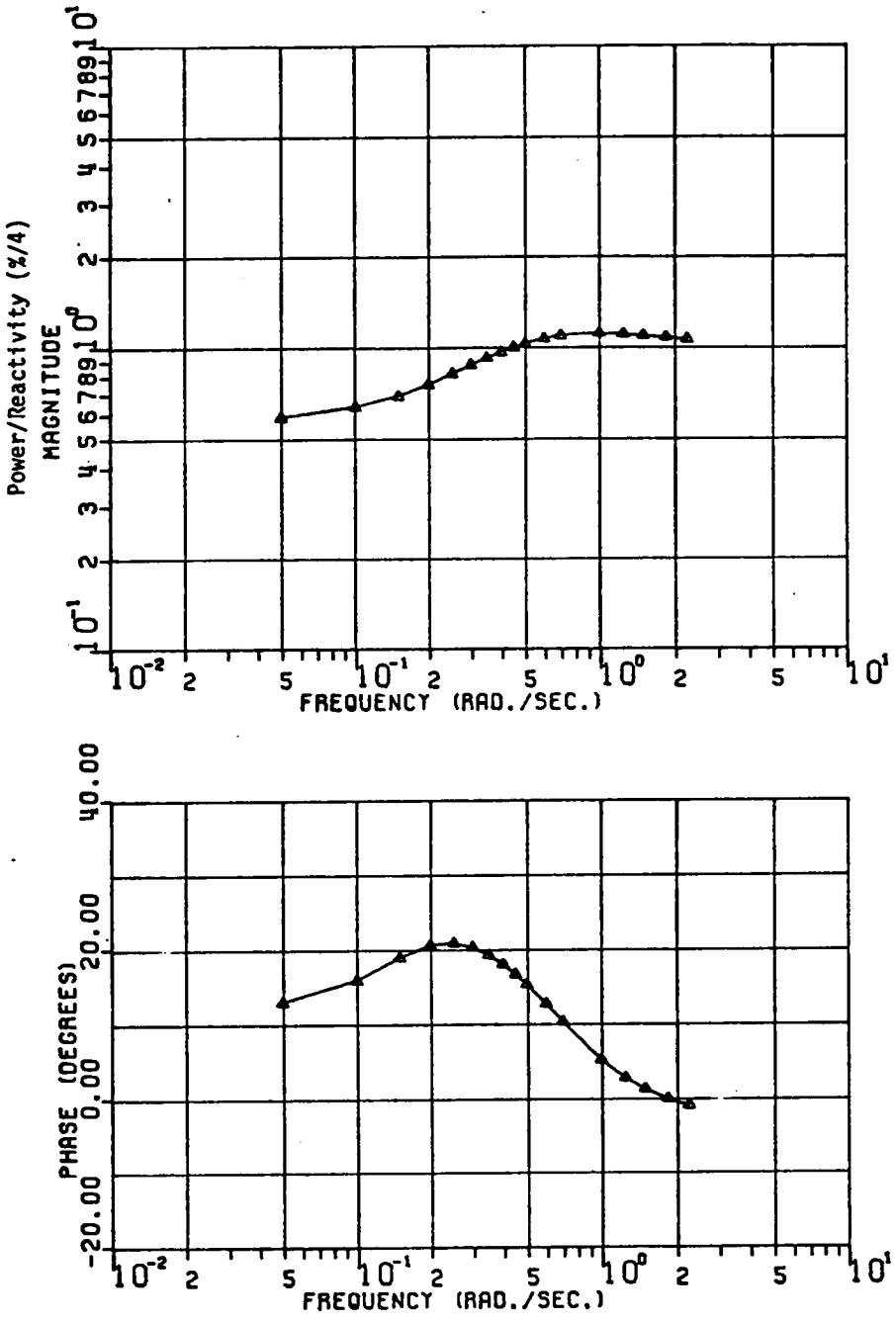


Figure 31. Frequency Response Based on Reference Coefficients Values: 95 Percent Power.

range was about ±1 percent of the nominal power. Oconee I was at 95 percent of full power, when the data for this case study were collected. The rod position and power level signals were recorded on an FM tape recorder after appropriate signal conditioning. The signal conditioning consisted of analog low pass filter and dc bias removal. Figure 32 shows a portion of the signals for rod position and power level for the test. The signal conditioning equipment must be compensated in the calculation of experimental frequency response. The average of frequency response results obtained with the HFFT computer program for ten periods are plotted in the Figure 33. In the calculation, fifty harmonic frequencies were analyzed. The fundamental frequency ($\frac{2\pi}{T}$) was 0.0495 rad/sec and highest frequency ($\frac{2\pi x50}{T}$) was 2.474 rad/sec.

A comparison was made between reference model predictions (see Figure 31) and the experimental results (see Figure 33). The phase plot for reference model and experiment are similar, especially between .1 and 1.0 radian per second. The magnitude of both cases are close to unity as in the "flat" portion at frequencies around 2 radians per second (as it must be). The major differences are in the frequency range below than .4 radian per second, in which the magnitude of reference model is greater than the experimental results.

Results and Discussion

Katz[21] pointed out that the effective coefficient of heat transfer from fuel to coolant (h_{fc}), the Doppler coefficient (α_f), and the coolant temperature coefficient (α_c) have dominant effects

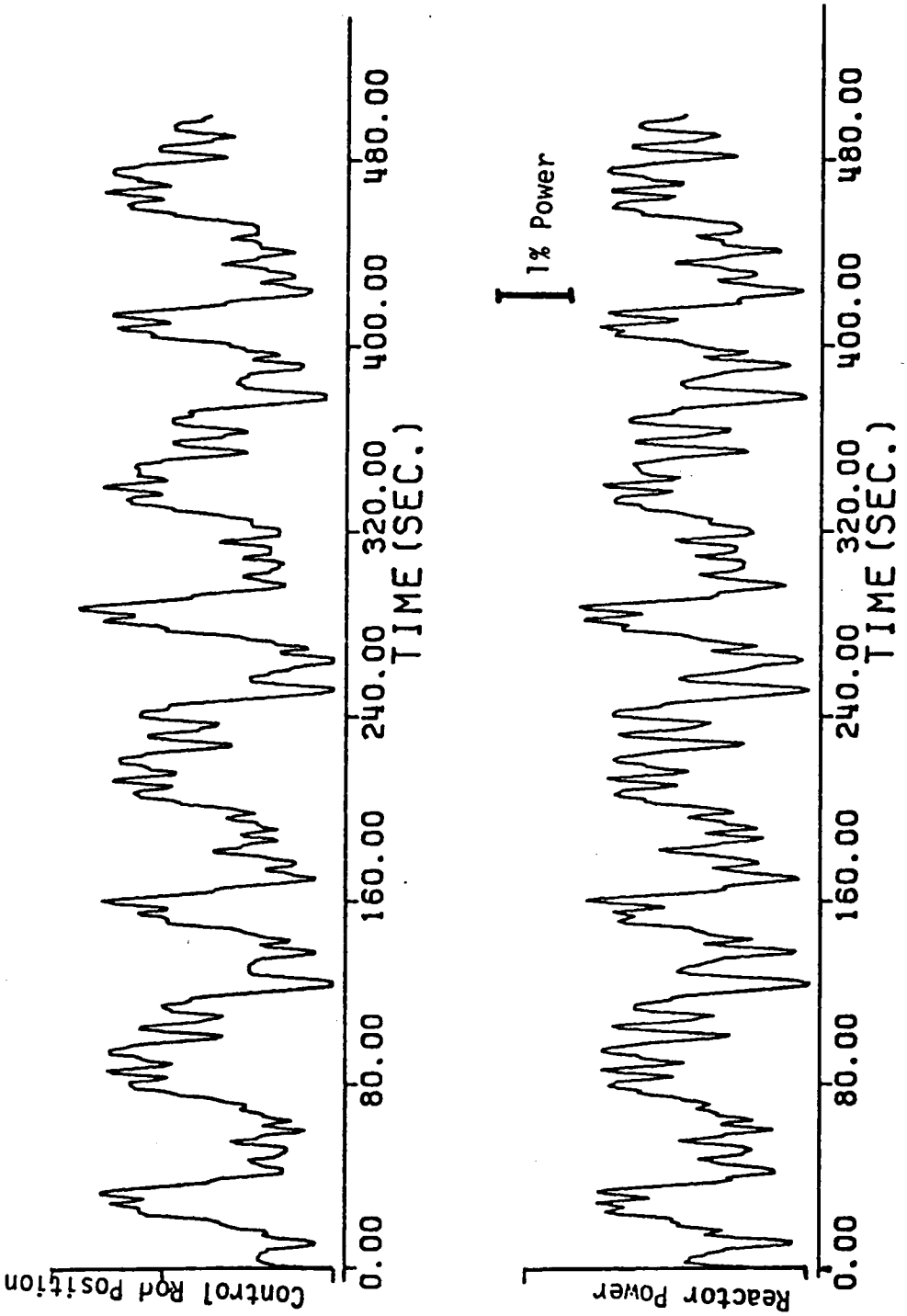


Figure 32. The Experiment Response Data in Time-Domain.

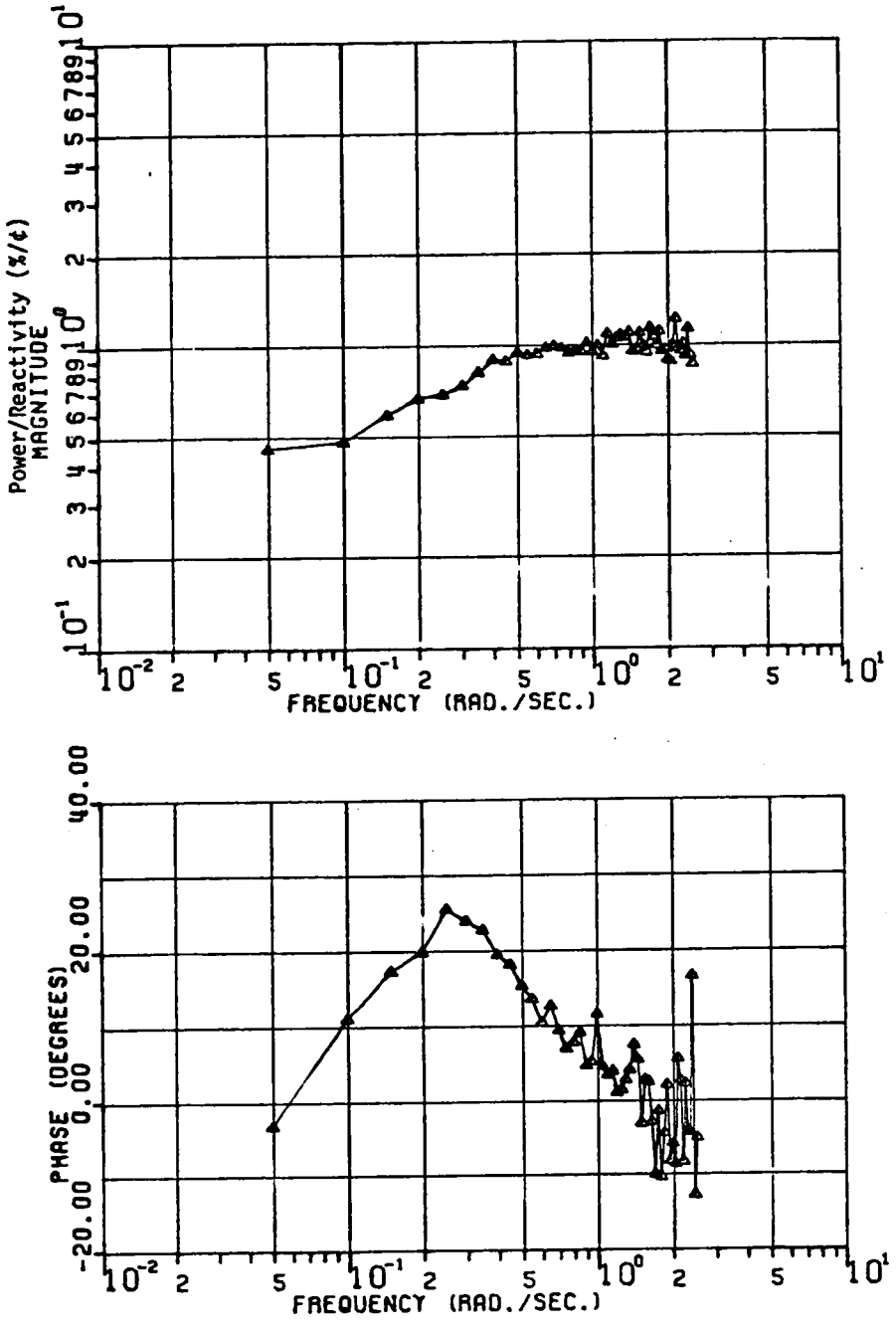


Figure 33. Frequency Response Calculated from Experiment Data.

on the power/reactivity frequency response at frequencies lower than 1.0 rad/sec. These three important coefficients will be chosen as the parameters to be identified.

Let $P_1 = \alpha_f/\alpha_{fo}$, $P_2 = h_{fc}/h_{fco}$ and $P_3 = \alpha_c/\alpha_{co}$ be the coefficients defined relative to the reference values, where $\alpha_{fo} = -1.1 \times 10^{-5}$ $\delta\rho/°F$, $hf_{co} = 194$ Btu/hr ft^2 °F and $\alpha_{co} = -2.0 \times 10^{-5}$ $\delta\rho/°F$. From the equations in Section 4.2, page 97, we can identify elements of the system matrix which contain these parameters. The algebra table which relates these elements to the parameters, can be set up as shown in Table 4.7. Figure 34 is the map of the system matrix B. The elements that contain parameters to be identified are indicated by the symbol *, and the symbol # indicates that the corresponding row is the output state variable.

After the elementary row/column operations (see Appendix C), all the elements that contain the parameters to be identified and the diagonal elements (indicated by symbol # in Figure 34) of the output state variable were shifted to upper left corner of the matrix as shown in Figure 35. The dimension of A_{11} and B_{11} should be four. However, the program found out that the elements are all zero from columns 5 to 29 in row 5 (see Figure 35). It means that the sub-matrix, $(j\omega A_{22} - B_{22})$, with dimension (25 x 25) is singular. In order to avoid the singularity problem in matrix inversion, row 5 will be treated just like a row that contains a parameter and will be shifted into submatrix B_{11}. Thus, the final dimension of A_{11} and B_{11} is five.

TABLE 4.7

INPUT DATA FOR ALGEBRA TABLE: CASE STUDY I

Index				The Exponent Value of		
I	J	M	Constant	P_1	P_2	P_3
1	3	1	-0.44000E 00	1.000	0.0	0.0
1	4	1	-0.80000E 00	0.0	0.0	1.000
3	3	1	-0.20090E 00	0.0	1.000	0.0
3	4	1	0.20090E 00	0.0	1.000	0.0
4	3	1	0.63000E-01	0.0	1.000	0.0
4	4	1	-0.26320E 01	0.0	0.0	0.0
4	4	2	-0.63000E-01	0.0	1.000	0.0
5	3	1	0.62000E-01	0.0	1.000	0.0
5	4	1	0.26320E 01	0.0	0.0	0.0
5	4	2	-0.62000E-01	0.0	1.000	0.0

I \ J	0000000001111111112222222222 1234567890123456789012345678 9
1	#P**.....PPPPP
2	PN.....
3	P.**.....
4	..**....P.....
5	..**N.....
6	....PN.....
7	.....PN.....
8	.......N.....P.....
9	.......PN.....
10	..PNPPPNPNNNNNPPPP..NNPP.....
11	......P...N...P.....P.....
12	..........PN...PNN..PNPP.....
13	..........PN...PN..NNPP.....
14	..........PN..NP..NNPP.....
15	..........P...N.NNP.NNPP.....
16	..........P...NNN.PNNPP.....
17	..........P...NN..NNPP.....
18	..........P..PN..PPPP.....
19	..........PPPPNPNNPP.....
20	..........PPPPNNNNPP.....
21	..........NN..NNPP.....
22	..........PPPPNNPNPP.....
23	..........PP.NPPNN.....
24	..........PP.PPPNN.....
25	P.....N....
26	P.....N...
27	P.....N..
28	P.....N.
29	P.....N

Legend:

I row index number

J column index number

· zero element

N negative element

P positive element

* element with parameter

diagonal element of output state

Figure 34. Signs of System Matrix B for Case Study I.

I \ J	000000000111111111122222222223 123456789012345678901234567890123
1	#**P.....PPPPP
2	P**.....
3	.**.....P.....
4	.**.N.....
5	P..N.....
6	....PN.....
7	.....PN.....
8	.....N.....P.....
9	.....PN.....
10	.PN.PPPNPNNNNNPPPP..NNPP.....
11	.....P...N...P.....P.....
12	.....PN...PN.N..PNPP.....
13	.....PN...PN..NNPP.....
14	.....PN..NP..NNPP.....
15	.....P...N.NN.P.NNPP.....
16	.....P...N.NN.PNNPP.....
17	.....P...NN..NNPP.....
18	.....P..PN..PPPP.....
19	.....PPPPN.PNNPP.....
20	.....PPPPNNNNNPP.....
21	.....NN..NNPP.....
22	.....PPPPNNPNPP.....
23	.....PP.NPPNN.....
24	.....PP.PPPNN.....
25	P.....N.....
26	P.....N...
27	P.....N..
28	P.....N.
29	P.....N

Legend:

I row index number

J column index number

. zero element

N negative element

P positive element

* element with parameter

diagonal element of output state

Figure 35. Signs of System Matrix B After Row/Column Shifting.

Results of a PARARI code calculation are shown in Table 4.8. The value of the error function decreases monotonically. After the fifth iteration, the improvement is very slow. The frequency response for the optimized parameters is shown in Figure 36 and the improved agreement between theory and experiment is apparent. The program uses the optimized parameters values at the last iteration to calculate the curvature, $J_{ii\ell}$, (see Section 3.5, page 84) for the extended frequency range from 0.001 up to 10.0 rad/second. The curves of $J_{ii\ell}$ for each parameter are shown in Figure 37. The curvature for parameter, P_3, is very small (in the test frequency range) as compared to the others, so, we have less confidence in the estimated value of P_3. The relatively larger values of $J_{11\ell}$ and $J_{22\ell}$ are in the dynamic test frequency range from 0.03 up to 1.0 rad/second, i.e., from the test data we can accurately estimate parameters P_1 and P_2. It is interesting to see that the maximum value of $J_{11\ell}$ and $J_{22\ell}$ appear at 0.4 and 0.05 rad/sec respectively.

The same case was run on PARAGP code, which uses normalized gains and phase angles (in degree units) to generate the error function. At first we set the gain and phase weighting factor (W_1 and W_2, see Appendix A) equal to unity. The parameters P_2 and P_3 changed drastically during the optimization and could not converge to the optimized value. This is due to the domination of the error function by the large variation of the experimental phase angle (see Figure 33, page 120) in the test frequency range. In order to improve the situation, the phase angle weighting factor, W_2, was

TABLE 4.8

RESULTS OF PARARI COMPUTER CODE RUN: CASE STUDY I

Iteration Number	Error Function Value	$P_1(\alpha_f/\alpha_{fo})$	$P_2(h_{fc}/h_{fco})$	$P_3(\alpha_c/\alpha_{co})$
1	12.61	0.85	0.667	1.0
2	4.83	1.12	0.70	1.0
3	2.455	1.284	1.19	0.998
4	2.425	1.283	1.18	0.996
5	2.395	1.277	1.16	0.993
6	2.378	1.271	1.15	0.991
7	2.364	1.264	1.14	0.989
8	2.354	1.261	1.13	0.987
9	2.348	1.258	1.12	0.986
10	2.344	1.256	1.11	0.984

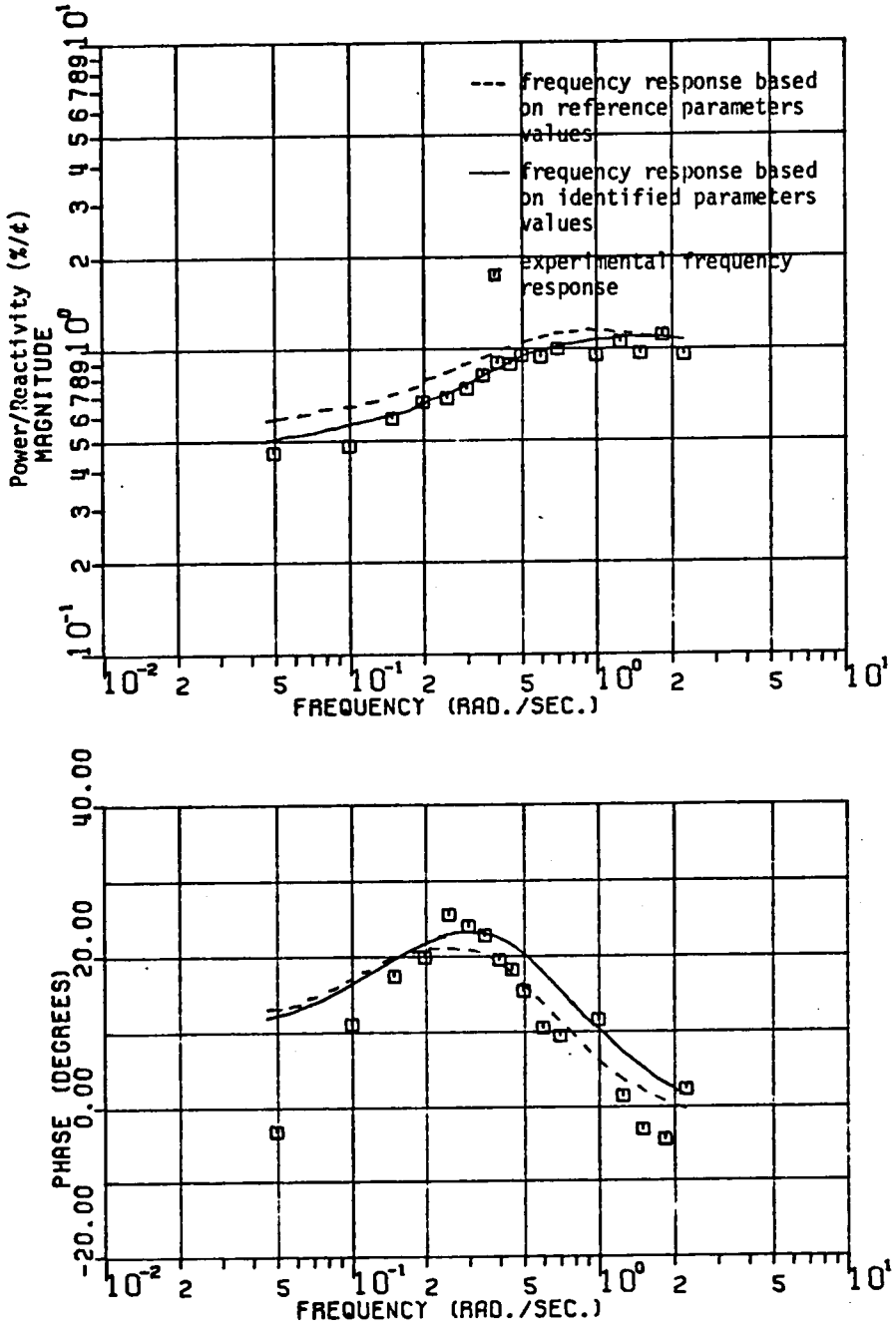


Figure 36. Comparison Between Theoretical and Experimental Frequency Response (PARARI Calculation).

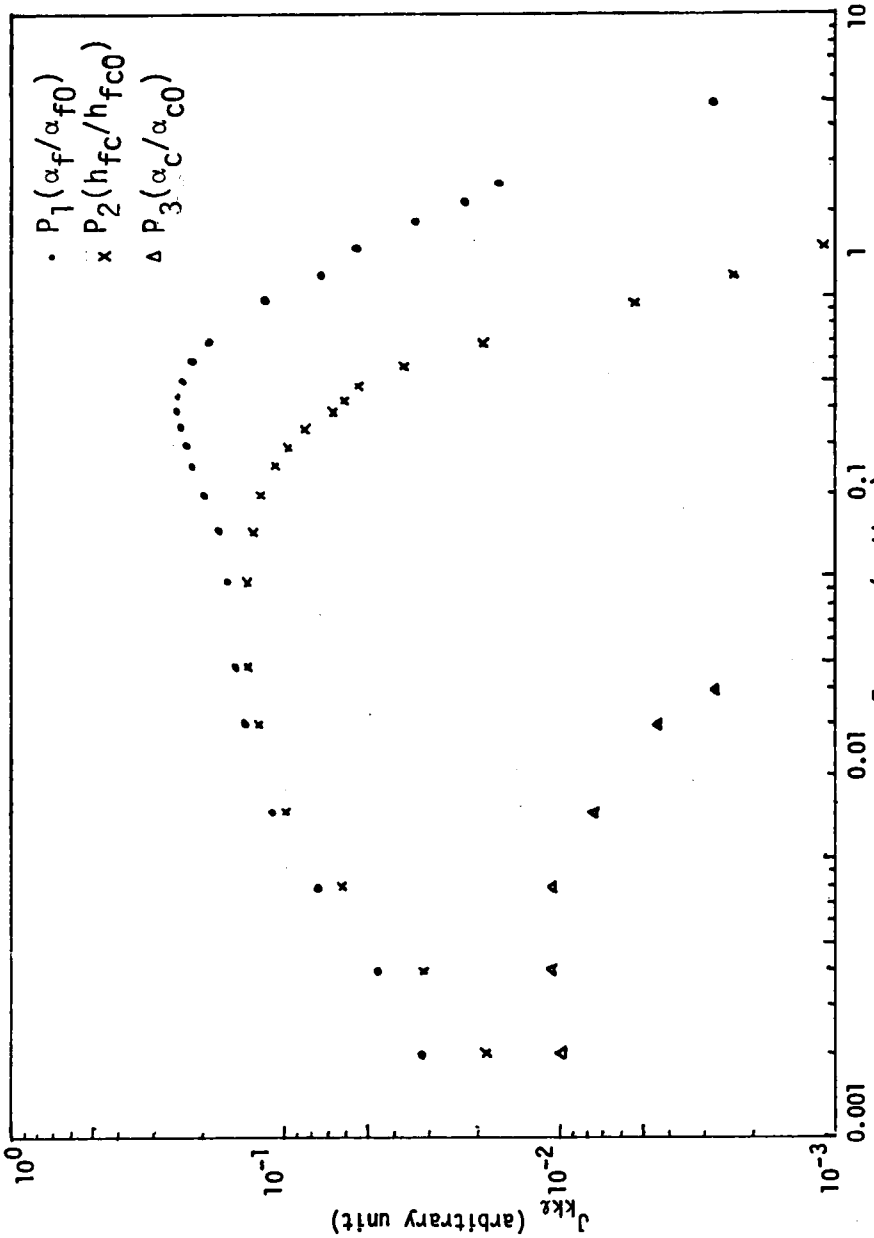


Figure 37. The Curves of $J_{kk\ell}$ Versus Frequencies for Case Study I.

reduced to 0.25 and the gain weighting factor, W_1, was increased to 5.0. The results of the PARAGP code calculations are shown in Table 4.9. As compared with the PARARI code calculations, the differences of P_1 and P_3 are small. The P_2 estimation has a 10 percent difference. As pointed out by Butterfield and Cummins[25] the set of optimized parameters values generally depends on the error function adopted. The differences in this study for the different error functions is considered reasonable. Comparison between the optimized theoretical model, which was obtained by the PARAGP code calculation, and the experimental frequency response is shown is Figure 38. It is apparent that the optimized theoretical model has a better fit in gain than in phase angle, since PARAGP code uses more weight for the error in gain (compare Figures 36 and 38).

Since the curvature, J_{33}, of P_3 is very small, the case was rerun with two parameters P_1 and P_2 only, and the estimated values of parameters are essentially the same as obtained in the three parameter cases. For this two parameter case, the information matrix (see Equation 3.32), J is

$$J = \begin{bmatrix} 3.064 & -1.28 \\ -1.28 & 1.39 \end{bmatrix} .$$

Following the procedures described in Section 3.5, page 89, we have

rotation angle, $\theta = -56.82°$,

major axes, $\overline{OP} = 1.17$,

minor axes, $\overline{OQ} = 0.52$,

and the level surface is plotted in Figure 39.

RESULTS OF PSI [illegible] RUN: [illegible]

Iteration Number	Eigenvalue	(α_F/α_{F_0})	(b_{Fc}/b_{Fco})	$P_3(\alpha_c/\alpha_{co})$
1	22.72	0.85	0.967	1.0
2	3.38	1.15	0.69	1.0
3	5.16	1.21	0.93	0.99
4	5.27	1.22	0.95	0.98
5	5.01	1.24	0.97	0.97
6	5.0	1.24	0.98	0.97
7	4.98	1.24	0.98	0.968
8	4.96	1.25	0.99	0.95
9	4.95	[illegible]	1.01	0.94

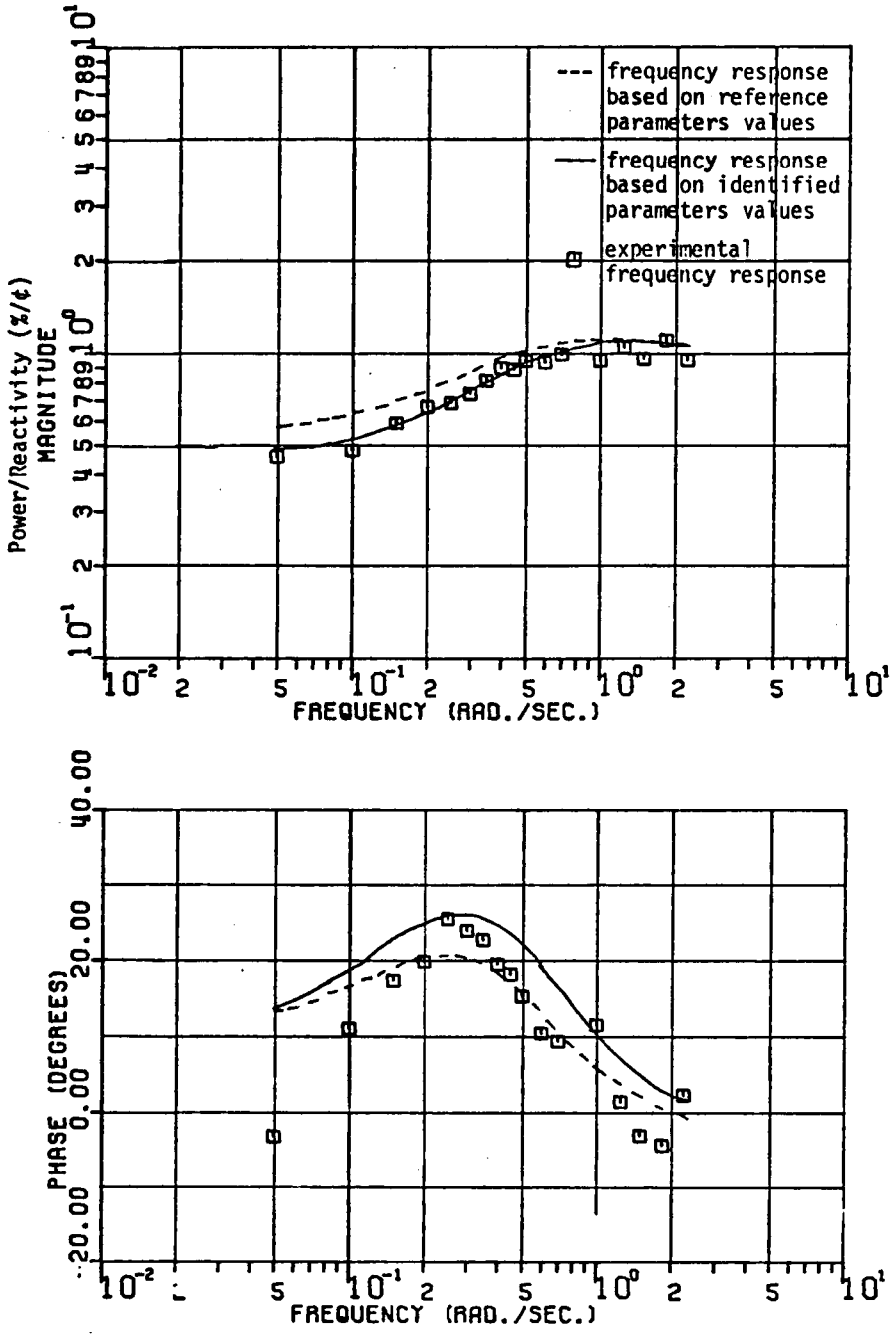


Figure 38. Comparison Between Theoretical and Experimental Frequency Response (PARAGP Calculation).

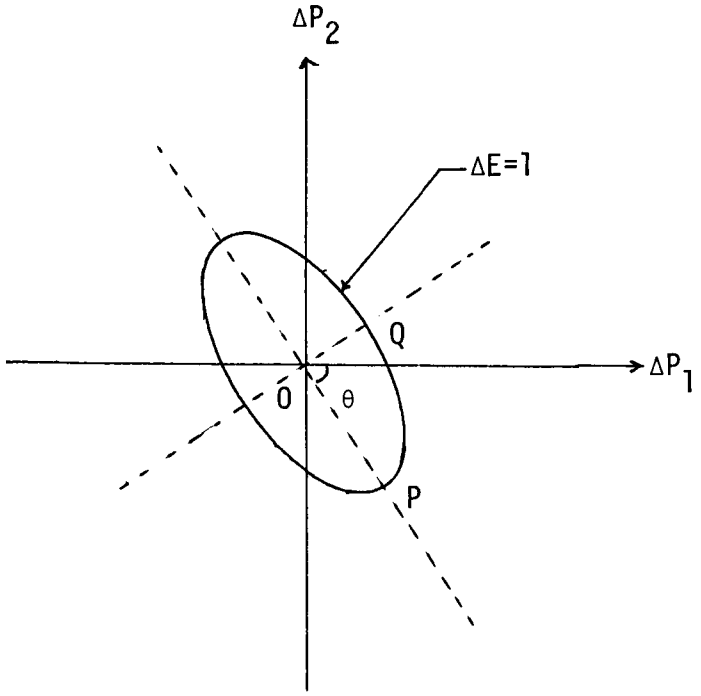


Figure 39. The Contour Map for Case Study I.

Notice that $\overline{OP}$ sin θ is larger than $\overline{OP}$ cos θ. From Figure 39 or the diagonal elements of J, we know that P_1 can be better estimated than P_2 (see the discussion in Section 3.5, page 84). This may provide some explanation, why the P_2 had 10 percent difference when different error functions were used.

In conclusion, the Doppler coefficient, α_f, about 25 percent higher and the fuel-to-coolant heat transfer coefficient, h_{f-c}, about 6 percent higher in magnitude than reference design value are considered to be the correct values.

Each analysis required 70 seconds on an IBM 360 Model 65. For the same results, it took 14 minutes and 40 seconds to run the case on the program which did not adopt the partitioned matrix algorithm.

CHAPTER 5

DEMONSTRATION OF THE METHOD-CASE STUDY II: FORT ST. VRAIN STEAM GENERATOR

5.1 Introduction

The partitioned matrix technique which was developed in Chapter 3, page 81, can be applied to the general set of n first order differential equations with constant coefficients such as Equation (1.2). The equation is repeated as follows:

$$A\dot{\bar{x}} = B\bar{x} + \bar{f}g. \qquad (5.1)$$

In Chapter 4, page 97, the technique was applied to the Oconee I theoretical model, in which the differential matrix, A, is the identity matrix. In order to demonstrate the adequacy of the method for theoretical models with non-identity differential matrices, the model of the Fort St. Vrain once-through steam generator was chosen for the analysis. The selected input and output are helium flow and main steam outlet temperature, respectively. The simulated responses from the Fort St. Vrain steam generator model with reference design parameter values are treated as test data. The heat transfer coefficients between the tube and water/steam at three nodes were changed. Then, the PARARI and PARAGP codes were run to determine whether they can identify the original values of these parameters in the noise-free case.

5.2 A Description of the System

The Fort St. Vrain once-through steam generator and its model were described in Chapter 2, page 6. The frequency response for steam outlet temperature/helium flow is shown in Figure 9, page 50, for reference parameter values. For convenience in comparing the results, the frequency response is replotted in Figure 40 with the symbol ⊡ , and it will be treated as the experimental data.

The heat transfer coefficients between tube and water/steam at 3 nodes are defined (see Equation 2.12) as follows:

$$h_i = (Ks_i \, Ws_i^{-Cs_i} + 0.5 \, R_i)^{-1} \quad (\text{for } i = 1, 2, 3)$$

and the design reference values are:

h_{10} = 966.6 Btu/hr ft^2 °F,
h_{20} = 1031.68 Btu/hr ft^2 °F,
h_{30} = 1067.03 Btu/hr ft^2 °F.

Let $P_1 = h_1/h_{10}$, $P_2 = h_2/h_{20}$, and $P_3 = h_3/h_{30}$ be the coefficients defined relative to the reference values. For the reference model, the selected adjustable parameter, P_i, are equal to unity. Then, the values were arbitrarily changed as follows:

$$P_1 = 1.25, \; P_2 = 1.2, \text{ and } P_3 = 0.7. \qquad (5.2)$$

Using these new parameter values, the new system matrix A and B can be generated, and the frequency responses can be calculated.

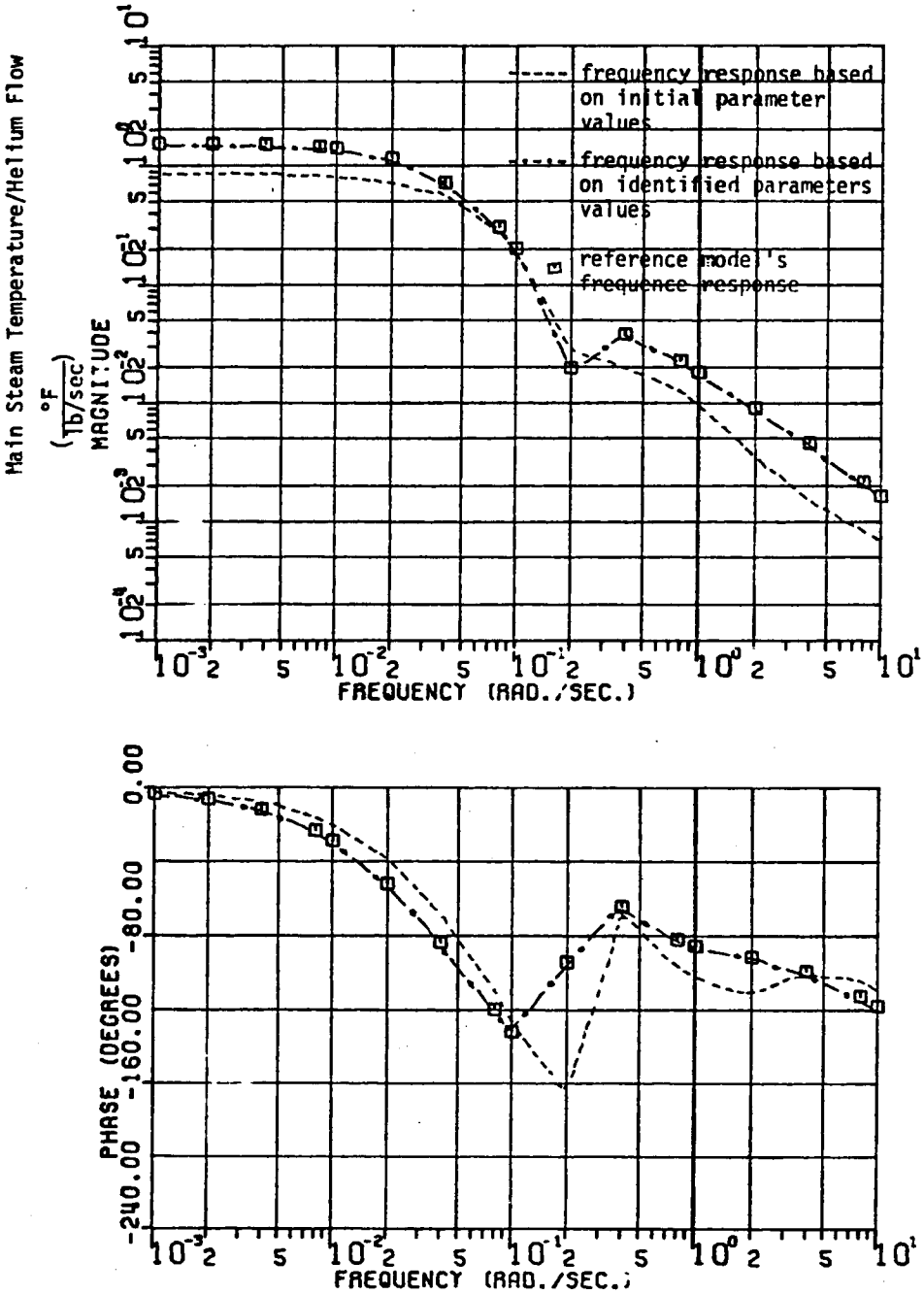


Figure 40. Comparison Between the Results of PARAGP Calculation and Reference Model's Frequency Response (Case Study II).

as shown in Figure 40. The difference as compared to the frequency response of the reference theoretical model is apparent.

The PARAPE computer code was run with the parameter values in Equation (5.2) as the initial parameter estimates and these were adjusted in such a way as to reduce the error function (sum of squares of differences). When the error function approaches zero, the parameters P_i should approach unity.

5.3 Results and Discussion

The elements of the system matrix which contain the parameters can be identified from the linearized equations in Chapter 2, page 22. The algebra table can be set up as shown in Table 5.1. Figure 41 is the map of the system matrix B. (* indicates the elements containing parameters to be identified, # indicates the output state.) After the elementary row/column operation, one would like to have non-zero diagonal elements in the shifted matrix. Otherwise, it tends to have a singular sub-matrix B_{22}. For example, if all the parameters appear in the first row, then the corresponding columns will be shifted to the left of the matrix sequentially. Since there are quite a few zero elements in the off-diagonal elements of the system matrix (see Figure 41), this would shift zeroes to the diagonal elements. However, if we shift the corresponding ith row of the shifted ith column to the top-most of the matrix accordingly, then the final matrix will not have zero diagonal elements (provided that matrix B does not have zero diagonal elements initially). In doing so, the dimension of sub-matrix B_{22} or A_{22} remain unchanged. The symbol

TABLE 5.1

THE ALGEBRA TABLE FOR CASE STUDY II

Index				The Exponent Value of		
I	J	M	Constant Value	P_1	P_2	P_3
8	1	1	0.87740E 02	1.0	0.0	0.0
8	8	1	-0.26119E 04	1.0	0.0	0.0
8	8	2	-0.93724E 03	0.0	0.0	0.0
9	2	1	0.91430E 02	0.0	1.0	0.0
9	9	1	-0.59587E 03	0.0	0.0	0.0
9	9	2	-0.17634E 04	0.0	1.0	0.0
10	3	1	-0.14256E 03	0.0	0.0	1.0
10	10	1	-0.29305E 04	0.0	0.0	1.0
10	10	2	-0.95852E 03	0.0	0.0	0.0
10	13	1	0.18321E 04	0.0	0.0	1.0
11	1	1	-0.11367E 03	1.0	0.0	0.0
11	8	1	0.26118E 04	1.0	0.0	0.0
11	11	1	0.13950E 04	1.0	0.0	0.0
12	2	1	-0.37370E 02	0.0	1.0	0.0
12	9	1	0.17634E 04	0.0	1.0	0.0
12	11	1	-0.15413E 04	0.0	1.0	0.0
12	12	1	0.15413E 04	0.0	1.0	0.0
13	3	1	0.12583E 03	0.0	0.0	1.0
13	10	1	0.29490E 04	0.0	0.0	1.0
13	12	1	-0.18133E 04	0.0	0.0	1.0
13	13	1	-0.28448E 03	0.0	0.0	0.0
13	13	2	-0.17624E 04	0.0	0.0	1.0

I \ J	00000000011111111112 12345678901234567890
1	+..............PN..
2	.+..............PN.
3	..+..............PN
4	...PP........N.....
5	....PP........N....
6	.....PP........N...
7	......N............
8	*......*.....P..NN..
9	.*......*.....P..NN.
10	..*.....*..*..P..NN
11	*N.....*..*.....PN..
12	P*P.....*.**.....PN.
13	.N*.....*.*#.....PN
14	...NP..P..N..N.....
15	....NP..P.PN..N....
16	.....NP..P.P...N...
17	N..............N...
18	PN..............N..
19	.PN..............N.
20	..P..............N

Legend:

I row index number

J column index number

. zero element

N negative element

P positive element

* element with parameter

diagonal element of output state

Figure 41. The Signs of System Matrix B for Case Study II.

(+) indicates that the corresponding rows and columns will be shifted to the left-upper corner of matrix.

Figure 42 shows the map of the system matrix B after shifting. (Note: the program does the same shifting on matrix A.) It is clear from Figure 42, that the dimension of A_{11} and B_{11} is nine.

The results of a PARAGP code run are shown in Table 5.2. The error function decreases quickly from 5.08 to 0.0001. The optimized parameters are found at the 8th iteration, and they are all close to unity (the original values of parameters) as they should be. In this case, we know the answer in advance and the results show that the PARAGP code can identify these parameters. The frequency response of the model with the optimized parameter values is exactly the same as for the reference model (see Figure 40).

The curvatures, $J_{ii\ell}$, for each parameter were calculated and the curves are plotted in Figure 43. The curvatures of these three parameters are all largest in the frequency range 0.02 to 1.0 rad/sec. This suggests that if one intends to get better estimates of heat transfer coefficients from tube to secondary coolant from the actual dynamic test data, the power of the input signal should be concentrated in this frequency range (especially where the maximum values appeared) as much as possible. The SIGNAL computer code which was developed by Buckner,[27] can produce a Multi-Frequency Binary Signal (MFBS) such that most of the power of the input signal will be concentrated in the specified frequencies.

I \ J	00000000011111111112 12345678901234567890
1	+..............PN..
2	.+..............PN.
3	..+..............PN
4	*..*.........P..NN..
5	.*..*.........P..NN.
6	..*..*..*......P..NN
7	*N.*..*.........PN..
8	P*P.*.**.........PN.
9	.N*..*.*#.........PN
10	.........PP....N....
11	..........N.........
12	...........PPN......
13	.........P..P.N.....
14	...P..N....NPN......
15	....P.PN.P..N.N.....
16	.....P.P.NP....N....
17	N..............N...
18	PN..............N..
19	.PN..............N.
20	..P..............N

Legend:

I row index number

J column index number

. zero element

N negative element

P positive element

* element with parameter

diagonal element of output state

Figure 42. The Signs of System Matrix B After Elemental Row/Column Shifting.

TABLE 5.2

THE RESULTS OF PARAGP CODE RUN FOR THE FORT ST. VRAIN STEAM GENERATOR

Iteration Number	Error Function Value * 10^2	$P_1(h_1/h_{10})$ Value	$P_2(h_2/h_{20})$ Value	$P_3(h_3/h_{30})$ Value
1	508.20	1.25	1.2	0.7
2	500.92	1.22	1.06	1.02
3	34.91	1.18	1.04	1.03
4	20.75	1.14	1.02	1.04
5	7.52	1.11	1.01	1.03
6	3.35	1.07	1.01	1.01
7	0.42	1.02	1.004	0.99
8	0.005	1.002	1.00	1.00

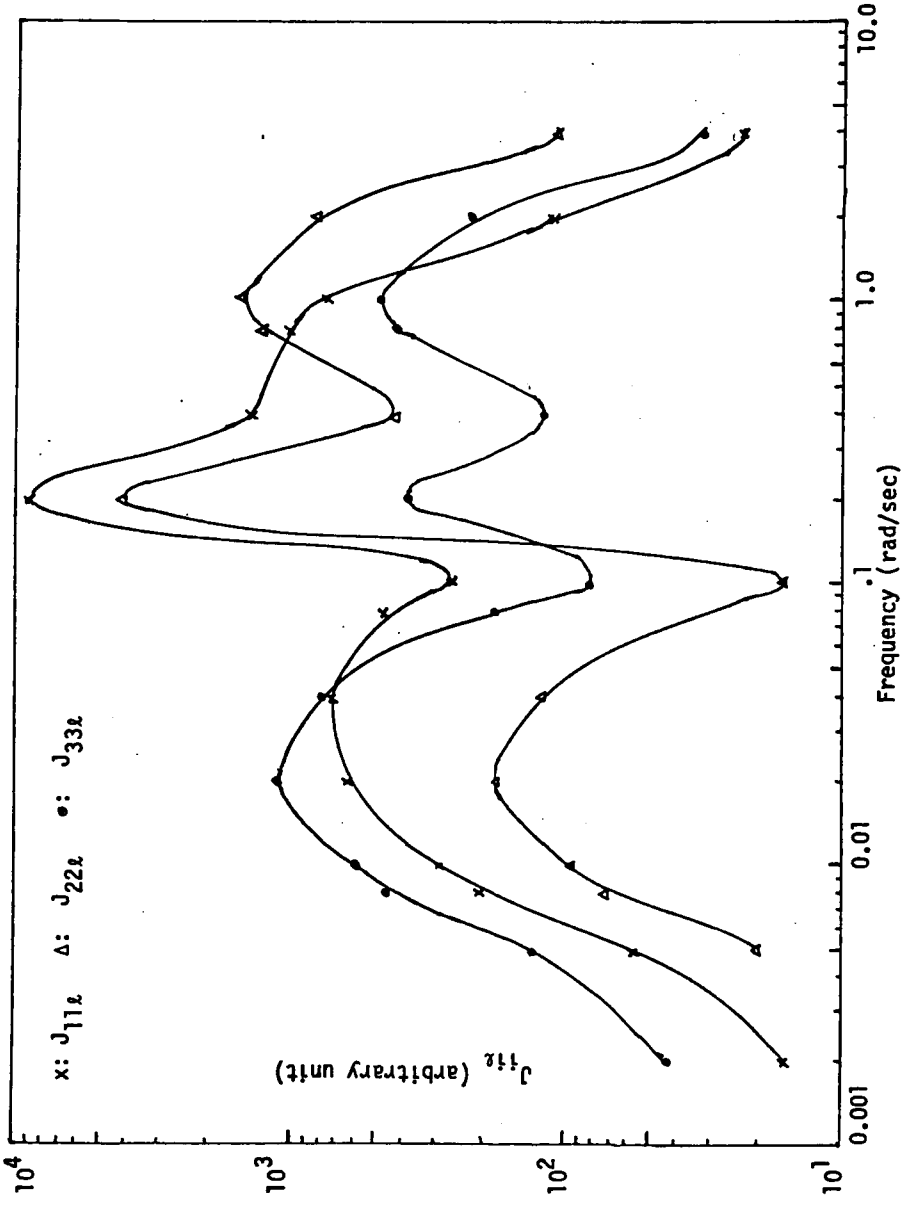


Figure 43. The Curves of $J_{ii\ell}$ Versus Frequencies for Case Study II Steam Generator.

For the same case, the results of PARARI code run are not good. The error function reduced slowly and the parameters did not converge to the original values (see Table 5.3). In the PARARI calculation, the error function is generated by the square difference of the real and imaginary parts of the frequency response. The magnitude values at frequencies above 0.1 rad/sec are two orders smaller than the magnitude at low frequency (see Figure 40). This means that this error function is not sensitive to the change of the parameters at high frequencies. This is the main reason of the failure. It is not the case in the PARAGP calculation, where the error function is the sum of square differences of normalized gain and phase angle (see Appendix A).

The analysis required 1 minute and 40 seconds on an IBM 360 Model 65.

TABLE 5.3

THE RESULTS OF PARARI CALCULATION FOR THE FORT ST. VRAIN STEAM GENERATOR

Iteration Number	Error Function Value * 10^2	$P_1(h_1/h_{10})$ Value	$P_2(h_2/h_{20})$ Value	$P_3(h_3/h_{30})$ Value
1	282.5	1.25	1.20	0.70
2	48.8	1.21	1.18	0.95
3	15.17	1.19	1.17	1.01
4	6.55	1.18	1.17	1.04
5	4.81	1.18	1.169	1.05
6	4.13	1.17	1.168	1.056
7	3.80	1.17	1.167	1.06
8	3.62	1.17	1.66	1.061

CHAPTER 6

DEMONSTRATION OF THE METHOD-CASE STUDY III: FORT ST. VRAIN NUCLEAR STEAM SUPPLY SYSTEM

6.1 Introduction

The Nuclear Engineering Department of The University of Tennessee is assisting the General Atomic Company (GA) in planning and performing dynamic tests on the Fort St. Vrain Nuclear Power Station. The experimental data obtained from dynamic testing will have the following applications:

a. verification of the theoretical model (LAP) for Fort St. Vrain nuclear system
b. experimental determination of values for system design parameters.

The decision was made to follow a test plan similar to that of the Oconee 1 nuclear system dynamic test.[21] The first draft of the Fort St. Vrain plant test procedure has been completed. During the conduct of the test, the plant will be in normal power operation and no plant technical specifications shall be violated. A multi-frequency binary signal will be inserted to cause variations in selected inputs. The inputs to be used in the test are: (1) control rod position perturbation, (2) helium (primary coolant) flow perturbation, (3) feedwater flow perturbation, and (4) throttle

value perturbation. By measuring selected plant outputs and appropriate data processing, the frequency response of the reactor will be determined.

As described in Chapters 4 and 5, pages 96 and 134, the PARAPE computer code was applied successfully to identify the parameters of the linear dynamic models of systems with order 29 (using experimental test data) and 20 (using simulated test data). In order for the capability of the new parameter identification scheme to be demonstrated for the type of application envisioned at Fort St. Vrain, it must be shown that the method can handle large linear dynamic models (order near one hundred). The major objective of this chapter was to use the 81st order linear dynamic LAP model of the Fort St. Vrain nuclear system as an example to demonstrate that the new method is economical enough for routine use in identifying parameters from experimental data.

Due to the delay of Fort St. Vrain plant completion, the experimental data are not yet available. The best available source of information for evaluating the parameter identification method is the simulated dynamic response from the theoretical LAP model. The procedures are similar to those used in Chapter 5, page The selected input and output in the simulated test were control rod position and reactor power. Fuel and moderator (graphite) temperature coefficients of reactivity (α_{fi} and α_{mi}) were selected as the parameters to be identified in the analysis.

6.2 The Fort St. Vrain Nuclear Power Plant Description

Fort St. Vrain is located 35 miles north of Denver, Colorado. This plant, rated at 330 MW(e), was designed and built by General Atomic Company. The high-temperature gas-cooled reactor (HTGR) will provide 1000°F, 2400-psig steam with 1000°F reheat. Unique features of the HTGR include: (1) use of a pre-stressed concrete reactor vessel (PCRV), (2) high speed (9550 rpm) steam-driven helium circulators, (3) once-through steam generators (see Chapter 2, page 6).

A schematic flow diagram of the GA HTGR system is shown in Figure 44. The Fort St. Vrain reactor fuel consists of (U, Th) C_2 microspheres embedded in graphite; graphite is the moderator. The primary coolant is helium and the secondary coolant is water/steam. Contained in the PCRV are the reactor core, steam generators, and helium circulators.

The control rods are withdrawn by steel cables on pulleys driven by electric motors; insertion is by gravity. Helium coolant (762°F) enters the core at the top through orifice control valves. Helium (1427°F) leaves the core and travels downward to the steam generators. The cold helium exits at the bottom of the steam generator and flows into the four helium circulators. From the helium circulators, the helium flows upward through the annular space between the core barrel and PCRV, back to the core entrance.

The superheated steam, which is generated by the steam generator at about 1000°F and 2700 psi, is piped to the high pressure turbine (HPT) and then to the helium circulator turbines. All of the steam flows through the circulator turbines except for a

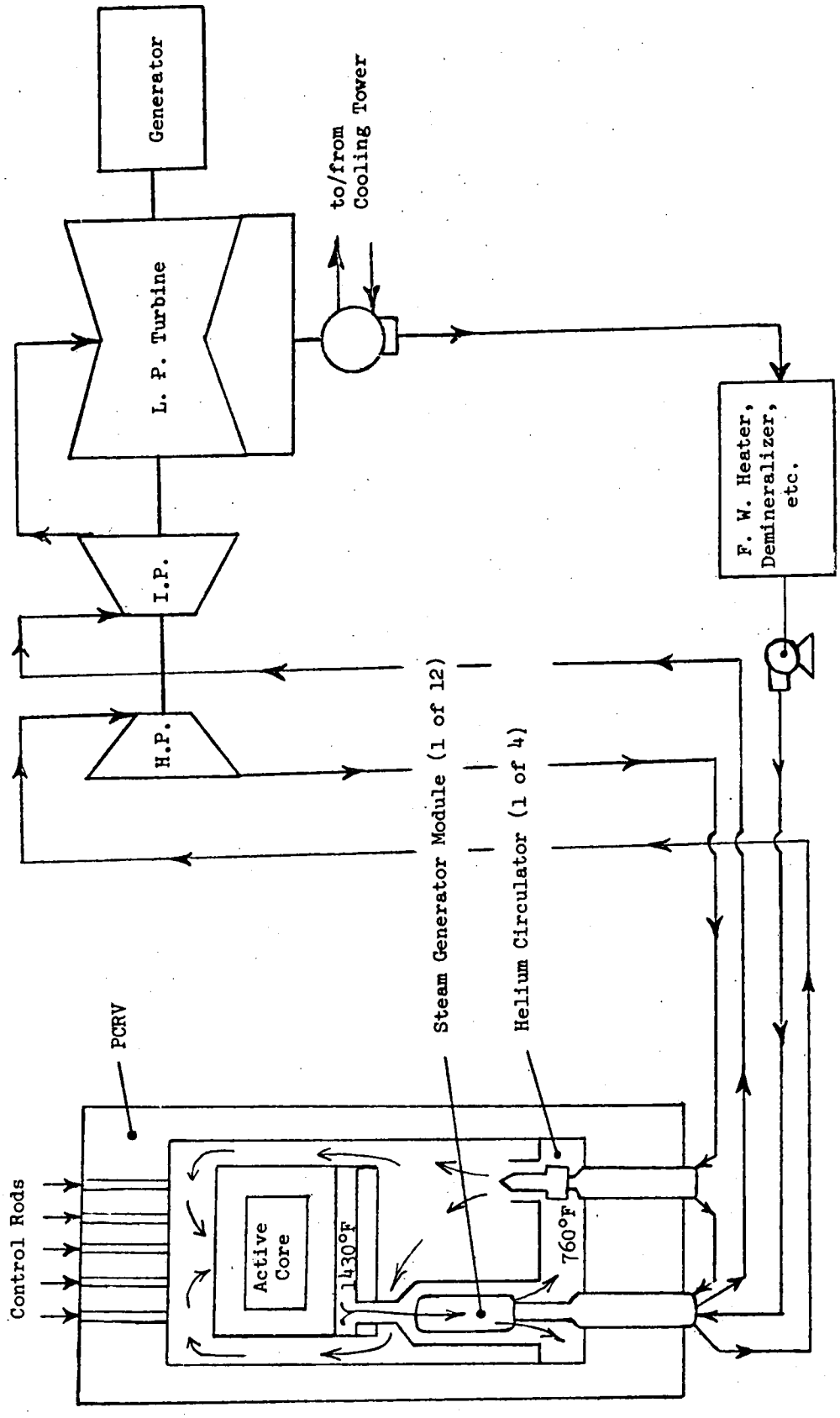


Figure 44. Schematic Diagram of Fort St. Vrain Nuclear Steam Supply System.

bypass flow of about 5 percent (see page 161) then re-enters the steam generator in the reheater section. The steam is reheated back to 1000°F and 618 psi, then flows to the intermediate and low pressure turbines. The exit is condensed and returned to the steam generator.

Tables 6.1 and 6.2 summarize values of neutronic and major design parameters important to Fort St. Vrain dynamic response. For the important parameters values for the steam generator, see Table 2.1, page 8.

6.3 Theoretical Model of the System[6]

The LAP theoretical model includes the neutronic, core heat transfer, graphite thermal shielding at the top and bottom of the core, steam generator and reheater, piping, high pressure turbine, and helium blower turbine. The equations for each component are briefly described below.

Neutronics

The neutronics equations used in the Fort St. Vrain modeling are the standard point reactor kinetics equations for power level and six delayed neutron groups which, after linearization, are

$$\frac{d\ \delta P/P_o}{dt} = -\frac{\beta_T}{\Lambda}\,\delta P/P_o + \sum_{i=1}^{6} \lambda_i\ \delta C_i/P_o + \frac{1}{\Lambda}\,\delta\rho \qquad (6.1)$$

$$\frac{d\ \delta C_i/P_o}{dt} = \frac{\beta_i}{\Lambda}\,\delta P/P_o - \lambda_i\ \delta C_i/P_o \qquad (i = 1, 2, \ldots, 6) \qquad (6.2)$$

TABLE 6.1

FORT ST. VRAIN NEUTRONICS PARAMETERS

Core	Λ^+ (sec)	β^+	α_f^+ ($\delta k/k/°F$)	α_m^+ ($\delta k/k/°F$)
Initial Core, BOL*, equilibrium Xenon and Samarium	$1.8(10)^{-4}$	0.0065	$-2.3(10)^{-5}$	$0.555(10)^{-5}$
Initial Core, EOL**, equilibrium Xenon and Samarium	$1.9(10)^{-4}$	0.0053	$-2.4(10)^{-5}$	$0.833(10)^{-5}$

Delayed Neutron Group	Fraction BOL* ($x10^{+3}$)	Fraction EOL** ($x10^{+3}$)	Half Life BOL* (sec)	Half Life EOL** (sec)
1	0.214	0.22	55.7	55.4
2	1.42	1.18	22.7	22.2
3	1.27	1.04	6.22	5.92
4	2.57	1.86	2.3	2.27
5	0.748	0.512	0.6	0.61
6	0.273	0.203	0.23	0.24

*BOL = beginning of life.

**EOL = end of life.

$^+\Lambda$ = neutron generation time.

β = total delayed neutron fraction.

α_f = fuel temperature coefficient of reactivity.

α_m = moderator temperature coefficient of reactivity.

TABLE 6.2

DATA ON MAJOR DESIGN CHARACTERISTICS FORT ST. VRAIN FSAR[29]

REACTOR	
Type	HTGR employing a U^{235}-thorium fuel cycle, helium cooling, and graphite moderation.
Number of primary coolant loops	2
Net electrical output (to main power transformer), MW	330
Reactor thermal power, MW	842
CORE AND FUEL ASSEMBLIES	
Number of fuel elements in core	1482
Number of controls	74 (37 pairs)
Number of control rod drives	37
Effective core diameter, ft	19.6
Fuel element stack height, ft	15.6
Top reflector thickness, in	39
Bottom reflector thickness, in	46.8
Reactor vessel inside height, ft	75
Fuel elements type	Hexagonal graphite blocks containing blended beds of fuel particles

TABLE 6.2 (Continued)

CORE DESIGN OPERATING CONDITIONS	
Average power density, KW/liter	6.3
Max. power density, KW/liter	20.0
Heat transfer surface area, sq. ft	62,600
Heat flux, Btu/hr-ft^2	average 45,000 maximum 140,000
Fuel temperature, °F	average 1,500 maximum 2,300
Helium temperature at core outlet, °F	average 1,444 maximum 1,800
PRIMARY COOLANT SYSTEM	
Total helium flow rate in steam generators, lb/hr	3.41×10^6
Helium pressure at rated load, psia	700
Ratio of gross circulator power to gross thermal output	0.02
System pressure drop, psi	14
Helium circulator type	Single-state axial compressor
Number of helium circulators	4 (2 per loop)

TABLE 6.2 (Continued)

TURBINE PLANT	
Main turbine	Tandem-compound double-flow
Throttle steam pressure, psig	2,400
Throttle steam temperature, °F	1,000
Hot reheat steam pressure, psia	600
Reheat steam temperature, °F	1,000
Nominal design back pressure, in. Hg abs	2.5

where

$$\delta\rho = \sum_{i=1}^{4} \alpha_{fi}\, \delta T_{fi} + \sum_{i=1}^{4} \alpha_{mi}\, \delta T_{mi} + \delta\rho_{rod} \qquad (6.3)$$

α_{fi} = temperature coefficient of reactivity for ith fuel node

T_{fi} = temperature of ith fuel node

α_{mi} = temperature coefficient of reactivity for ith moderator node

T_{mi} = temperature of ith moderator node.

Core Thermal

In this theoretical model, there are four fuel nodes, six moderator (graphite) nodes and six primary coolant (helium) nodes in the core as shown in Figure 45. The typical fuel node equation is:

$$\frac{d}{dt}(C_{fi}T_{fi}) = Q_i - K_{fmi}(T_{fi} - T_{mi}) \qquad (6.4)$$

where

$i = 1, 2, 3, 4$

C_{fi} = heat capacity of the fuel node

Q_i = the amount of fission thermal energy which is released in the ith fuel node

K_{fmi} = heat transfer coefficient between the ith fuel node and the ith moderator node.

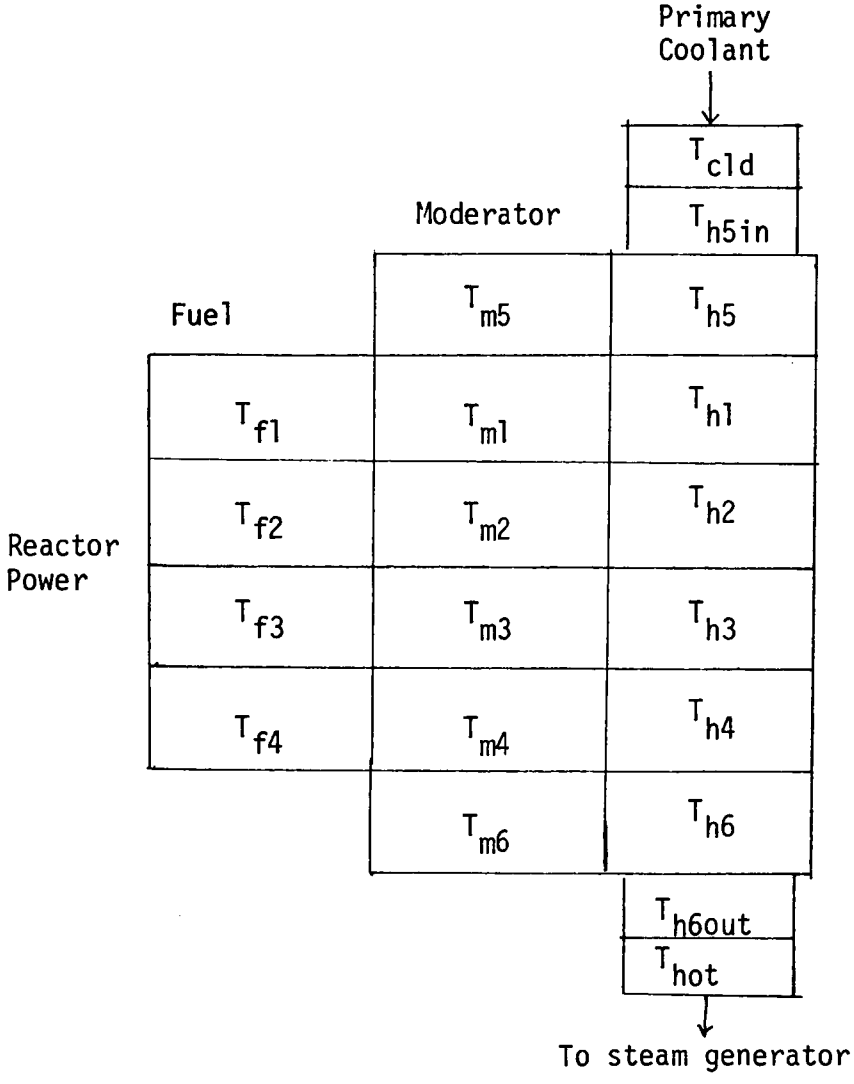


Figure 45. Core Thermal Model for Fort St. Vrain Nuclear System.

Linearizing the fuel node thermal balance Equation (6.4) gives

$$C_{fi} \frac{d}{dt} \delta T_{fi} = \delta Q_i - K_{fmi} \delta T_{fi} + K_{fmi} \delta T_{mi}. \qquad (6.5)$$

A typical equation for a moderator node is as follows

$$\frac{d}{dt} (C_{mi} T_{mi}) = K_{fmi}(T_{fi} - T_{mi}) - K_{mhi} \cdot F_h^{\,b}(T_{mi} - T_{hi}) \qquad (6.6)$$

where

$i = 1, 2, \ldots, 6$. Note that the first term on the right-hand side of Equation (6.5) is zero when $i = 5$ and 6.

C_{mi} = the heat capacity of the moderator node

T_{hi} = temperature of primary coolant node

K_{mhi} = heat transfer constant between the ith moderator node and its coolant node

$F_h^{\,b}$ = helium flow raised to the b power. In this case, $b = 0.8$, for heat transfer inside round tubes.

The moderator equation is now linearized assuming that the heat capacity does not change with temperature

$$C_{mi} \frac{d}{dt} \delta T_{mi} = K_{fmi} \delta T_{fi} - (K_{fmi} + K_{mhi} \bar{F}_h^{\,b}) \delta T_{mi}$$

$$- b K_{mhi} \bar{F}_h^{b-1}(\bar{T}_{mi} - \bar{T}_{hi}) \delta F_h \qquad (6.7)$$

where

$\bar{F}_h$, $\bar{T}_{mi}$, $\bar{T}_{hi}$ = steady state values.

A typical coolant node thermal balance equation is

$$\frac{d}{dt}(C_{hi}T_{hi}) = K_{mhi}F_h^b(T_{mi} - T_{hi}) + F_h\, C_p\, T_{hini} - F_h\, C_p\, T_{houti} \tag{6.8}$$

where

$i = 1, 2, \ldots, 6$

C_{hi} = heat capacity of the coolant node

C_p = the specific heat of helium

T_{hini} = helium temperature at inlet to ith coolant node

T_{houti} = helium temperature at outlet from ith coolant node.

The relationship between coolant inlet, midpoint, and outlet temperature is given by the arithmetic average

$$T_{hi} = 0.5\,(T_{hini} + T_{houti}). \tag{6.9}$$

In linearizing Equations (6.8) and (6.9), we have

$$C_{hi}\frac{d}{dt}T_{hi} = \bar{F}_h^b\, K_{mhi}\, \delta T_{mi} - \bar{F}_h^b\, K_{mhi}\, \delta T_{hi} + \bar{F}_h\, C_p\,(\delta T_{hini} - \delta T_{houti}) + b\bar{F}^{b-1}\, K_{mhi}\,(\bar{T}_{mi} - \bar{T}_{hi})\,\delta F_h + C_p\,(\bar{T}_{hini} - \bar{T}_{houti})\,\delta F_h \tag{6.10}$$

and

$$\delta T_2 = 0.5(\delta T_{hini} + \delta T_{houti}). \tag{6.11}$$

Assumptions in the core thermal model include: (1) no axial heat flow in fuel and graphite nodes, (2) specific heat of helium is constant, (3) no spatial variation of helium flow.

Helium Transport Delays

The temperatures in the piping between the core exit and steam generator entrance and the piping between steam generator exit and core inlet are each modeled as a well-mixed tank. The linearized equations are:

$$\frac{d}{dt}\delta T_{hhot} = \frac{1}{\tau_h}(\delta T_{h6} - \delta T_{hhot}) \tag{6.12}$$

$$\frac{d}{dt}\delta T_{hcld} = \frac{1}{\tau_c}(\delta T_{hcl} - \delta T_{hcld}) \tag{6.13}$$

where

T_{hhot} = temperature of helium in the pipe between core exit and steam generator inlet

T_{h6} = reactor outlet helium temperature

T_{hcld} = temperature of helium in the pipe between steam generator exit and core inlet

T_{hcl} = steam generator outlet helium temperature

τ_h = coolant transport time in hot leg piping

τ_c = coolant transport time in cold leg piping.

Secondary Coolant Pressure-Flow Equations

The secondary side pressure-flow modeling consists of the equations necessary to describe the water or steam flow rate and

pressure throughout the secondary coolant path. The nodal structure of the secondary pressure-flow model is shown on Figure 46. Nodes $\bar{P}_1$, $\bar{P}_2$, and $\bar{P}_3$ are the pressures in the steam generator. The equations for these nodes were derived in Chapter 2, page 14. Essentially, the basic modeling approach is conservation of mass. The flow into or from a node (except the nodes in the high pressure turbine and blower turbine) is determined from the relation

$$\text{Flow Rate} = K_f \sqrt{P_{up} - P_{dn}} \tag{6.14}$$

where

K_f = flow constant,

P_{up} = upstream pressure

P_{dn} = downstream pressure.

The nozzle flow equations for frictionless expansion of a perfect gas are used to calculate flow through each of the three expansions (P_{hpt}, P_{hpt1}, P_{hpt2}, and P_{hpte}) in the high pressure turbine, and the single expansion (P_{bt} and P_{bte}) in the blower turbine (see Figure 46).

The flow into or from these nodes is given by the following relation

$$\text{Flow Rate} = \frac{K_{hp} P_{up}}{\sqrt{T_{up}}} \sqrt{\left(\frac{P_{dn}}{P_{up}}\right)^{2/k} - \left(\frac{P_{dn}}{P_{up}}\right)^{k+1/k}} \tag{6.15}$$

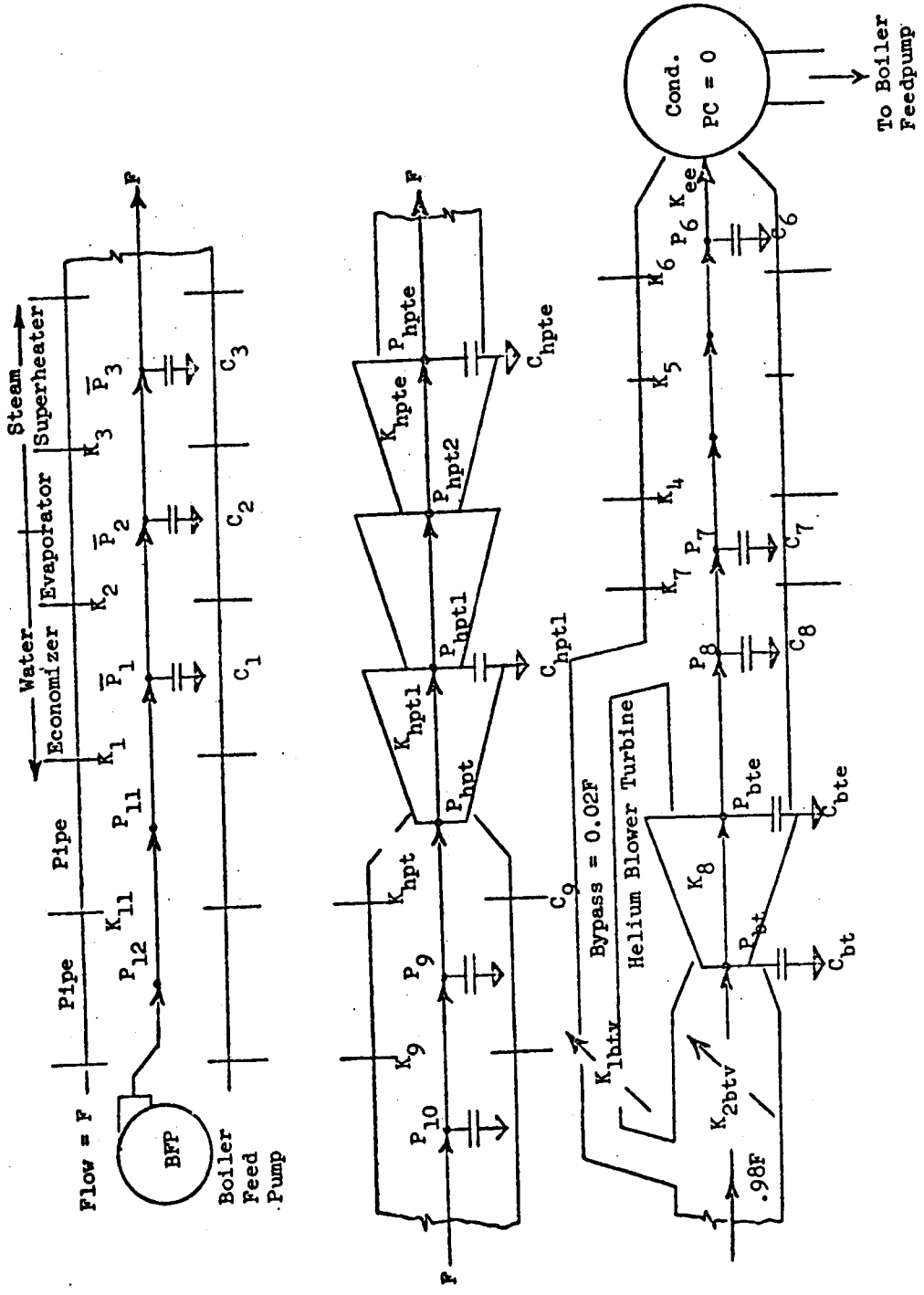


Figure 46. Pressure/Flow Model for Secondary Coolant Flow.

where

K_{hp} = flow constant

T_{up} = temperature at entrance to the node

k = ratio of specific heat = Cp/Cv.

The typical equation for each node is

$$\frac{d}{dt} M - F_{sin} - F_{sout} = 0 \tag{6.16}$$

where

M = the mass of steam/water in the node

F_{sin} = the flow of steam/water to the node

F_{sout} = the flow of steam/water from the node.

For the steam nodes, the mass storage term M is determined using the perfect gas law

$$M = \rho V = \frac{P}{RT} \tag{6.17}$$

where

ρ = density if steam at the node

V = total volume of the node

R = gas constant for steam

T = steam temperature of the node.

For the water nodes (the nodes before entering the steam generator), the change of mass storage term M is determined by the relation

$$\delta P = \beta \frac{\delta \rho}{\rho} = \frac{\beta}{M} \delta M \tag{6.18}$$

where

β = the bulk modulus.

After substituting Equation (6.14) (or (6.15)) and Equation (6.17) (or (6.18)) into Equation (6.16), the equations are linearized (see Reference 28 for the details). Then, the linear differential equations which relate the pressure, P, at each node to the other state variables can be obtained. (In this case, the state variables are the temperature and pressure at each node.)

Secondary Coolant Thermal Balance Equations

The thermal equations for the secondary system describes heat transfer between helium, tube metal, and water/steam in the steam generator and reheater and the transfer of energy from steam to turbine shaft in the high pressure and blower turbines. The equations for the steam generator were derived in Chapter 2, page 12. The nodal structure for the reheater, high pressure turbine and blower turbine is shown on Figure 47. There are two nodes for the helical U-tube integrated reheater.

Reheater Section. Typical nodal energy balance equations will be given for helium, tube, and steam nodes at the reheater section.

a. Helium side

The equations for helium nodes in the reheater section are

$$\frac{d}{dt}\left(M_{hi}\, T_{hbi}\, C_p\right) - F_h\, C_p\, T_{hai} + F_h\, C_p\, T_{hci} + \frac{A_i\left(T_{hbi} - T_{tbi}\right)}{K_{ht}\, F_h^{-\alpha} + R_t} = 0 \qquad (6.19)$$

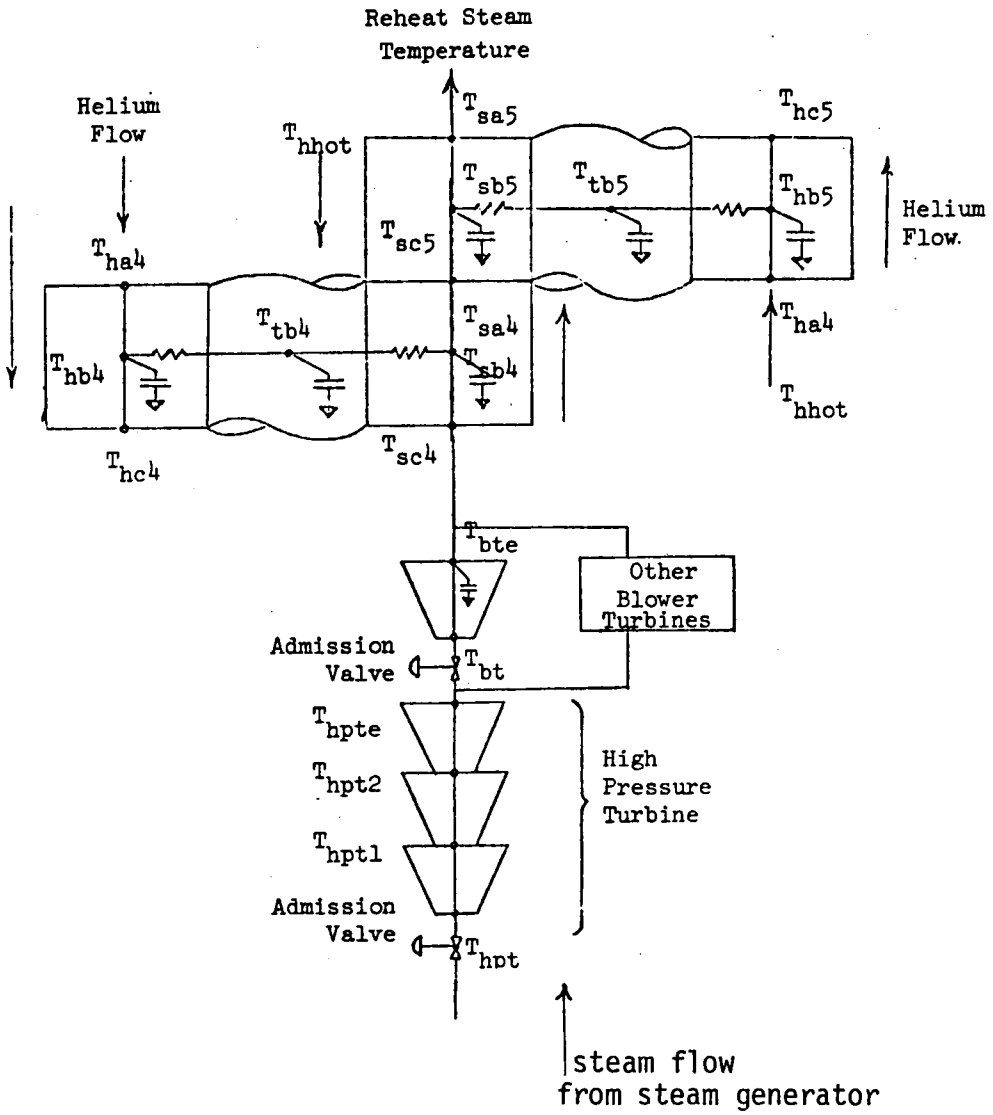


Figure 47. Thermal Model of Reheater and Turbines.

where

i = 4, 5 (see Figure 47)

M_{hi} = mass of helium in ith node

T_{hbi} = temperature at midpoint of ith helium node

T_{hai} = the entrance temperature at ith helium node

T_{hci} = the exit temperature at ith helium node

T_{tbi} = midpoint temperature of reheater metal node

α = exponent used in heat transfer correlation in this case is 0.615

K_{ht} = constant for helium to metal heat transfer

A_i = ith node heat transfer area

R_t = thermal resistivity of the metal times the tube thickness.

Arithmetic averaging is used to relate helium entrance, midpoint, and exit temperature

$$T_{hbi} = 0.5\ (T_{hci} + T_{hai}). \tag{6.20}$$

As seen on Figure 47, helium flows in parallel through the reheater nodes, with exit temperature T_{ha3} being considered the average of the two reheater helium outlet temperatures. Thus,

$$T_{ha3} = 0.5(T_{hc4} + T_{hc5}) = T_{hb4} + T_{hb5} - T_{hhot}. \tag{6.21}$$

b. Metal tube side

The typical balance equations for tube metal nodes are

$$M_{ti}\, C_{Pti}\, \frac{d}{dt}\,(T_{tbi}) + \frac{A_i(T_{tbi} - T_{sbi})}{K_{ts}\, F_{sini}^{-b} + R_t}$$

$$- \frac{A_i(T_{hbi} - T_{tbi})}{K_{ht}\, F_h^{-\alpha} + R_t} = 0 \qquad (6.22)$$

where

M_{ti} = mass of ith tube node

C_{Pci} = specific heat of ith tube node

K_{ts} = constant for tube to steam heat transfer

F_{sini} = steam flow in the ith steam node.

Steam flow, F_{sini}, is calculated by the same relationship used in Equation (6.14)

$$F_{sini} = K_i \sqrt{P_{i-1} - P_i}$$

c. Steam side

The thermal balance equations for the steam nodes are

$$\frac{d}{dt}\,[M_{si}\, C_p\, T_{sbi}] + H_{outi}\, F_{souti} - H_{ini}\, F_{sini}$$

$$- \frac{A_i\,(T_{tbi} - T_{sbi})}{F_{sini}^{-b} + R_t} = 0 \qquad (6.23)$$

where

M_{si} = mass of steam in ith node

H_{outi} = enthalpy at ith node exit

H_{ini} = enthalpy at ith node inlet.

The steam flow rate, F_{souti} is given by the relation

$$F_{souti} = K_{i+1} \sqrt{P_i - P_{i+1}} \cdot$$

Turbine Thermal Balances. The energy balance equations for steam flow in the high pressure turbine (HP) and blower turbine are based on the following thermodynamic relationship for each node

$$q_{stored} - q_{in} + q_{out} + P_{ower} = 0$$

or

$$\frac{d}{dt}(M C_p T) - F_{sin} H_{in} + F_{sout} H_{out} + W = 0 \qquad (6.24)$$

where

$W = F_{sin} \Delta H = F_{sin} C_p \Delta T$

q = rate change of the energy in the node

$\Delta H/\Delta T$ = change in enthalpy/temperature of steam between the turbine expansion node entrance and exit.

The steam flow rate, F_s, is calculated using Equation (6.15) which is strictly true only for adiabatic, frictionless flow. Furthermore, the flow is further limited to subsonic flow in each expansion node.

$$C_p \Delta T = K_b T_o [1 - (P_1/P_o)^{k-1/k}] \qquad (6.25)$$

where

$$K_b = \frac{\bar{H}_{in} - \bar{H}_{out}}{\bar{T}_o[1 - (\bar{P}_1/\bar{P}_o)^{k-1/k}]}$$

T_o, P_o = temperature and pressure at entrance to expansion

P_1 = pressure at exit from expansion

$\bar{P}, \bar{T}, \bar{H}$ = refer to steady values.

As seen in Figure 47, the high pressure turbine is modeled as three nozzle expansions with corresponding variables T_{hpt1}, T_{hpt2}, and T_{hpte}. The blower turbine is modeled as one expansion, with corresponding variable T_{hpt}. The time delays due to transport in pipes between components are assumed to be zero. That is,

$$T_{hpt} = \begin{bmatrix}\text{high pressure turbine}\\ \text{inlet temperature}\end{bmatrix} = T_{sa3} = \begin{bmatrix}\text{steam generator}\\ \text{exit temperature}\end{bmatrix}$$

$$T_{bt} = \begin{bmatrix}\text{blower turbine}\\ \text{inlet temperature}\end{bmatrix} = T_{hpte} = \begin{bmatrix}\text{high pressure turbine}\\ \text{exit temperature}\end{bmatrix}$$

$$T_{sc4} = \begin{bmatrix}\text{reheater steam}\\ \text{inlet temperature}\end{bmatrix} = T_{bte} = \begin{bmatrix}\text{blower turbine}\\ \text{exit temperature}\end{bmatrix} .$$

Energy storage in all but the blower turbine node is assumed to be zero.

This concludes the description of the thermal balance equations for each node of the secondary coolant loop. The linear differential equations which relate the state variable (temperature) at each node

to the other state variables (temperature and pressure) can be obtained by linearizing the thermal balance equations (see Reference 28 for the details of the linearization procedures).

Helium Flow Rate

The helium flow rate, F_h, throughout the primary coolant flow path is assumed to be directly proportional to the blower turbine shaft angular velocity, ω.

$$F_h = R_{rkh}\ \omega \tag{6.26}$$

where

R_{rkh} = the conversion constant.

The blower turbine angular velocity is determined by conservation of angular momentum. That is, the time rate of change of angular momentum equals the net torque

$$\frac{I}{g_c}\frac{d\omega}{dt} = T_t - T_b \tag{6.27}$$

where

I = moment of inertia of blower turbine rotor shaft

g_c = 32 ft-lbm/lb_F - sec^2

T_t = torque exerted on shaft by the force of steam flowing in the blower turbine

T_b = torque exerted on shaft by helium in blower.

T_b is approximated using the relation

$$T_b = K_b\ \omega^2 \tag{6.28}$$

where

K_b = the empirical drag constant.

The above equation for T_b assumes that K_b does not vary with angular velocity.

T_t is determined by using an energy balance equation

$$\omega T_t = F_s \Delta H = F_s C_p \Delta T. \tag{6.29}$$

Subsonic, frictionless, and adiabatic flow of a perfect gas through the expansion node is assumed. Using Equation (6.25) and Equation (6.15), the quantities ΔH and F_s can be determined. After substituting these quantities into Equation (6.27) and linearization, the linear differential equation which relates the helium flow rate, F_h, to the other state variables can be obtained (see Reference 28 for the details).

Overall System

The linear differential equations which have been developed to represent the components of the Fort St. Vrain Nuclear Steam Supply System can be cast into state variable form:

$$A \frac{d\bar{x}}{dt} = B\bar{x} + \bar{f}g$$

where

$$\bar{X} = \begin{bmatrix} X_1 \\ X_2 \\ \vdots \\ X_{49} \\ X_{50} \\ \vdots \\ X_{81} \end{bmatrix} = \begin{bmatrix} \delta\bar{P}_1 \\ \delta\bar{P}_2 \\ \vdots \\ \delta\rho \\ \delta P/P_o \\ \vdots \\ \delta T_{sb5} \end{bmatrix}$$

A = the differential system matrix

B = the algebraic system matrix

$$\bar{f} = \begin{bmatrix} \delta f_1 \\ \delta f_2 \\ \vdots \\ \delta f_{49} \\ \vdots \\ \delta f_{81} \end{bmatrix} = \begin{bmatrix} 0 \\ 0 \\ \vdots \\ 5.9\text{x}10^{-3} \\ \vdots \\ 0 \end{bmatrix}$$

For the reactivity perturbation case, only the 49th element of the forcing vector is non-zero. The indeces of the state variables of the model are listed in Table 6.3. This 81st order model included 58 differential and 23 algebra equations. The values of non-zero elements of the A and B matrices are given in Table 6.4 and Table 6.5. The frequency response for reactor power level/rod reactivity was computed using the PARAPE code with the non-optimization option (see Appendix D), and the results are plotted in Figure 48 using

TABLE 6.3

STATE VARIABLE INDEX FOR FORT ST. VRAIN SYSTEM

State Variable	Index Number	Definition
$\bar{P}_1$-$\overline{TG}_3$	1-20	The twenty state variables of the steam generator (see Table 2.1, page 8).
M_{st}	21	Throttle steam temperature.
TG_4	22	Helium temperature at steam generator inlet
F_h	23	Helium flow rate.
T_{hcld}	24	Helium temperature at the pipes between steam generator and core.
T_{f1}-T_{f4}	25,28,31,34	Fuel temperature at each node.
T_{m1}-T_{m6}	26,29,32,35, 39,51	Moderator temperature at each node.
T_{h1}-T_{h6}	27,30,33,36, 40,53	Helium temperature at each node in the core.
T_{cld}	37	Helium temperature at core inlet.
T_{h5a}	38	Helium entrance temperature at 5th helium node in the core.
T_{h4c}	41	Helium exit temperature at 4th helium node in the core
q	42	Thermal power and neutron flux conversion factor.
C_1-C_6	43-48	1st to 6th precursor concentrations.
ρ	49	The reactivity term.
P	50	Neutron flux level.
T_{hot}	52	Helium exit temperature at 6th node.

TABLE 6.3 (Continued)

State Variable	Index Number	Definition
P_{12}	54	Section of pipe between P_{11} node and feedwater pump.
P_{11}	55	Section of pipe between P_{12} node and entrance to economizer.
P_{10}	56	Section of pipe between superheat and P_9 node.
P_9	57	Section of pipe between P_{10} and throttle valve
P_{hpt}	58	Pressure between throttle valve and 1st HPT expansion.
P_{hpt1}	59	Pressure between HPT 1st and 2nd expansion node.
P_{hpt2}	60	Pressure between HPT 2nd and 3rd expansion node.
P_{hpte}	61	HPT exit pressure.
P_{bt}	62	Pressure between blower turbine valve and entrance to 1st expansion node
P_{bte}	63	Blower turbine exit pressure.
P_8	64	Section of pipe between blower turbine exit and P_7 node
P_7	65	Section of pipe between reheat and blower turbine.
P_4	66	1st reheater node pressure
P_5	67	2nd reheater node pressure.
P_6	68	Section of pipe leading from reheater to low pressure turbine throttle valve.

TABLE 6.3 (Continued)

State Variable	Index Number	Definition
T_{hpt1}	69	Temperature at same section as P_{hpt1}.
T_{hpt2}	70	Temperature at same section as P_{hpt2}.
T_{hpte}	71	Temperature at same section as P_{hpte}.
T_{bte}	72	Temperature at same section as P_{bte}.
T_{hb4}	73	Temperature of 4th helium node (in reheater).
T_{tb4}	74	Temperature of 4th tube node.
T_{sb4}	75	Temperature of 4th steam node.
T_{sa5}	76	Temperature of steam at the entrance of 2nd node.
T_{hhot}	77	Helium temperature between the core and steam generator inlet.
T_{sa4}	78	Steam temperature at the entrance of reheater.
T_{hb5}	79	Helium temperature at 5th node (reheater).
T_{tb5}	80	Tube temperature at 5th node.
T_{sb5}	81	Steam temperature at 5th node.

TABLE 6.4

ELEMENTS OF A MATRIX FOR CASE STUDY III

I	J	Value	I	J	Value
1	1	2.61100E-01	1	11	3.38100E 01
2	2	1.01500E 00	2	11	2.28600E 01
2	12	1.47400E 01	3	3	3.13900E-01
3	12	1.05200E 01	3	13	-5.05800E-01
7	7	1.00000E 00	8	8	7.41000E 03
8	11	-7.91700E 03	9	9	4.71100E 03
9	11	-7.91700E 03	9	12	-1.09600E 04
10	10	7.51100E 03	10	12	-1.09600E 04
11	1	4.14200E 02	11	11	-6.98900E 02
12	2	9.45500E 02	12	11	1.57900E 04
12	12	8.68800E 03	13	3	3.67400E 02
13	12	9.52200E 03	13	13	-4.25700E 02
14	11	-3.11100E 02	14	14	3.67500E 01
15	11	3.11100E 02	15	12	-3.11100E 02
15	15	1.97900E 01	16	12	3.11100E 02
16	16	2.59200E 01	21	21	3.00000E 01
23	23	1.00000E 00	24	24	1.50000E 00
25	25	2.01700E 03	26	26	6.09200E 03
27	27	2.92200E 01	28	28	4.36200E 03
29	29	1.33000E 04	30	30	4.99000E 01
31	31	4.41500E 03	32	32	1.36200E 04
33	33	4.18300E 01	34	34	2.20100E 03
35	35	6.83200E 03	36	36	1.93400E 01
39	39	1.53900E 04	43	43	1.00000E 00
44	44	1.00000E 00	45	45	1.00000E 00
46	46	1.00000E 00	47	47	1.00000E 00
48	48	1.00000E 00	50	50	1.00000E 00
53	53	1.99800E 04	54	54	2.71000E-02
55	55	7.27800E-03	56	13	-6.38900E-02
56	56	3.64800E-02	57	13	-4.46100E-01
57	57	2.67900E-01	58	58	1.29500E-02
59	59	1.73300E-02	61	61	4.26700E-01
62	62	4.18100E-02	63	63	9.40800E-02
64	64	1.00900E 00	65	65	2.57700E-01
66	75	-1.82900E-02	67	81	-1.56500E-02
68	68	1.12500E 00	69	69	2.31800E 01
72	72	1.32000E 03	73	73	2.08500E 01
74	74	1.60000E 03	75	75	1.25000E 01
77	77	1.00000E 00	79	79	2.01400E 01
80	80	1.60000E 03	81	81	1.17900E 01

TABLE 6.5

ELEMENTS OF B MATRIX FOR CASE STUDY III

I	J	Value	I	J	Value
1	17	1.00000E 00	1	18	-1.00000E 00
2	18	1.00000E 00	2	19	-1.00000E 00
3	19	1.00000E 00	3	20	-1.00000E 00
4	4	7.50000E-01	4	5	2.50000E-01
4	14	-1.00000E 00	5	5	6.70000E-01
5	6	3.30000E-01	5	15	-1.00000E 00
6	6	3.00000E-01	6	7	7.00000E-01
6	16	-1.00000E 00	7	7	-2.00000E 00
7	22	2.00000E 00	8	1	8.77400E 01
8	8	-3.54900E 03	8	14	9.37200E 02
8	17	-8.58400E 01	8	18	-2.86100E 01
8	23	1.28300E 02	9	2	9.14300E 01
9	9	-2.35900E 03	9	15	5.95800E 02
9	18	-4.74800E 01	9	19	-2.33800E 01
9	23	9.01200E 01	10	3	-1.42600E 02
10	10	-3.89900E 03	10	13	1.83200E 03
10	16	9.50000E 02	10	19	-3.52900E 01
10	20	-8.23500E 01	10	23	1.69000E 02
11	1	-1.13700E 02	11	2	-2.59300E 01
11	8	2.61200E 03	11	11	1.39500E 03
11	17	4.71600E 02	11	18	-7.48700E 02
12	1	2.59300E 01	12	2	-3.78800E 01
12	3	2.76200E 01	12	9	1.76300E 03
12	11	-1.54100E 03	12	12	1.54100E 03
12	18	8.24800E 02	12	19	-1.02900E 03
13	2	-2.76200E 01	13	3	1.25800E 02
13	10	2.94900E 03	13	12	-1.81300E 03
13	13	-2.04700E 03	13	19	1.08800E 03
13	20	-1.48600E 03	14	4	-5.95500E 02
14	5	5.95500E 02	14	8	9.37200E 02
14	11	-1.45900E 03	14	14	-9.37200E 02
14	23	1.33200E 02	15	5	-5.95500E 02
15	6	5.95500E 02	15	9	5.95800E 02
15	11	1.61200E 03	15	12	-1.61200E 03
15	15	-5.95800E 02	15	23	9.35300E 01
16	6	-5.95500E 02	16	7	5.95500E 02
16	10	9.50000E 02	16	12	1.89600E 03
16	16	-9.50000E 02	16	23	1.75400E 02
17	1	-6.18100E 00	17	17	-1.00000E 00
17	55	6.18100E 00	18	1	7.24500E 00
18	2	-7.24500E 00	18	18	-1.00000E 00
19	2	1.86000E 00	19	3	-1.86000E 00
19	19	-1.00000E 00	20	3	1.37700E 00

TABLE 6.5 (Continued)

I	J	Value	I	J	Value
20	20	-1.00000E 00	20	56	-1.37700E 00
21	13	1.00000E 00	21	21	-1.00000E 00
22	22	-1.00000E 00	22	73	1.00000E 00
22	77	-1.00000E 00	22	79	1.00000E 00
23	23	-3.91700E 00	23	62	2.16700E 00
23	63	-2.32400E 00	23	71	7.89400E-02
24	4	1.00000E 00	24	24	-1.00000E 00
25	25	-5.96300E 02	25	26	5.96300E 02
25	42	1.65400E-01	26	23	-1.30500E 02
26	25	5.96300E 02	26	26	-7.93900E 02
26	27	1.97600E 02	27	23	-1.14900E 01
27	26	1.97600E 02	27	27	-1.31900E 03
27	37	1.12100E 03	28	28	-1.14900E 03
28	29	1.14900E 03	28	42	4.36100E-01
29	23	-3.44100E 02	29	28	1.14900E 03
29	29	-1.53300E 03	29	30	3.83800E 02
30	23	-3.03100E 01	30	27	2.24300E 03
30	29	3.83800E 02	30	30	-1.50500E 03
30	37	-1.12100E 03	31	31	-1.32200E 03
31	32	1.32200E 03	31	42	3.57100E-01
32	23	-2.81700E 02	32	31	1.32200E 03
32	32	-1.78800E 03	32	33	4.65900E 02
33	23	-2.48200E 01	33	27	-2.24300E 03
33	30	2.24300E 03	33	32	4.65900E 02
33	33	-1.58700E 03	33	37	1.12100E 03
34	34	-2.36600E 02	34	35	2.36600E 02
34	42	4.14500E-02	35	23	-3.27100E 01
35	34	2.36600E 02	35	35	-3.22700E 02
35	36	8.60900E 01	36	23	-2.88100E 00
36	27	2.24300E 03	36	30	-2.24300E 03
36	33	2.24300E 03	36	35	8.60900E 01
36	36	-1.20700E 03	36	37	-1.12100E 03
37	37	5.95600E 02	37	38	-5.95600E 02
37	39	-7.90900E 02	37	40	7.90900E 02
38	24	1.00000E 00	38	38	-1.00000E 00
39	39	-7.90900E 02	39	40	7.90900E 02
40	37	-1.00000E 00	40	38	-1.00000E 00
40	40	2.00000E 00	41	27	-2.00000E 00
41	30	2.00000E 00	41	33	-2.00000E 00
41	36	2.00000E 00	41	37	1.00000E 00
41	41	-1.00000E 00	42	42	1.00000E 00
42	50	-4.13700E 03	43	43	-1.24300E-02
43	50	6.22100E-03	44	44	-3.05000E-02
44	50	4.14000E-02	45	45	-1.11400E-01
45	50	3.70300E-02	46	46	-3.01300E-01
46	50	7.46500E-02	47	47	-1.13600E 00
47	50	2.17400E-02	48	48	-2.98100E 00

TABLE 6.5 (Continued)

I	J	Value	I	J	Value
48	50	7.93600E-03	49	25	-1.65500E-06
49	26	5.67700E-07	49	28	-9.37900E-06
49	29	3.82200E-06	49	31	-6.01300E-06
49	32	2.49800E-06	49	34	-8.19900E-08
49	35	3.34700E-08	49	49	-1.00000E 00
50	43	1.24300E 00	50	44	3.05000E 00
50	45	1.11400E 01	50	46	3.01300E 01
50	47	1.13600E 02	50	48	2.98100E 02
50	49	2.90700E 05	50	50	-1.89000E 01
51	41	-1.00000E 00	51	51	2.00000E 00
51	52	-1.00000E 00	52	41	-5.95600E 02
52	51	8.42900E 02	52	52	5.95600E 02
52	53	-8.42900E 02	53	51	8.42900E 02
53	53	-8.42900E 02	54	54	-8.24500E-01
54	55	8.24500E-01	55	17	-1.00000E 00
55	54	8.24500E-01	55	55	-8.24500E-01
56	20	1.00000E 00	56	56	-1.23900E 00
56	57	1.23900E 00	57	56	1.23900E 00
57	57	-2.11700E 00	57	58	8.77900E-01
58	21	2.19400E-01	58	57	1.75600E 00
58	58	-2.27600E 00	58	59	3.25700E-01
59	21	-2.19400E-01	59	58	5.19900E-01
59	59	-1.03100E 00	59	60	4.47100E-01
59	69	2.31900E-01	60	59	7.05400E-01
60	60	-1.28100E 00	60	61	4.73500E-01
60	69	-2.31900E-01	60	70	2.47100E-01
61	60	8.33800E-01	61	61	-4.52100E 00
61	62	3.99100E 00	61	64	5.65300E-02
61	70	-2.47100E-01	62	61	1.99600E 00
62	62	-2.75700E 00	62	63	5.24700E-01
62	71	1.28800E-01	63	62	7.61600E-01
63	63	-2.32200E 01	63	64	2.26900E 01
63	71	-1.28800E-01	64	61	2.82600E-02
64	63	2.26900E 01	64	64	-4.46400E 01
64	65	2.19200E 01	65	64	2.19200E 01
65	65	-3.55000E 01	65	66	1.35800E 01
66	65	1.35800E 01	66	66	-3.25100E 01
66	67	1.89300E 01	67	66	1.89300E 01
67	67	-2.39400E 01	67	68	5.00600E 00
68	67	5.00600E 00	68	68	-5.53600E 00
68	76	1.57100E-01	69	21	7.28400E 02
69	57	2.51100E 03	69	58	-3.28200E 03
69	59	5.03100E 02	69	69	-4.12100E 02
70	21	-3.06500E 02	70	58	7.26200E 02
70	59	-1.48200E 03	70	60	6.79900E 02
70	69	7.20800E 02	70	70	-3.99000E 02
71	59	9.60100E 02	71	60	-1.74300E 03

TABLE 6.5 (Continued)

I	J	Value	I	J	Value
71	61	7.18000E 02	71	69	-3.15600E 02
71	70	7.17500E 02	71	71	-3.99400E 02
72	61	2.66700E 03	72	62	-3.71800E 03
72	63	7.44600E 02	72	71	3.48200E 02
72	72	-2.01200E 02	73	23	7.54000E 01
73	73	-6.32600E 02	73	74	8.70200E 01
73	77	5.95600E 02	74	23	3.29400E 01
74	65	-2.63100E 02	74	66	2.63100E 02
74	73	8.70200E 01	74	74	-1.17600E 02
74	75	3.05800E 01	75	65	1.78700E 04
75	66	-4.48200E 04	75	67	2.69600E 04
75	72	2.09600E 02	75	74	3.05800E 01
75	75	-3.05800E 01	75	78	-1.76700E 02
76	76	-1.00000E 00	76	78	-1.00000E 00
76	81	2.00000E 00	77	52	1.00000E 00
77	77	-1.00000E 00	78	72	-1.00000E 00
78	75	2.00000E 00	78	78	-1.00000E 00
79	23	6.64700E 00	79	77	5.95600E 02
79	79	-6.82600E 02	79	80	8.70200E 01
80	23	2.50700E 01	80	66	-2.00300E 02
80	67	2.00300E 02	80	79	8.70200E 01
80	80	-1.17600E 02	80	81	3.05800E 01
81	66	2.71600E 04	81	67	-3.47700E 04
81	68	7.61600E 03	81	76	-1.73800E 02
81	78	1.76700E 02	81	80	3.05800E 01
81	81	-3.05800E 01			

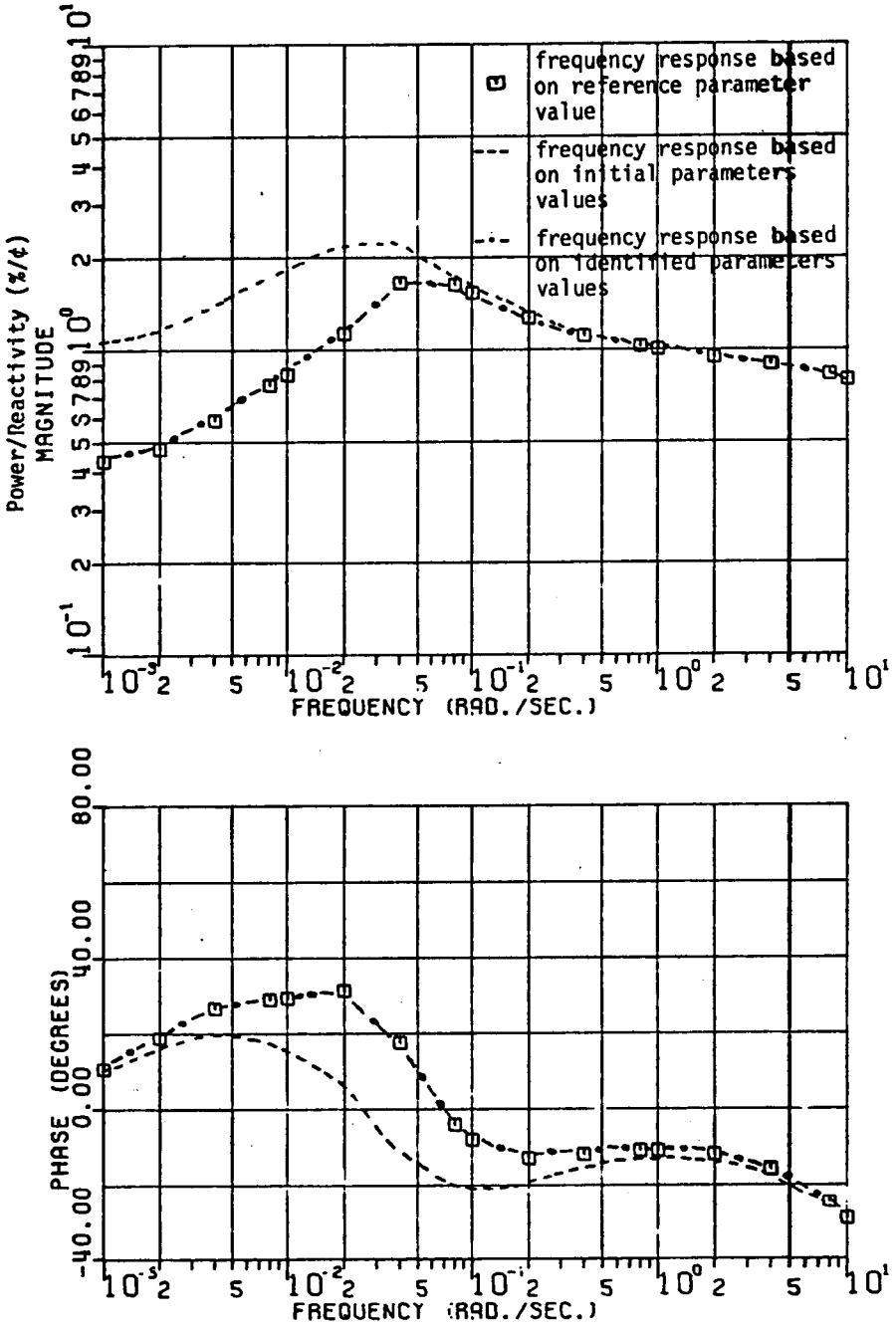


Figure 48. Comparison Between the Results of PARARI Calculation and Reference Model's Frequency Response.

symbol, ◻ . This analysis required 10 minutes and 50 seconds on an IBM-360 model 65. The frequency response of the reference model will be treated as the experimental data in this case study.

The fuel temperature coefficients of reactivity, α_{fi}, and the moderator temperature coefficients of reactivity, α_{mi}, are chosen as the coefficients to be adjusted. The reference values for these coefficients (in $\frac{\Delta K}{K}/°F$ unit) are:

$$\alpha_{f10} = 1.655 \times 10^{-6} \text{ , } \alpha_{m10} = 5.677 \times 10^{-7}$$

$$\alpha_{f20} = 9.378 \times 10^{-6} \text{ , } \alpha_{m20} = 3.822 \times 10^{-6}$$

$$\alpha_{f30} = 6.013 \times 10^{-6} \text{ , } \alpha_{m20} = 2.498 \times 10^{-6}$$

$$\alpha_{f40} = 8.20 \times 10^{-8} \text{ , } \alpha_{m20} = 3.347 \times 10^{-8}.$$

Let

$$P_1 = \alpha_{f1}/\alpha_{f10} = \alpha_{f2}/\alpha_{f20} = \alpha_{f3}/\alpha_{f30} = \alpha_{f4}/\alpha_{f40}.$$

and

$$P_2 = \alpha_{m1}/\alpha_{m10} = \alpha_{m2}/\alpha_{m20} = \alpha_{m3}/\alpha_{m30} = \alpha_{f4}/\alpha_{m40},$$

be the parameters defined relative to the reference coefficients values. Then, the values of parameters P_1 and P_2 were arbitrarily changed as follows:

$$P_1 = 0.7 \text{ and } P_2 = 1.2. \tag{6.30}$$

Using these new parameter values, the new system matrices A and B were generated, and the frequency responses were calculated and plotted in Figure 48. The differences relative to the reference model are

at the frequencies lower than 0.2 rad/sec. This is because α_f and α_m have large effects at low frequencies only.

The PARAPE computer code was run with the parameter values in Equation (6.30) as the initial parameter estimates; and the code adjusted these parameters to reduce the differences between theory and simulated experiment. The optimized parameter should converge to unity if the search is successful.

6.4 Results and Discussion

The elements of the system matrix which contain the adjustable parameters can be identified from the equations in the previous section. All the elements which contain the parameter are in Equation (6.3). The algebra table was set up as shown in Table 6.6. After the row/column shifting, the program found that the dimension of the sub-matrices were ten.

The results of a PARARI code run are shown in Table 6.7. The value of the error function decreases quickly from 6.66 to 0.02. The optimized parameters are found at the tenth iteration, they are close to unity (the "true" values of parameters). The estimates of P_1 and P_2 have three percent and nine percent deviation from unity. The frequency response of the model with the optimized parameter values is plotted in Figure 48. There are no significant differences between the optimized results and the reference results.

For the same case, the results of a PARAGP code run are shown in Table 6.8.

TABLE 6.6

THE ALGEBRA TABLE FOR CASE STUDY III

Index I	Index J	Index M	Constant Value * 10^{-6}	The Exponent Value of P_1	The Exponent Value of P_2
49	25	1	-1.655	1.0	0.0
49	26	1	0.567	0.0	1.0
49	28	1	-9.378	1.0	0.0
49	29	1	3.822	0.0	1.0
49	31	1	-6.013	1.0	0.0
49	32	1	2.498	0.0	1.0
49	34	1	-0.082	1.0	0.0
49	35	1	0.0335	0.0	1.0

TABLE 6.7

THE RESULTS OF PARARI CODE RUN FOR THE FORT ST. VRAIN NUCLEAR SYSTEM

Iteration Number	Error Function Value * 10^2	$P_1(\alpha_f/\alpha_{fo})$	$P_2(\alpha_m/\alpha_{mO})$
1	666.25	0.7	1.2
2	0.594	1.044	1.089
3	0.277	1.036	1.0913
4	0.225	1.033	1.0917
5	0.203	1.032	1.0919
6	0.193	1.031	1.0919
7	0.186	1.030	1.0919
8	0.182	1.0298	1.0917
9	0.179	1.0293	1.0916
10	0.177	1.0288	1.0914

TABLE 6.8

THE RESULTS OF PARAGP CODE RUN FOR THE FORT ST. VRAIN NUCLEAR SYSTEM

Iteration Number	Error Function Value * 10^2	$P_1(\alpha_f/\alpha_{fo})$	$P_2(\alpha_m/\alpha_{mo})$
1	3018.4	0.7	1.2
2	76.7	1.102	1.075
3	1.87	1.04	1.095
4	0.72	1.034	1.096
5	0.605	1.033	1.097
6	0.556	1.0325	1.0971
7	0.532	1.0320	1.0971
8	0.519	1.0316	1.0972
9	0.512	1.0314	1.0972
10	0.507	1.0311	1.0972

The results between the PARARI and PARAGP code calculations are almost the same at both runs (unlike the results of case study II in Chapter 5, page 137). As shown in Table 6.8, the error function decreases from 30.18 to 0.005 and the optimized values of P_1 and P_2 were found at the tenth iteration with 3.1 percent and 9.7 percent deviation from unity.

The curvatures, $J_{ii\ell}$, for each parameter were calculated and the curves are plotted in Figure 49. The curvature of P_1 is constantly larger than the curvature of P_2. This is the main reason why P_2 has a larger deviation from unity than P_1. For the Fort St. Vrain system, the maximum value of the curve for α_{fi} appear at a lower frequency (0.04 rad/sec) than the Oconee I system (see Figure 37, page 128). This is because the high temperature gas cooled reactor (HTGR) has a larger core and heat capacity than the pressurized water reactor (PWR).

It is very interesting to see that the curves in Figure 49 are parallel to each other at the frequencies lower than 0.08 rad/sec. Also, this is the frequency range where the large differences exist between the model based on starting parameter estimates and the reference model (see Figure 48). This means that the change of α_{fi} and α_{mi} will have similar effects at low frequencies on the power level/reactivity frequency response. This provides us the explanation of why the error function almost approaches zero, the optimized P_1 and P_2 still had deviations from unity.

The curvature results suggest that if one intends to get better estimates of α_{fi} or α_{mi} from dynamic test data, the power

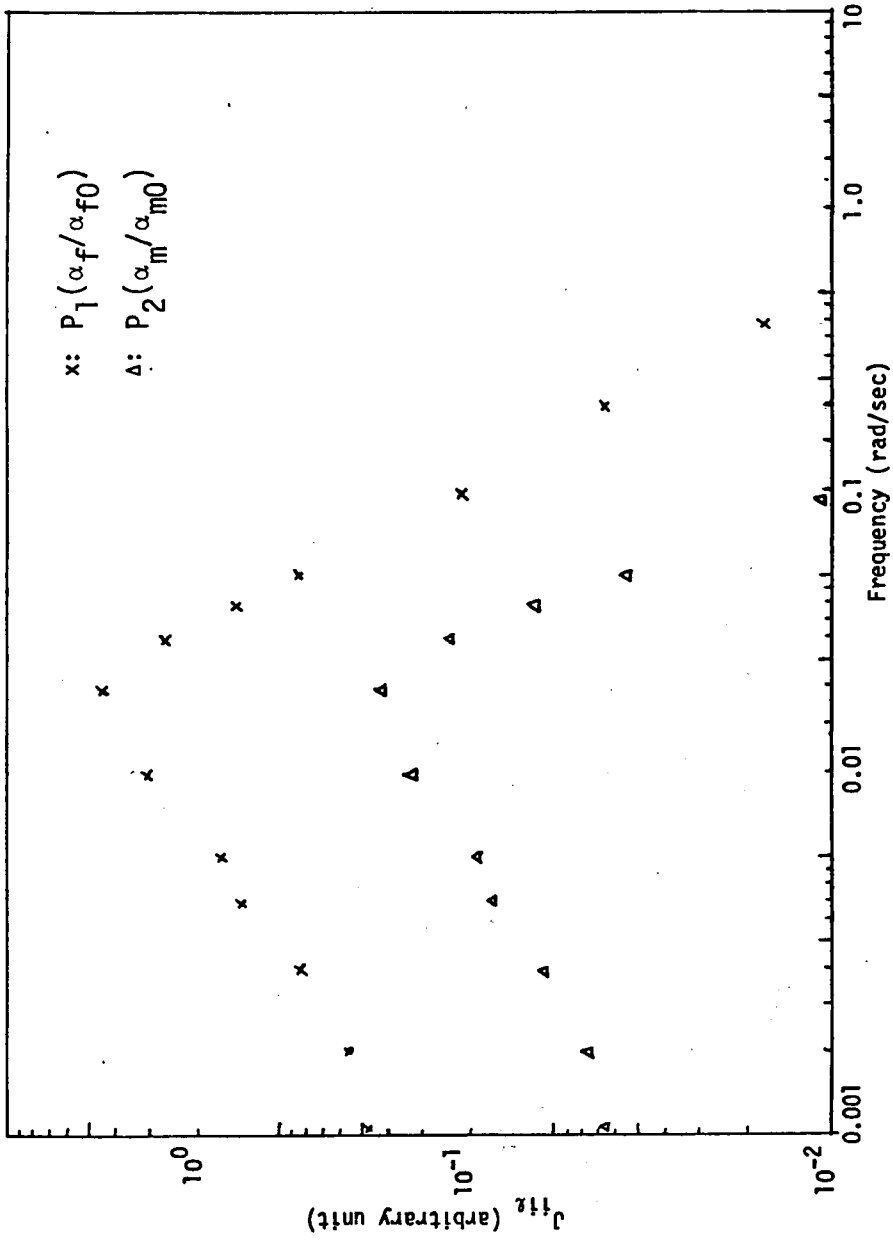


Figure 49. The Curves of J_{iil} Versus Frequencies for Fort St. Vrain Nuclear System.

of the input signal should be concentrated in the frequency range 0.04 to 0.1 rad/sec. This is the frequency range where the larger values of curvature appeared.

The computer time required was 12 minutes and 50 seconds in each analysis on an IBM 360 model 65. Recall that 10 minutes and 50 seconds was required in the case run by the code with non-optimization option. So, by using the partitioned matrix technique in the optimization scheme, it only took 2 minutes for the ten iterations in the parameter optimization.

CHAPTER 7

CONCLUSIONS AND RECOMMENDATIONS

7.1 Conclusions

A new method was developed for identification of parameters in large dynamic systems. The identification is achieved by an optimization procedure that adjusts system parameters to minimize differences between experimental frequency responses and theoretical frequency responses obtained from the dynamic model (up to 110th order systems can be handled). The identification uses a new matrix partitioning technique in order to achieve the computational efficiency needed to deal with very large models. The primary intended use of the method is to analyze results from tests to be performed at the Fort St. Vrain plant.

The work included a study of methods for assessing the identifiability of parameters by fitting dynamic test data. The Fisher Information Matrix was found to be useful for this purpose. Basically, the Fisher Information Matrix is a matrix whose diagonal elements are the curvature of the error in the calculated frequency response versus a selected parameter. Large diagonal elements indicate that the error function depends strongly on the parameter and identification is likely. It was also found that the frequency dependence of the sensitivity function is important in determining identifiability. The measurements should include frequencies where the sensitivity to the parameter of interest is largest. Also, it

was found that separate, unique identification of parameters with parallel curves of sensitivity versus frequency is impossible regardless of how large the magnitudes of the sensitivities are.

These methods were demonstrated in three test cases. One used actual test data (from the Oconee I pressured water reactor) and a twenty-ninth order model. The other two used simulated experiments. The models for these were twentieth order and eighty-first order. These demonstrated that the computational requirements are reasonable for large systems and that the procedure can find correct parameters if all of the identifiability conditions are satisfied. In this connection, the non-uniqueness of estimates for parameters with parallel curves of sensitivity versus frequency was demonstrated in a test case.

As an adjunct to the identification work, it was necessary to develop a model for the Fort St. Vrain steam generator to be included in the overall plant model. This model was developed and is discussed in Chapter 2, page 6. It is a three-node, moving boundary, linear model for the system. It was used successfully in the overall system model in one of the simulated test cases.

In general, the work has provided a systematic method for parameter identification in the planned future tests at Fort St. Vrain as well as other systems described by large linear dynamic models.

7.2 Recommendations

The results of the PARAPE code calculation are different when different forms of error function are used. The PARARI code which uses the sum of the squared difference in real and imaginary parts of the frequency response as the error function failed to find the true values of parameters in case study II. The values of weighting factors W_1 and W_2 (see Appendix A), which are used in the error function for the PARAGP code, have large effects on the results too as shown in case study I. In order to obtain more information about the way to choose the best form of error function and values of weighting factors for each case, additional work is necessary.

It is very difficult to evaluate the uniqueness or the identifiability of the physical parameters to be estimated in large linear dynamic systems from dynamic test data. The plots of curvature, $J_{ii\ell}$, presented in this dissertation not only indicate the goodness of the parameter estimates, but also provide clues to evaluate the identifiability of the parameters. The clue is the parallelism between the curves as shown in case study III. If the curves are parallel over the test frequency range, this indicates that these parameters could not be simultaneously identified from the dynamic test data. Further theoretical and experimental investigation is necessary to completely characterize the use of curvature plots to assess identifiability.

LIST OF REFERENCES

LIST OF REFERENCES

1. Sumner, A., "Optimal Identification of Some Parameters of a Nuclear Dynamical System," Transaction from Third Congress of the International Federation of Automatic Control, 1, Book 2: 26A.1-4 (June 1966).

2. Davidson, E. J., "The Identification of Parameter in Large Linear Dynamic Systems," International Journal of Control, 5: 123-130 (February 1967).

3. Yore, E. E. and Y. Takahashi, "Identification of Dynamic System by Digital and Computer Modeling in State Space," Journal of Basic Engineering, 89: 295-299 (June 1967).

4. Hays, J. R., W. C. Clements, Jr., and T. R. Harris, "The Frequency Domain Evaluation of Mathematical Models for Dynamic Systems," A. E. Ch. E. Journal, 374-378 (March 1967).

5. Kowalik, J. and M. R. Osborne, Methods for Unconstrained Optimization Problems, American Elseview Publishing Company, Inc., New York, New York (1968).

6. Richardson, D. C., "Linear Modeling and Control of High Temperature Gas-Cooled Reactor (HTGR) Power Plant," Gulf-GA-A12062, April 1972.

7. Savery, C. W., et al., "TAP - A Fortran IV Program for the Transient Analysis of the HTGR Power Plant Performance," Gulf General Atomic, 1966.

8. Leech, W. D., Personal communication, General Atomic, 1974.

9. Harrington, R. M., Personal communication, The University of Tennessee, 1974.

10. Ball, S. J. and R. K. Adams, "MATEXP: A General Purpose Digital Computer Program for Solving Ordinary Differential Equations by the Matrix Exponential Method," ORNL-TM-1933, Oak Ridge National Laboratory (August 1967).

11. Hooke, R. and T. A. Jeeves, "Direct Search Solution of Numerical and Statistical Problems," J. Assoc. Comput. Mach., 8:212 (1961).

12. Rosenbrock, H. H., "An Automatic Method for Finding the Greatest or Least Value of a Function," Computer J., 3:175 (1960).

13. Spendley, W., G. R. Hext, and F. R. Hamsworth, "Sequential Application of Simplex Designs in Optimization and Evolutionary Operation," Technometrics, 4:441 (1962).

14. Fletcher, R. and C. M. Reeves, "Functions Minimization by Conjugate Gradients," Computer J., 7:149 (1964).

15. Kerlin, T. W. and J. L. Lucius, "The SFR-3 Code--A Fortran Program for Calculating the Frequency Response of a Multivariable System and Its Sensitivity to Parameter Changes," ORNL-TM-1573, Oak Ridge National Laboratory (June 1966).

16. Noble, B., Applied Linear Algebra, Prentice-Hall, Inc., Englewood Cliffs, New Jersey (1969).

17. Buckner, M. R., "A Study of the Application of System Identification Techniques in the Analysis of Nuclear Reactor Dynamics," M. S. Thesis, Nuclear Engineering Department, The University of Tennessee (December 1968).

18. Eykhoff, P., System Identification, John Wiley and Sons, Ltd..(1974).

19. Kendall, M. G. and A. Stuart, The Advanced Theory of Statistics, Vol. 1 and 2, Griffin, London (1961).

20. Kerlin, T. W., Frequency Response Testing in Nuclear Reactors, Academic Press, New York (1974).

21. Katz, E. M., "Planning, Performing, and Interpreting Dynamic Measurements in Pressurized Water Reactors," Ph. D. Dissertation, Nuclear Engineering Department, The University of Tennessee (June 1975).

22. Ball, S. J., "Approximate Models for Distributed Parameter Heat Transfer Models," ISA Transactions, Vol. 3, No. 1, 38-47 (January 1964).

23. Chen, A. T., "A Dynamic Simulation of a Large Once-Through Steam Generator in a Pressurized Water Reactor Power System" Ph. D. Dissertation, Nuclear Engineering Department, The University of Tennessee (to be published).

24. Thakkar, J. G., "Correlation of Theory and Experiment for the Dynamics of a Pressurized Water Reactor," M. S. Thesis, Nuclear Engineering Department, The University of Tennessee (March 1975).

25. Butterfield, M. H. and J. D. Cummins, "Plant Disturbance and Model Verification," Specialist Meeting on Reactor Noise: From Critical Assemblies to Power Reactors, Rome, Italy (October 1974).

26. Duke Power Company, Oconee I Final Safety Analysis Report (1974).

27. Buckner, M. R., "Optimum Binary Signals for Frequency Response Testing," USAEC Report ORNL-TM-3198, Oak Ridge National Laboratory (November 1970).

28. Harrington, R. M., "Analysis of the Fort St. Vrain Nuclear Plant in Supporting of a Dynamic Testing Program," M. S. Thesis, Nuclear Engineering Department, The University of Tennessee (August 1974).

29. Public Service Company of Colorado, Fort St. Vrain Nuclear Generating Station: Final Safety Analysis Report (1975).

30. Dick, D. E. and H. J. Wertz, "Analog and Digital Computation of Fourier Series and Integrals," IEEE Trans. on Electronic Computer, EC-1611, 8-13 (February 1967).

31. Acton, F. S., Numerical Methods that Work, Harper and Row, New York (1970).

32. Kerlin, T. W., "Class Notes on Experimental Methods in Reactor Dynamics" (1973).

APPENDIXES

APPENDIX A

THE ERROR FUNCTION BASED ON THE DIFFERENCE OF GAIN AND PHASE IN THE FREQUENCY DOMAIN

There are two versions of the PARAPE code for the IBM 360 model 65. One uses the error function given by Equation (3.1), as described in Chapter 3, page 66. The other one which uses the difference of gain and phase to generate the error function is of the following form:

$$E = W_1^2 \sum_{\rho=1}^{N} \left(\frac{MG_{P\ell} - MG_{c\ell}}{\sigma_{g\ell}\, MG_{P\ell}}\right)^2 + W_2^2 \sum_{\rho=1}^{N} \left(\frac{\theta_{P\ell} - \theta_{c\ell}}{\sigma_{\theta\ell}\, \theta_{P\ell}}\right)^2 \qquad (A.1)$$

where

N = the total number of frequency observation points

$MG_{P\ell}$ (or $\theta_{P\ell}$) = the magnitude (or phase angle) of the experimental frequency response at the ℓth frequency

$MG_{c\ell}$ (or $\theta_{c\ell}$) = the magnitude (or phase angle) of the model's frequency response at the ℓth frequency

$\sigma_{g\ell}$ (or $\sigma_{\theta\ell}$) = standard deviation of the magnitude (or phase angle) of the experimental frequency response at the ℓth frequency due to the noise contamination in the measurement

W_1 = the weighting factor for the difference in magnitude (normally equal to one).

W_2 = the weighting factor for the difference in phase angle (normally equal to one).

If the test data is contaminated by noise, then, after the Fourier transform by the HFFT code, the phase angle (in degree units) could have large variation (as the case for the Oconee I system, see Figure 33, page 120). In order to eliminate the chance that the error function is dominated by the phase angle difference between model and experiment, one must reduce the weighting factor W_2 or increase the weighting factor W_1. Otherwise, the parameter estimation might not converge to the correct value.

The error function sensitivity with respect to a parameter, P_k, is:

$$\frac{\partial E}{\partial P_k} = -2 \sum_{\ell=1}^{N} \left[\frac{W_1^2 (MG_{P\ell} - MG_{c\ell})}{\sigma_{g\ell}^2 MG_{P\ell}^2} \frac{\partial MG_{c\ell}}{\partial P_k} + \frac{W_2^2 (\theta_{P\ell} - \theta_{c\ell})}{\sigma_{\theta\ell}^2 \theta_{P\ell}^2} \frac{\partial \theta_{c\ell}}{\partial P_k} \right]. \qquad (A.2)$$

Differentiate Equation (A.2) with respect to P_m, to obtain:

$$\frac{\partial^2 E}{\partial P_k \partial P_m} = -2W_1^2 \sum_{\ell=1}^{N} \left[\frac{(MG_{P\ell} - MG_{c\ell})}{\sigma_{g\ell}^2 MG_{P\ell}^2} \frac{\partial^2 MG_{c\ell}}{\partial P_k \partial P_m} - \frac{1}{\sigma_{g\ell}^2 MG_{P\ell}^2} \frac{\partial MG_{c\ell}}{\partial P_k} \frac{\partial MG_{c\ell}}{\partial P_m} \right]$$

$$-2W_2^2 \sum_{\ell=1}^{N} \left[-\frac{(\theta_{P\ell} - \theta_{c\ell})}{\sigma_{\theta\ell}^2 \theta_{P\ell}^2} \frac{\partial^2 \theta_{c\ell}}{\partial Pk \partial Pm} - \frac{1}{\sigma_{\theta\ell}^2 \theta_{P\ell}^2} \frac{\partial \theta_{c\ell}}{\partial P_k} \frac{\partial \theta_{c\ell}}{\partial P_m} \right].$$

At the optimized parameter vector ($\bar{P}$), $MG_{c\ell}$ (or $\theta_{c\ell}$) is close to $MG_{P\ell}$ (or $\theta_{P\ell}$). So,

$$\frac{\partial^2 E}{\partial P_k \partial P_m} = 2 \sum_{\ell=1}^{N} \left[\frac{W_1^2}{\sigma_{g\ell}^2 MG_{c\ell}^2} \frac{\partial MG_{c\ell}}{\partial P_k} \frac{\partial MG_{c\ell}}{\partial P_m} + \frac{W_2^2}{\sigma_{\theta\ell}^2 \theta_{c\ell}^2} \frac{\partial \theta_{c\ell}}{\partial P_k} \frac{\partial \theta_{c\ell}}{\partial P_m} \right]. \qquad (A.3)$$

The values of the magnitude ($MG_{c\ell}$), the phase angle ($\theta_{c\ell}$), the magnitude sensitivity ($\frac{\partial MG_{c\ell}}{\partial P_k}$) and phase angle sensitivity ($\frac{\partial \theta_{c\ell}}{\partial P_k}$) are easily determined as shown in the following development:

$$MG_{c\ell} = [R_{c\ell}^2 + I_{c\ell}^2]^{1/2}$$

$$\theta_{c\ell} = \tan^{-1} \left(\frac{I_{c\ell}}{R_{c\ell}}\right).$$

Differentiating the above with respect to P_k gives

$$\frac{\partial MG_{c\ell}}{\partial P_k} = \frac{R_{c\ell} \frac{\partial R_{c\ell}}{\partial P_k} + I_{c\ell} \frac{\partial I_{c\ell}}{\partial P_k}}{MG_{c\ell}}$$

and

$$\frac{\partial \theta_{c\ell}}{\partial P_k} = \frac{R_{c\ell} \frac{\partial I_{c\ell}}{\partial P_k} - I_{c\ell} \frac{\partial R_{c\ell}}{\partial P_k}}{MG_{c\ell}^2}.$$

Since the values of $R_{c\ell}$, $I_{c\ell}$, $\frac{\partial R_{c\ell}}{\partial P_k}$, and $\frac{\partial I_{c\ell}}{\partial P_k}$ can be found from Equations (3.24a), (3.24b), (3.24c), and (3.24d) in Chapter 3, page 79, the above quantities can be determined easily.

APPENDIX B

HFFT-A METHOD FOR DIGITAL FOURIER ANALYSIS

B.1 Description of the Method

The calculation of Fourier transforms on a digital computer requires the numerical evaluation of

$$F(j\omega) = \frac{1}{T} \int_0^T X(t)\, e^{-j\omega t}\, dt. \qquad (B.1)$$

The most common method for calculating the discrete Fourier transform (DFT) is to approximate the integral as follows:

$$F'(j\omega_k) = \frac{1}{T} \int_0^T X(t)\, e^{-j\omega_k t}\, dt \simeq \sum_{P=0}^{N-1} X_p \exp(-j\omega_k t_p)\frac{\Delta t}{T}$$

$$= \frac{1}{N} \sum_{p=0}^{N-1} X_p \exp(-j\omega_k t_p)$$

$$= \frac{1}{N} \sum_{P=0}^{N} X_p \exp -jP\theta_k \qquad (B.2)$$

where

T = the period

X_p = pth sample of $x(t)$

N = number of samples = $\frac{T}{\Delta t}$

Δt = time interval between samples

$\theta_k = \frac{2K\pi}{N}$

$F'(j\omega_k)$ = DFT approximation to $F(j\omega_k)$.

The real and imaginary parts are

$$R_k = \frac{1}{N} \sum_{P=0}^{N-1} X_p \text{ Cos } P\ \theta_k \qquad (B.3)$$

$$I_k = -\frac{1}{N} \sum_{P=0}^{N-1} X_p \text{ Sin } P\ \theta_k. \qquad (B.4)$$

The calculation procedure would require 2N multiplications for each frequency and the sine and cosine functions would have to be calculated or looked up in a stored table.

A less obvious, but more efficient, procedure[30,31] may be developed by using a simple recursion relation which gives a result that is easily transformed into the desired Fourier integrals. The recursion relationship involves the calculation of a new quantity C(P), defined as follows

$$C(P) = X(P) + 2 \cos \theta_k\ C(p-1) - C(p-2) \qquad (B.5)$$

and with C(-2) = C(-1) = 0. This defined relationship may be solved for X(P) and substituted into Equations (B.3) and (B.4) to give

$$R_k = \frac{1}{N} \sum_{P=0}^{N-1} [C(P) - F(k)\ C(P-1) + C(P-2)] \cos P\theta_k$$

$$I_k = -\frac{1}{N} \sum_{P=0}^{N-1} [C(P) - F(k)\ C(P-1) + C(P-2)] \sin P\theta_k$$

where

$$F(k) = 2 \cos \theta_k.$$

These series may be expanded and rearranged[32] to give the final results:

$$R_k = \frac{1}{N}\left[-C(N-2) + C(N-1)\cos\theta_k\right] \qquad (B.6)$$

$$I_k = \frac{1}{N}\left[C(N-1)\sin\theta_k\right]. \qquad (B.7)$$

We observe that the algorithm (called the HFFT) only requires the evaluation of C(P) for each data point for each frequency using Equation (B.5). This involves a single multiplication and two additions. When the data sampling is complete, convert the values of C(N-2) and C(N-1) into the desired Fourier integrals using Equations (B.6) and (B.7).

If the output and input signals are Fourier analyzed at a harmonic frequency, the frequency response is obtained as follows:

$$G(j\omega_k) = \frac{\frac{1}{T}\int_0^T \delta O(t)\, e^{-j\omega_k t}\, dt}{\frac{1}{T}\int_0^T \delta I(t)\, e^{-j\omega_k t}\, dt}$$

$$= \frac{RO_k + j\ IO_k}{RI_k + j\ II_k} \qquad (B.8)$$

where

$$RO_k = Re\{F[\delta O(t)]_{\omega_k}\} \qquad (B.8a)$$

$$IO_k = Im\{F[\delta O(t)]_{\omega_k}\} \qquad (B.8b)$$

$$RI_k = Re\{F[\delta I(t)]_{\omega_k}\} \qquad (B.8c)$$

$$II_k = Im\{F[\delta I(t)]_{\omega_k}\}. \qquad (B.8d)$$

These lead to the following results

$$\text{Gain} = |G(j\omega_k)| = \left[\frac{RO_k^2 + IO_k^2}{RI_k^2 + II_k^2}\right]^{1/2} \qquad (B.9)$$

$$\text{Phase} = x\{G(j\omega_k)\} = \tan^{-1}\left[\frac{IO_k\ RI_k - RO_k\ II_k}{RO_k\ RI_k + IO_k\ II_k}\right]. \qquad (B.10)$$

If the input signal is given by

$$\delta I(t) = \sum_{k=-\infty}^{\infty} C_k\ e^{j\omega_k t}$$

where

$$C_k = RI_k + jII_k \quad (j = \sqrt{-1})$$

then the output is

$$\delta O(t) = \sum_{k=-\infty}^{\infty} D_k\ e^{j\omega_k t}$$

where

$$D_k = C_k\ G(j\omega_k).$$

The cross power spectrum, P_{IO}, and the power spectrum of the input, P_{II}, are given by

$$P_{II} = C_k\ C_{-k} = RI_k^2 + II_k^2 \qquad (B.11)$$

$$P_{IO} = D_k\ C_{-k} = G(j\omega_k)\ C_k\ C_{-k}$$

$$= G(j\omega_k)\ P_{II}. \qquad (B.12)$$

It is necessary to use an averaging procedure in the data analysis for two reasons: the effective bandwidth of the Fourier analysis becomes too narrow when data records become long making the analysis too sensitive to small errors, and the calculation experiences numerical difficulties when the number of points treated is large (~10,000). This may be overcome by the following procedure.

1. Bring in a block of data (<10,000 points) and analyze. For periodic signals, this block should contain an integral number of periods. At the end of a block, save the necessary values from the recursion calculation C(N-1) and C(N-2).
2. Reinitialize the recursion calculation and bring in another block. Repeat this until the whole data record has been analyzed.
3. Use the stored values from the recursion calculation to calculate the Fourier coefficients and to perform necessary averages.

A FORTRAN language computer program for the HFFT algorithm is given. The code's name is "HFFT." In this computer code, the quantities in Equations (B.8), (B.11), and (B.12) are used in three different average procedures as follows.

1. The Fourier coefficients for input and output are calculated, averaged, and finally ratioed to form the frequency response estimate,

2. Cross power spectrum P_{OI} and input power spectrum P_{II} are calculated, averaged, and ratioed to form the frequency response estimate,
3. The frequency response for each block is calculated and then averaged to give the final estimate.

These different procedures are known to have different sensitivities to noise and to periodicity errors. All three procedures are included to allow investigation of these effects.

The simplicity of the programming required is illustrated in the "HFFT" input instructions. For each harmonic frequency, the printout results include: the input and output Fourier coefficients, power spectrum and cross-power spectrum, the frequency response for each averaging procedure.

B.2 HFFT Input Instructions

(1) Title card (12A6)

Any 72 Alphanumeric characters.

(2) FORMAT (F10.0)

WO = The period (seconds)

(3) FORMAT (6I-10, F10.0)

INT	NAV	L	NBLK	IN	IO	DT
I-10	I-10	I-10	I-10	I-10	I-10	F10.0

If user desired to decrease the effective sampling rate by skipping some of the points, set INT = the number of points to be skipped between data points to be used in the analysis. Otherwise, INT = 0.

NAV = 1, process the input and output data after subtracting bias (bias = average value of the signal).

= 0, process the input and output data as read in.

L = total number of harmonics for print out.

NBLK = number of blocks.

IN = the index number of channel on tape which is selected as input signal.

IO = the index number of channel on tape which is selected as output signal.

DT = time interval between samples.

(4) FORMAT (16I-5)

KI(1)	KI(2)	KI(3)	Up to 16
I-5	I-5	I-5	per card

KI(s) = the selected harmonic number for calculation and print out (s = 1, 2, . . ., L).

(Note: The computer program is available from author on request.)

APPENDIX C

THE ELEMENTARY ROW/COLUMN OPERATION ON A GENERAL COMPLEX SQUARE MATRIX

Let Equation (1.2) in Chapter 1, page 2 represent the model of the dynamic system under study. The equation is repeated as follows

$$\dot{A\bar{x}} = B\bar{x} + \bar{f}g. \qquad (C.1)$$

Upon Laplace transforming this equation and rearranging, the following is developed

$$M\bar{x}(s) = \bar{f}g(s) \qquad (C.2)$$

where

$s = j\omega$

$M = (sA-B)$ is the complex matrix with dimension (NEXNE).

The result of performing an elementary row exchange on the square matrix M can be achieved by forming the left-product $E\ell_{pq}M$ where $E\ell_{pq}$ is the matrix obtained by performing the Pth and qth raw exchange on the unit matrix, I. The elementary column exchange can be achieved by forming the right-product $M\ Er_{pq}$ where Er_{pq} is the matrix obtained by performing the pth and qth column exchange on the unit matrix, I. The matrix obtained by interchange the pth and qth rows/columns of the unit matrix I is

$$E\ell_{pq} = \begin{matrix} \\ \text{pth} \\ \\ \text{qth} \\ \\ \end{matrix} \begin{matrix} \text{pth} \quad \text{qth} \\ \left[\begin{array}{cccccccc} 1 & \cdots & 0 & \cdots & 0 & \cdots & 0 \\ & & \cdots & & & & \\ 0 & \cdots & 0 & \cdots & 1 & \cdots & 0 \\ & & \cdots & & & & \\ 0 & \cdots & 1 & \cdots & 0 & \cdots & 0 \\ & & \cdots & & & & \\ 0 & \cdots & 0 & \cdots & 0 & \cdots & 1 \end{array}\right] \end{matrix} = Er_{pq}. \qquad (C.3)$$

By the definition of elementary row/column operations, we have

$$E\ell_{pq} \cdot E\ell_{pq} = I = Er_{pq} \cdot Er_{pq}. \qquad (C.4)$$

Since if, starting with unit matrix I, we interchange rows/columns p and q, and then perform the same interchange on the results, we arrive back at I.

First, the row exchange of M will be considered. By forming the left-product of Equation (C.2) with $E\ell_{pq}$ and using Equation (C.3), we have

$$E\ell_{pq}\, M\, \bar{x} = E\ell_{pq}\, \bar{f}g \qquad (C.5)$$

It is clear that Equations (C.2) and (C.5) have the same solution for the state vector, $\bar{x}$. Note that during the row exchange, the pth and qth components of the forcing vector $\bar{f}$ exchanged accordingly. The state vector $\bar{x}$ remains unchanged. From the algebra table, sequence of elementary matrices $E\ell^1$, $E\ell^2$, . . . $E\ell^i$ can be found corresponding to the elementary row operations such that

$$E\ell\, M\, \bar{x} = E\ell \cdot \bar{f}g \qquad (C.6)$$

where $E\ell = E\ell^{i} \cdot E\ell^{i-1} \cdot \cdot \cdot E\ell^{1}$ will shift all the rows of M which contain the parameters to the top most rows sequentially.

As for the elementary column exchange, we have

$M\ I\ \bar{x} = \bar{f}g$

$M(Er_{pq} \cdot Er_{pq})\ \bar{x} = \bar{f}g$ (by Equation (C.3))

$(M\ Er_{pq})\ (E\ell_{pq}\ \bar{x}) = \bar{f}g$ (by Equation (C.2))

So, during the column exchange, the pth and qth components of state vector $\bar{x}$ are exchanged accordingly. The forcing vector $\bar{f}$ remains unchanged. Again, from the algebra table, a sequence of elementary matrix $Er^{1}, Er^{2}, \ldots, Er^{j}$ can be found corresponding to the elementary column operations such that

$$(M \cdot Er) \cdot (Eb \cdot \bar{x}) = \bar{f}g \qquad (C.7)$$

where $Er = Er^{j} \cdot Er^{j-1} \cdot \cdot \cdot Er^{1} = Eb$, will shift all columns of M which contain the parameters, to the left most columns sequentially. Note that if the ith state variable is the output to be measured, the ith column will be treated as the column containing the parameters. In this way, the output variable will surely be shifted into the final partitioned sub-matrix A_{11} or B_{11} (see Equation 3.25 in Chapter 3, page 81).

From Equations (C.6) and (C.7), the final matrix equation for the system is

$$(E\ell \cdot M \cdot Er) \cdot (Eb \cdot \bar{x}) = E\ell \cdot \bar{f}g \qquad (C.8)$$

(Note that $Er \cdot Eb = Er \cdot Er = I$).

From the above discussion, it was proven that the solution for state vector $\bar{x}$ would not change by the elementary row/column exchange of M, if one keeps a record on the exchange of the components in $\bar{x}$ and $\bar{f}$ accordingly. A sub-computer program in the PARAPE code has been written to implement these procedures (see Section 4.4, page 121, for an example).

APPENDIX D

DESCRIPTION OF COMPUTER CODE, PARAPE

A digital computer code for the IBM 360 model 65 computer was prepared to implement the techniques developed in this dissertation. The computational procedures parallel the development in Chapter 3, page 81. The current version of the code will handle system models consisting of up to 110 coupled first-order differential equations with the general form as Equation (1.2) in Chapter 1, page 2.

Input Requirements. The computer must be given the following information to perform a calculation:

1. Operational instructions.
2. The input matrices A and B.
3. The initial values of the selected parameters.
4. The algebraic relationships between matrix elements and parameters.
5. The selected frequency observation points.
6. The experimental (or reference) frequency response of the system.
7. The standard deviation and weighting factor at each observed frequency point.

The algebraic relationship between matrix elements and selected parameters is used to calculate partitioned matrix elements each time the newly changed parameters are used including the initial parameters.

Directions for Data Input. There are several types of data cards that must be prepared. They are given below.

Type 1

Title Card: 1-80 columns of alphanumeric characters.

Type 2

Column	1-5	6-10	11-15	16-20	21-25	26-30
Format	I5	I5	I5	I5	I5	I5
Input	NOR	NPLOT1	NPLOT2	IPRNAB	ICASE	IFISH

NOR = number of cases

NPLOT1 $\neq$ 0; plot the frequency response in gain and phase angle

= 0; no plot

NPLOT2 $\neq$ 0; plot the frequency responses in real and imaginary

= 0; no plot

IPRNAB $\neq$ 0; print out the non-zero elements of matrix A and B.

(If IPRNAB = 47, program will print 47 lines per page.)

= 0; no print

ICASE = 1; matrix A is identity

$\neq$ 1; matrix A is not identity

IFISH $\neq$ 0; calculate and print out the matrix, $\frac{\partial^2 E}{\partial P_i \partial P_j}$, in the extended frequency range which is defined in card type 3

= 0; no option.

Type 3

Column	1-10	11-20
Format	E10.4	E10.4
Input	WLO	WUP

If IFISH = 0, omit this card.

WLO = the lowest frequency point in the extended range

WUP = the highest frequency point in the extended range.

The range between WLO and WUP will include all the observed frequency points.

Type 4

Column	1-5	6-10	11-15	16-20	21-25	25-30	31-35
Format	I5	I5	I5	I5	I5	I5	I5
Input	N	NOW	NCTS	NOXI	NOFV	NOK	IPRNT

N = order of system matrix ($N \leq 110$)

NOW = number of observed frequency points

NCTS = number of outputs to be measured

NOXI = number of parameters being considered

NOFV = row number of the last non-zero entry in the forcing vector

NOK < 0; calculate the reference model's frequency response only (no parameter optimization)

IPRNT ≠ 0; print out the sensitivity of the magnitude and phase (or real and imaginary) with respect to changes in matrix element a_{ij} and b_{ij}

= 0; no print.

Type 5

Column	1-12	13-14	25-30
Format	E12.5	E12.5	I5
Input	EST	EPS	LIMIT

If NOK < 0, omit this card.

EST = an estimate of the minimum error function value (recommended value 10^{-5})

EPS = the value of the expected absolute error in parameter estimation, due to the round-off error in numerical calculation. A reasonable choice is 10^{-6}. If the improvement of parameter is less than EPS, program will stop.

LIMIT = maximum number of iterations.

Type 6

Column	1-10	Repeat, 7 per card
Format	7E10.4	
Input	FVEC	

FVEC = components of the forcing vector.

Type 7

Column	1-10	Repeat, 7 per card
Format	7E10.4	
Input	P_ℓ	

P_ℓ = initial value of the parameter, values are listed sequentially starting with P_1.

Type 8: Algebra table (refer to Chapter 3, page 78).

Column	1-3	4-6	7-9	10-19	20-26	27-33	-----	69-75
Format	I3	I3	I3	E10.4	8F7.2			
Input	I	J	m	F_m	E_{m1}	E_{m2}	-----	E_{m8}

I = row number of matrix B or A ($I \leq 110$)

J = column number of matrix B or A ($J \leq 110$)

m = number of the term

F_m = constant multiplier of term m

E_{mq} = exponent of the parameter in factor q of term m ($q \leq 10$).

If $q > 8$ in any E_{mq}, then an additional card is included with identical values of I, J, and m. For instance, E_{m10} would be the second entry (columns 27-33) of the second card with identical values of I, J, and m.

If ICASE = 1, input the elements of B matrix containing parameters and end with a blank card.

If ICASE ≠ 1, input B matrix first (end with a blank card), then input the A matrix (end with a blank card).

Type 9

Column	1-5	Repeat, 16 per card
Format	I5	
Input	ICOL	

ICOL = row numbers of outputs.

Type 10

Column	1-1	Repeat, 80 per card
Format	I1	
Input	IPNA1(I)	

If ICASE = 1, omit this card.

IPNA1(I) = 1, if Ith row is differential state variable

= 2, if Ith row is algebraic state variable

Type 11

Column	1-5	6-10	11-20	Repeat, 3 per card
Format	I5	I5	E10.4	
Input	I	J	b_{ij}	

I = row number

J = column number

b_{ij} = value of elements of the system matrix B.

Note: End Type 11 cards with a blank card.

Type 12

Column	1-5	6-10	11-20	Repeat, 3 per card
Format	I5	I5	E10.4	
Input	I	J	a_{ij}	

If ICASE = 1, skip these cards.

I = row number

J = column number

a_{ij} = value of element of the system matrix A.

Note: End Type 12 cards with a blank card.

Type 13

Column	1-5	6-20	21-35	36-50
Format	I5	E15.7	E15.7	E15.7
Input	KI	FREQI	GAN	PHA

If NOK < 0, skip these cards.

KI = the index number of observed frequency point

FREQI = the frequency in rad/sec

GAN = the gain of the experimental frequency response

PHA = the phase of the experimental frequency response.

Note: Repeat Type 13 card NOW times.

Type 14

Column	1-5	6-20	21-35	36-50
Format	I5	E15.7	E15.7	E15.7
Input	KI	FREQI	RE2	IM2

If NOK < 0, skip these cards.

RE2 = the real part of frequency response

IM2 = the imaginary part of frequency response.

Note: Repeat Type 14 card NOW times.

Type 15

Column	1-10	11-20
Format	F10.0	E10.4
Input	WEIGT1	WEIGT2

If NOK < 0, omit this card.

WEIGT1 = a weighting factor for the summation of the real part (or gain) of error function (normally equal to 1.0)

WEIGT2 = a weighting factor for the summation of the imaginary part (or phase) of error function (normally equal to 1.0)

Type 16

Column	1-10	Repeat, 7 per card
Format	F10.0	
Input	CORA(I)	

If NOK < 0, omit these cards.

CORA(I) = the standard deviation of the real part (or gain) at Ith observed frequency point.

Type 17

Column	1-10	Repeat, 7 per card
Format	F10.0	
Input	CORP(I)	

If NOK < 0, omit these cards.

CORP(I) = the standard deviation of the imaginary part (or phase) at Ith observed frequency point.

Type 18

Column	1-10	Repeat, 7 per card
Format	F10.0	
Input	OMEGA(I)	

OMEGA(I) = the selected Ith observed frequency point.

(Note: The computer program is available from author on request.)

VITA

Sen-I Chang was born in Taichung, Taiwan, Republic of China on October 15, 1943. His parents are Yao-Len Chang and the former Twi Wang. After receiving the Bachelor of Science degree in physics from Chung Cheng Institute of Technology in February 1967, he was employed by the Institute of Nuclear Energy Research (INER).

Beginning in March 1969, he worked at Oak Ridge National Laboratory (ORNL) for two years under the job training program which was arranged in INER and ORNL. At the same time, he entered The University of Tennessee as a part-time graduate student in the Nuclear Engineering Department, and received the Master of Science degree in Nuclear Engineering in December 1970.

In September 1972 he re-entered The University of Tennessee to work towards the Ph.D. degree in Nuclear Engineering. After receiving the Doctor of Philosophy degree in March 1976, he will return to Taiwan, Republic of China and work for INER.